CHALMERS
UNIVERSITY OF TECHNOLOGY

Experimental and modelling study of platinum volatilization from model Diesel Oxidation Catalysts

Master's thesis in the programme of Innovative and Sustainable Chemical Engineering

CAROLINA BRAGA

THESIS FOR THE DEGREE OF MASTER OF SCIENCE

Experimental and modelling study of platinum volatilization from model Diesel Oxidation Catalysts

CAROLINA BRAGA

Supervisors: Prof. Louise Olsson and Dr. Kirsten Leistner

Examiner: Prof. Louise Olsson

CHALMERS UNIVERSITY OF TECHNOLOGY

Department of Chemistry and Chemical Engineering

Gothenburg, Sweden 2017

Experimental and modelling study of platinum volatilization from model Diesel Oxidation Catalysts

CAROLINA BRAGA

Department of Chemistry and Chemical Engineering
Chemical Engineering – Competence Center for Catalysis
Chalmers University of Technology
SE-412 96 Göteborg
Sweden
Telephone: +46 (0)31-772 1000
In collaboration with Cummins Inc.

Abstract

This study investigates platinum volatilization from a model diesel oxidation catalyst (DOC). To comply with future emissions regulations, new solutions for decreasing the amounts of NOx released from vehicles have been proposed, with urea-Selective Catalytic Reduction (urea-SCR) being one of the most promising for heavy-duty diesel engines. DOCs, placed upstream from the urea-SCR, often contain platinum and platinum group metals, which are good oxidizers for other species present in the diesel exhaust. However, it has been observed that ultra-low levels of platinum migrate from the DOC and contaminate the SCR catalyst, reducing the catalyst performance towards NOx reduction due to deactivation. A better understanding of the Pt migration behaviour and its effect on the SCR system is of high importance for further development of diesel exhaust aftertreatment systems. Experimental studies were performed using model Pt/Al_2O_3 catalysts as DOCs. The effects of temperatures to which the DOCs were exposed, durations of exposure and oxygen concentrations were investigated by flow reactor experiments and ICP-MS analysis. It was observed that the rate of Pt volatilization increases non-linearly with increasing temperature and with increasing oxygen concentration in the ranges of 550°C-850°C and 2% O_2 – 8% O_2, respectively. When it comes to the relation with duration of exposure, a small increase with increasing duration was observed. Based on the ICP-MS results obtained for these tested parameters, a model of the simplified kinetics of Pt evaporation from model DOC was developed with the help of the commercial software AVL BOOST™. The model was based on the global reaction $Pt(s)+O_2 \leftrightarrow PtO_2(g)$, and an Arrhenius expression was used in the reaction rate to account for the effects of temperature. A fairly good fit to the experimental data was obtained. However, further adjustments need to be made to take into account the fact that the backward reaction is still active at temperatures as low as 550°C. The effect of doping the model DOC with palladium was also explored. Pd has been reported to act as a stabiliser to Pt, reducing its volatilization. Surprisingly, the amount of Pt evaporated was found to be higher for the Pd-doped catalyst when compared to the model DOC, based on ICP-MS analysis. One possible reason could be that the Pd addition might decrease the noble metal particle sintering and that Pt is more easily evaporated from small particles. A commercial DOC provided by Cummins, Inc. was tested and the results compared to the ones obtained with the model DOC; the levels of Pt migration were lower for the commercial catalyst, however the capturing monoliths after the commercial DOC exhibited higher ammonia oxidation activity.

Keywords: platinum migration, diesel oxidation catalyst, kinetic model, ultra-low platinum contamination.

Acknowledgements

This thesis work was done at the Division for Chemical Engineering at Chalmers University of Technology, in collaboration with the Competence Center for Catalysis (KCK) and Cummins Inc.

First of all, I would like to thank my supervisors Louise Olsson and Kirsten Leistner.

Thank you, Louise, for the opportunity and for the support throughout this work.

Thank you, Kirsten, for all the shared knowledge and for always being so helpful, I am extremely grateful for that.

I would also like to thank all the colleagues in the Chemical Engineering Department for their help and for good moments during the year.

I am also grateful to the colleagues from Cummins for the valuable discussions.

Lastly, I would like to thank my family and friends for their immeasurable support that made this possible.

Contents

1 Introduction

1.1 Context

Emissions from vehicles are a major contributor to air pollution. During the 1940s and the 1950s, the increase in the number of vehicles started to show the first impacts in air quality (Twigg 2007). In the 1960s, for instance, the ground-ozone levels, which are mainly related to nitrogen oxides (NOx) emissions, reached six times the maximum established limit for public health in Los Angeles (Dunn-Rankin et al. 2008), requiring actions to be taken.

The first air quality regulations started to be implemented during the 1960s under California's lead. The milestone in emission control came in 1970 with the Clean Air Act. From that point on, engine modifications were not sufficient to reduce the emissions to the established limits, and catalytic systems were introduced (Twigg, 2007). New regulations for emission control from vehicles are continuously updated, making the limits stricter and increasing the challenge in developing more efficient systems.

The main primary pollutants from engine exhaust gases are unburnt hydrocarbons (HC), carbon monoxide (CO) and NOx (Twigg, 2007, Heck and Farrauto, 2001). When the composition of the exhaust gases is kept close to stoichiometric air to fuel ratio, the traditional three-way catalyst can be successfully used to almost completely remove these three pollutants over the life of the vehicle in modern cars (Twigg, 2007). However, the growing interest in fuel-efficient vehicles with reduced carbon dioxide emissions and in lean-burn engines, in particular, diesel, has created new scenarios when it comes to emissions control (Twigg, 2007, Heck and Farrauto, 2001).

Diesel exhaust always presents an excess of oxygen, which makes the control of NOx difficult since these species should be reduced (Twigg, 2007). Lean-NOx control techniques have been developed to keep the NOx emission limits within the regulations, being Selective Catalytic Reduction (SCR) one of them (Twigg, 2007).

The term "SCR" comprises different technologies, being urea-SCR one of the most promising for reducing NOx emissions from heavy-duty vehicles to meet stricter regulations (Koebel et al., 2000, Toops et al., 2010). In this system, urea is converted to ammonia (NH_3), which then reacts with NOx, selectively reducing it to N_2 and H_2O (Heck and Farrauto, 2001).

A typical heavy-duty SCR system consists of an SCR catalyst located downstream of a Diesel Oxidant Catalyst (DOC) and of a Diesel Particulate Filter (DPF) (Chen et al., 2013). The DOC and the DPF typically contain Platinum Group Metals (PGM), such as Pt and/or Pd, that oxidises HC, CO and NO (Chen et al., 2013). During the regeneration of the DPF, the temperature in the DOC can reach values up to 850°C, which results in the volatilization of precious metals, particularly Pt (Cavataio et al., 2009). It was found that Pt from the upstream DOC can contaminate the SCR catalyst. This generates a problem in emission control since very low amounts of deposited Pt can oxidise the NH_3 that should act as a reducing agent in the urea-SCR system. This situation significantly affects the conversion of NOx and consequently the emission levels of this species (Jen et al., 2008, Cavataio et al., 2009).

1.2 Aim of the project

The SCR catalyst functionality is severely affected by precious metal contamination from upstream DOC catalyst (Cavataio et al. 2009; Jen et al. 2008). It has been observed that trace levels of Pt that migrate from the DOC to the SCR catalyst poisons and deactivates it (Cavataio et al. 2009; Jen et al. 2008). The deactivated region shows high oxidation rate of NH_3 into NO_x and formation of N_2O, leading to significant reduction in NO_x conversion (Jen et al. 2008).

Urea-SCR is one of the most promising techniques for reducing NO_x emissions from heavy-duty vehicles in order to meet stricter regulations (Koebel et al. 2000; Toops et al. 2010). On the other hand, Pt and/or Pd based catalysts are typically used in lean-burn engines (Heck & Farrauto 2001). Therefore, considering the previous discussion, quantifying the amount of Pt deposited on the downstream catalyst and investigating how different parameters (i.e. temperature, time duration, oxygen concentration) affects Pt migration are important issues to make progress in emission control in lean-burn engines.

To better understand Pt migration and its impact on urea-SCR systems, answers to the following questions were sought:

- How is Pt migration affected by the temperature to which the DOC is exposed to?
- How is Pt migration affected by the duration of the DOC exposure to a specific temperature?
- How is Pt migration affected by the O_2 concentration?
- How much Pt contaminates the downstream capturing monolith?
- How can the Pt evaporation be kinetically modelled?

1.3 Delimitations

As the aim of this study was to gain a better understanding of platinum migration from the DOC, no investigation of the direct effects on the SCR catalyst was performed.

No kinetic models describing Pt evaporation from DOCs were found to the date when this work was written. Therefore, the strategy of starting with a model based on the simplified kinetics of the Pt oxidation reaction was adopted.

It was assumed both in the analysis of the experimental results, as in the development of the kinetic model that no significant amounts of Pt deposited on the walls of the reactor tube.

2 Theory

The interest for fuel-efficient vehicles and for reducing emissions of greenhouse gases, especially carbon dioxide, has brought attention to diesel vehicles. Diesel engines are compression-ignited: diesel fuel is injected in a chamber with highly compressed air at a temperature that is high enough for combustion to occur. The excess air makes this process "lean", being diesel engines classified as lean-burn engines. The lean nature of the process makes the combustion cooler which leads to less NOx formation when compared to spark-ignited engines (Heck & Farrauto 2001).

Emissions from diesel engines are, however, more complex than those of gasoline engines, which makes the exhaust catalytic treatment in this type of system additionally challenging (Heck et al. 2009). Diesel engine emissions typically consist of three phases: solids, liquids and gases. The solids and liquids form the so-called total particulate matter (TPM), being composed of soot, inorganic oxides and liquids. The liquids, formed by diesel fuel and oil are known as soluble organic fraction (SOF). The gaseous phase consists of gaseous HC, NOx, CO and sulphur dioxide (SO_2) (Heck et al. 2009).

In the upcoming sessions, a brief description of a typical exhaust aftertreatment system for diesel engines is presented followed by more specific theory regarding different elements of this system, being the level of details adjusted according to the relevance for the development of this work.

2.1 Exhaust aftertreatment system for diesel engines

Different technologies have been investigated for NOx conversion in diesel engines. The high excess of oxygen present in this type of exhaust eliminates the reduction capacity of CO and HC that in three-way catalytic converters serve this purpose (Schäfer & van Basshuysen 1995). Some investigated alternatives have been: selective non-catalytic reduction, non-selective catalytic reduction, selective catalytic reduction (SCR) and DeNOx or lean-burn catalyst (Schäfer & van Basshuysen 1995). More information about the different technologies can be found in the literature. Due to the scope of this work, only SCR systems are further discussed.

A typical heavy-duty SCR system consists of an SCR catalyst located downstream of a DOC and of a DPF (Chen et al., 2013). A representation of the system is presented in Figure 1. The individual elements are discussed in the upcoming sections.

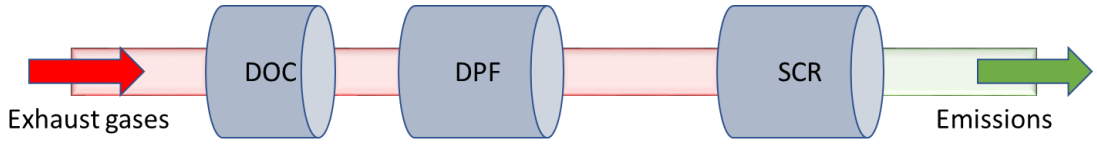

Figure 1 Representation of a typical heavy-duty SCR system.

2.1.1 Diesel Oxidation Catalyst

DOCs are the main catalytic device for removal of SOF in the aftertreatment system. They are typically found as monolithic honeycomb catalysts and are kept in metallic exhaust devices that resemble the gasoline equivalents. The basis for the technology was developed in the USA in the late 1980s to bring trucks into compliance with 1994's emission standards (Heck et al. 2009).

As diesel engines operate in lean mode, they are significantly cooler than gasoline engines, which operate in stoichiometric conditions. This fact brought new challenges in catalytic emission control since it inserted a liquid phase into the system and required, therefore, a catalyst able to not only operate at much lower temperatures but also to handle both liquids and gases (Heck & Farrauto 2001).

Initially, the overall idea with a DOC was to have a catalyst capable of oxidising the SOF without oxidising SO_2, since the latter leads ultimately to the formation of H_2SO_4, which is undesired (Heck & Farrauto 2001; Heck et al. 2009).

Catalytic metals such as Pt and Pd present good activity towards hydrocarbon conversion at lower temperatures but are also very active for SO_2 oxidation (Heck & Farrauto 2001). Different approaches were adopted to face that situation, among which: addition of V_2O_5, which blocked Pt activity towards SO_2 oxidation without affecting SOF conversion (Domesle et al. 1992; Wyatt et al. 1993); use of Pd as a catalytic metal instead of Pt since it has a lower SO_2 activity (Horiuchi et al. 1991); the elimination of the use of noble metals by employing base metal oxides (Farrauto et al. 1993,1995 in Heck et al. 2009).

The approach proposed by Farrauto et al. (1993,1995) in Heck et al. (2009) was based on base metal oxides and resulted in high conversion of SOF. The approach consisted in combining bulk CeO_2 with γ-Al_2O_3. The addition of small amounts of Pt deposited directly on CeO_2 turned out to decrease even further SO_2 oxidation.

Conversion of gaseous HC and CO also were of interest in DOC application. Exclusively increasing the amounts of Pt result in higher activity towards the conversion of these species but also forms particulate matter via sulphate formation. An approach was to add inhibitors to sulphate formation, such as the already mentioned vanadium (Domesle et al. 1992; Wyatt et al. 1993) and rhodium (Fukano et al. 1993 in Heck et al. 2009).

In the 1990s, treated zeolites started to be used to further reduce the emissions of CO and HC to comply with regulations. The zeolites adsorbed the hydrocarbons at low temperatures and released them when the exhaust temperature increased, allowing for oxidation on the Pt function. A typical formulation initially used was Pt on CeO_2 mixed with metal-exchanged zeolite such as ZSM-5 (Heck et al. 2009).

Since the mid-2000s, efforts for lowering the sulphur level in the fuel have resulted in bigger flexibility for catalyst composition. From 2007 on, the DOCs started to have an important part in regeneration of the diesel particulate filter (DPF), which functionality will be briefly discussed in the next section, by providing a lower lightoff of the particulate matter on the DPF and a higher gas temperature for regeneration, by the oxidation of HC (Heck et al. 2009).

Furthermore, the DOC can act on the adjustment of the NO_2/NOx ratio. Higher ratio results in an increase in the rate of soot oxidation at low temperatures in the DPF and favours NOx conversion in SCR catalysts and NOx traps catalysts (Heck et al. 2009; Hauff et al. 2013).

2.1.2 Diesel Particulate Filter

With the stricter regulations proposed by the USA Environmental Protection Agency in the 2000s, the use of DPFs for reducing TPM emissions became once more relevant (Khair 2003). DPFs became first known as traps in the mid-, late 1970s but with the advances in i.e. design engineering made at that time, sufficiently low emissions were achieved without the need of these control devices in order to comply with the regulations (Khair 2003).

Diffusion is the filtration method most used in DPFs for automotive applications. In this method, the particles get trapped in the porous wall of the filter, being also able to diffuse through an existing layer of particulate matter that has already been deposited on the wall. As the deposit layer increases, the flow through this element becomes harder, increasing the exhaust backpressure, which can harm the engine performance. To avoid that, regeneration of the filter is necessary (Khair 2003).

Regeneration occurs by combustion of the accumulated soot, so heat and oxygen are necessary. As diesel engines operate in excess oxygen, the oxygen supply is guaranteed. However, since the exhaust temperature from diesel engines is low, auxiliary systems are needed to ensure the regeneration process. There are two types of regeneration: passive and active. Active regeneration refers to when the addition of heat to the exhaust is done, which can be achieved by use of e.g. electrical heating or addition of extra fuel that creates reaction heat. Passive regeneration refers to when the regeneration process can be achieved without the addition of heat (Khair 2003) and often requires NO_2.

Elemental carbon demands at least 600°C to oxidise, which is seldom achieved in diesel exhaust. To help the regeneration process, soot ignition temperature can be lowered with the use of catalysts (Khair 2003).

It has been observed that passive regeneration can be benefited by placing an oxidation catalyst upstream from the DPF. A platinum catalyst eases the formation of NO_2, which reacts with the carbon captured in the DPF, forming CO_2 and N_2 ideally. In order for this process to be successful, the NOx/carbon ratio must be at least 8:1 but preferably 20:1 (Khair 2003).

Catalysed soot filters are another alternative, in which the catalytic coating composed of noble metals i.e. platinum or copper zeolites applied on the DPF. The surface filter area being restricted, limiting the formation of NO_2 is one of the challenges in this technique; but also catalyst choice and exhaust temperature profile need to be considered (Khair 2003).

Combining DOC and DPF is an effective method for regeneration if the lightoff temperature in the DOC is achieved. However, there are times in which the exhaust temperature is too low, and then an active regeneration method will be required. When active regeneration is performed, the exhaust temperature is raised to high values, reaching 650°C at the filter face (Kong et al. 2005). As previously discussed, this scenario has led to the problem of Pt migration, affecting the performance and causing deactivation in the SCR catalyst.

2.1.3 Selective Catalytic Reduction (SCR)

It is well known that three-way catalyst technology has been efficiently used for removing NOx produced in gasoline engines. However, as diesel engines operate in lean conditions, the same technology cannot be applied. SCR has been appointed as one of the most promising technologies for NOx conversion in diesel exhaust (Toops et al. 2010; Koebel et al. 2000).

SCR systems are mainly based on zeolites, which have the advantage of not relying on the use of noble metals. Besides that, it exhibits a high tolerance to sulphur and can be operated in a broad range of temperatures. However, the regeneration of the DPF, which exposes the system to higher temperatures, has brought up some concerns regarding the durability and performance of the SCR catalyst (Toops et al. 2010). Among those is the one related to Pt contamination due to migration from the DOC/DPF, explored in this work.

In SCR processes, a reducing agent is used for the purpose of reacting specifically with NOx, and not with the excess oxygen present in the lean exhaust gas. There are different reducing agents that have been explored for this application, such as HC, H_2 and NH_3 (Brandenberger et al. 2008).

NH_3-SCR is a technology that has been widely used for DeNOx of stationary sources (Koebel et al. 2000; Brandenberger et al. 2008). In vehicle applications, it is based on the addition of urea that acts as a "non-toxic" source of NH_3, which is the reducing agent (Koebel et al. 2000).

NOx from diesel exhaust gases is mainly composed by NO, which represents over 90% of the total amount (Koebel et al. 2000). Therefore, the main reaction in NH_3-SCR catalysts is (Koebel et al. 2000; Brandenberger et al. 2008):

$$4NH_3 + 4NO + O_2 \rightarrow 4N_2 + 6H_2O \quad (1)$$

Another reaction present in the system is the one where NH_3 reacts with equimolar amounts of NO and NO_2. This reaction is much faster than Reaction (1) (Koebel et al. 2000; Brandenberger et al. 2008):

$$4NH_3 + 2NO + 2NO_2 \rightarrow 4N_2 + 6H_2O \quad (2)$$

If the fraction of NO_2/NOx is higher than 50%, NH_3 reacts with pure NO_2 (Brandenberger et al. 2008):

$$4NH_3 + 3NO_2 \rightarrow 3.5N_2 + 6H_2O \quad (3)$$

As temperature increases to values above 400°C, nitrous oxide might be formed (Koebel et al. 2000). At even higher temperatures NH_3 can be oxidised to NO, which restrains the maximum NOx conversion in the system, decreasing its performance. The reactions are represented by (4) and (5), respectively (Koebel et al. 2000):

$$4NH_3 + 4NO + 3O_2 \rightarrow 4N_2O + 6H_2O \quad (4)$$
$$4NH_3 + 5O_2 \rightarrow 4NO + 6H_2O \quad (5)$$

At low temperatures N_2O formation is also observed, and, in the presence of NO_2, this is related to the formation and decomposition of ammonium nitrates. N_2O is also formed in the presence of NO and it could lead to decomposition of different NH_3-NO species.

2.2 Platinum evaporation in diesel exhaust aftertreatment systems

As described in section 2.1, the typical exhaust layout in diesel engines that make use of urea-SCR systems consists of a DOC and a DPF located upstream of an SCR catalyst (Cavataio et al. 2009; Jen et al. 2008). When the DPF is actively regenerated, the bed temperature in the DOC can reach values up to 850°C, which creates conditions for noble metals, particularly Pt, to volatilize (Cavataio et al. 2009). The volatilized metal has been observed to deposit on the SCR catalyst, poisoning it (Cavataio et al. 2009; Jen et al. 2008; Chen et al. 2013).

As known, upcoming regulations are becoming stricter, which requires efficient catalysts. DOCs containing Pt and Pd are very efficient to reduce levels of HC and CO (Cavataio et al. 2009; Chen et al. 2013). Moreover, high levels of Pt in the DOC favour the oxidation of NO to NO_2, which is beneficial for subsequent SCR performance (Cavataio et al. 2009).

Cavataio et al. 2009 studied the correlation between SCR contamination and the Pt/Pd ratio in the DOC. It was found that the Pt-rich catalyst resulted in a major impact on NO_x conversion and N_2O formation while the Pd-rich catalyst resulted in no changes regarding those aspects.

According to the study, the Pd stabilises the Pt in DOCs, reducing volatilization and consequently, contamination of the SCR catalyst.

Jen et al. 2008 studied the effects of Pt trace level contamination in SCR catalysts. This was done both by using a diesel aftertreatment system containing a DOC, SCR and DPF and also by laboratory duplication of Pt contamination. A combination of a FeSCR and a CuSCR was used, and it was observed that the inlet portion of the FeSCR, which was placed before the CuSCR, became deactivated by Pt contamination. NOx conversion at 350°C was reduced to 48%, and the formation of N_2O levels of 38 ppm was observed at the inlet of the catalyst. The surface area of the deactivated region was also investigated to eliminate the possibility of deterioration in activity due to a loss in surface area because of exposure to high temperature. No changes were observed, indicating that the deactivation was indeed due to Pt contamination (Chen et al. 2013).

Yu et al. (2017) studied Pt poisoning on Cu/SAPO-34 catalysts used in NH_3-SCR systems. To do that, Pt-impregnated Cu/SAPO-34 samples were used with Pt loading varying from 0 to 1 wt%. NH_3-SCR, NH_3 oxidation and NO oxidation tests were performed to evaluate the impact of Pt contamination. The results from NH_3-SCR tests showed that the presence of Pt increased NO conversion at temperatures lower than 250°C and decreased it at temperatures higher than 300°C when compared to the results from a non-contaminated sample. A trend of higher conversion difference according to higher Pt loading was overall observed. It was also noticed that over Pt-impregnated samples, N_2O was formed at around 250°C and that the higher the Pt loading, the higher the N_2O concentration. NO_2 was generated above 250°C and also increased with increasing loading. The increase in NO conversion at lower temperatures and decrease at higher temperatures were due to N_2O and NO_2 formation.

When it comes to NH_3 oxidation results, Yu et al. (2017) found that Pt-impregnated samples exhibited a better NH_3 conversion when compared to a non-contaminated sample. Also, NO was the main product obtained at high temperatures. N_2O and NO_2 were also formed.

Several studies have shown that the amount of Pt deposition on the SCR catalyst varies according to the length, being higher at inlet portions than at the outlet (Jen et al. 2008; Cavataio et al. 2009; Chen et al. 2013).

The formation of N_2O is an important indicative of Pt contamination since it suggests the presence of catalytically active metals, being Pt the most likely candidate for the studied systems (Jen et al. 2008). Poisoning of FeSCR by hydrocarbons or sulphur also leads to a lower SCR performance. Nevertheless, no N_2O formation at the aforementioned levels were observed or such a high drop in NOx conversion at temperatures around 300°C when poisoning is due to those (Jen et al. 2008).

The Pt sites have been shown to be more active than other metal sites, i.e. Fe and Cu, present in SCR samples. At temperatures higher than 400°C, it was observed that NOx remake occurs. That is, in terms of net values, NOx is being formed instead of reduced, which indicates extreme levels of NH_3 oxidation (Cavataio et al. 2009).

Jen et al. 2008 found trace levels of Pt contamination between 0.0005 wt% and 0.001 wt% on the deactivated part of the SCR catalyst investigated, the Fe-zeolite portion. Moreover, it was found in the same study that levels as low as 0.0005 wt% Pt in doped samples showed a significant decrease in conversion.

Chen et al. 2013 investigated contaminated CuSCR catalysts obtained from field aftertreatment systems through Pt elemental analysis of the inlet part of those. A concentration of 0.00042 wt% was found, which was sufficient to generate NOx remaking at temperatures higher than 400°C.

Jen et al. 2008 also investigated if the Pt contamination of the SCR catalyst was due to volatilization of Pt under lean conditions or if it was simply due to the blow off of the washcoat from the DOC that was then deposited on the SCR catalyst. It was found that the cause of contamination was, in fact, Pt volatilization. The presence of excess O_2 and the high temperatures lead possibly to the formation of PtO_2, which is volatile, as discussed in section 2.3.

Chen et al. (2013) and Jen et al. (2008) studied the possibility of recovering Pt poisoned SCR catalysts. Treatment at high temperatures was observed to be effective in recovering contaminated SCR samples (Jen et al. 2008). However, exposing the system to 850°C, as proposed by Jen et al. 2008, could actually lead to secondary poisoning thanks to Pt redistribution over the SCR system or to hydrothermal damaging of the catalyst. Therefore, Chen et al. 2013 were interested in the possibility of recovery at lower temperatures. It was found that a treatment of 2 hours at 700°C was efficient for recovering the contaminated SCR catalysts as long as mechanical damage was not present in the sample. Pt elemental analysis also showed that the SCR performance recovery, in that case, was due to sintering and not migration since the amount of Pt before and after the treatment remained unchanged, eliminating the possibility of secondary poisoning.

Yu et al. (2017) also investigated the regeneration of aged Cu/SAPO-34 after hydrothermal treatment at 750°C. The ageing treatment resulted in an improvement in NH_3-SCR activity of the Pt-impregnated samples and reduced the formation of side-products NO_2 and N_2O when compared to the fresh samples. Hydrothermal treatment at higher temperatures (850°C) was also tested and showed that it could, not only inhibit Pt poisoning on Cu/SAPO-34 samples but contribute to its rejuvenation if the temperature does not destroy the framework. It was observed that hydrothermal treatment causes Pt sintering and the formation of platinum oxides, which decreases the NH_3 oxidation ability and SCR poisoning.

Regarding characterization techniques, as the levels of Pt that migrate are so low, they are restricted. XRD is limited to detecting Pt amounts higher than 0.002 wt% (Jen et al. 2008). Jen et al. 2008 developed a technique based on ethylene hydrogenation that allowed for detecting Pt trace levels deposited on Fe-based NH_3-SCR catalyst in levels as low as 0.0005 wt%. This technique is not metal specific though, and the presence of other metals that are active for ethylene hydrogenation could lead to misleading conclusions. ICP-MS is an alternative for quantifying the amount of Pt deposited on the downstream catalyst, being estimated to detect Pt levels as low as 0.00005 wt% (Chen et al. 2013).

As Pt is a very active catalyst towards NH_3 oxidation, NH_3 oxidation tests have been employed in several studies (Chen et al. 2013; Yu et al. 2017; Jen et al. 2008) as a straightforward way of evaluating the impacts of Pt contamination.

2.3 Noble metals behaviour in the presence of oxygen

Noble metals have been used as catalysts in several applications. Platinum in the form of gauzes, for example, has been widely employed in industrial catalytic oxidation of ammonia, which is an important step in the production of nitric acid (Cornils 2004). Palladium, for

instance, has been used in cross-coupling reactions with application in the pharmaceutical and fine chemicals industry (Torborg & Beller 2009). Chemical vapour transport is another important application that has been broadly investigated, where for example platinum and rhodium have been employed (Hannevold et al. 2005).

Its extent application in various fields has made that considerable research concerning noble metals behaviour has been carried out throughout the years. Despite that, some divergences among the studies are found and will thereby be noticed throughout this section. They are found in i.e. dissociation temperatures and heats of reaction, revealing the challenges of this area of study.

It is well known that, when heated in oxygen or air, all noble metals experience changes in weight. Those changes can be observed as weight loss or increase, depending on the phenomenon occurring (Beamish 1966).

Platinum, iridium, ruthenium and osmium tend to experience weight loss whereas rhodium, palladium and gold, weight increase. It has been noticed that some of these metals may experience a simultaneous loss and gain of weight, which can be attributed to the volatility of an oxide and formation of a stable oxide, respectively (Beamish 1966).

Evidence of volatility in the presence of oxygen at high temperatures have been observed for all six platinum group metals (platinum, palladium, iridium, ruthenium, osmium and rhodium) but not for gold. Nevertheless, gold can temporarily gain weight due to retaining of oxygen by adsorption in some cases (Beamish 1966).

At lower temperatures, oxidation of platinum group metals (PGM) results in the formation of a thin film, which can be visible or not, on the metal surface. When a certain temperature is reached, the oxide films are no longer stable, and the surface becomes clean due to the high dissociation pressure of oxides. At such high temperatures, the volatile oxides are formed (Jehn 1984).

Jehn (1984) presents the dissociation temperatures of some PGM oxides, which are the temperatures in which the dissociation pressures of the oxides in their solid state reaches atmospheric pressure (1.01 bar). That is, at oxygen pressures of 1.01 bar, the solid oxides are stable at temperatures below the dissociation temperature and unstable at temperatures above the dissociation temperature. These temperatures are presented in Table 1.

Alcock (1961), by studying the thermodynamics of PGM oxides in the temperature range of 1200 to 1800°C, elucidated the molecular formulae of the oxides formed in this interval. The PGM oxides formed were PtO_2, RhO_2, IrO_3, RuO_3 and OsO_3. Palladium has a higher vapour pressure as a metal, which made it difficult to measure the volatility due to oxide formation to determine the molecular formula. Free energy equations were also established, which allowed, assuming equilibrium, for calculating the maximum weight losses of the PGM in different atmospheres: inert gas, rough vacuum and 1 atm of pure oxygen. The results showed that higher oxygen partial pressure results in higher weight loss for all PGM (Alcock 1961).

Jehn (1984) also investigated which volatile oxides were formed during high-temperature evaporation of PGM. They were found to be: RuO_3, RuO_4, RhO, RhO_2, PdO, OsO_3, OsO_4, IrO, IrO_2, IrO_3, PtO, PtO_2 and PtO_3. The evaporation of species containing more than one metal atom is not probable to occur (Jehn 1984). During high-temperature oxidation, the weight loss of PGM shows a linear behaviour with time and increases with temperature and pressure.

When temperatures become very high and the oxygen pressures low, the weight loss is mostly attributed to pure metal evaporation (Jehn 1984).

Table 1 Dissociation temperatures of PGM at 1.01 bar oxygen atmosphere [extracted from (Jehn 1984)].

Oxide	Dissociation temperature (°C)
RuO_2	1580
Rh_2O_3	1140
PdO	877
IrO_2	1124
PtO_2	650

Among all PGM, palladium is the only one that exhibits a different behaviour when comparing weight variation in oxygen/air atmosphere and high vacuum. As this metal exhibits a very high metal vapour pressure and very low oxide vapour pressure, lower weight loss is observed in oxygen/air atmosphere, as opposite from the others PGM (Jehn 1984).

Of special interest for this work is the behaviour of platinum in the presence of oxygen. Platinum surfaces, being a PGM, are normally covered by a very thin film of oxide, as discussed. At room temperature, PtO_2 is solid with a heat of formation of -133.9 kJ/mol (-32 kcal/mol) (Chaston 1964). As the heat of formation is low, the platinum surface and oxygen reach equilibrium fast, and the reaction is ceased. With temperature increase though, the tendency of the film is to thicken. When temperatures between 280°C and 450°C (1 atm of O_2) are reached, as reported by Chaston (1964), PtO_2 cannot continue to exist as a solid and dissociates to Pt and O_2. It can be noticed that the dissociation temperature for PtO_2 reported by Jehn (1984), presented in Table 1, is higher than this range. Grandadam in Beamish (1966) observed that PtO_2, under atmospheric pressure, decomposed into PtO at 380-400°C, that then decomposed into Pt at 560°C.

It is important to have in mind that under equilibrium conditions, small concentrations of gaseous PtO_2 always exist (Chaston 1964). The vapour pressure of Pt is higher than that of solid PtO_2 below the dissociation temperature, but when the temperature reaches values above the dissociation temperature, PtO_2 exhibits a higher vapour pressure, which increases with temperature. Thus, above the dissociation temperature, as vapour pressure increases, volatilization of PtO_2 becomes more rapid, making it possible to measure it through weight loss on the Pt surface (Chaston 1964). However, even at high temperatures, the amount of gaseous PtO_2 in equilibrium with Pt is very low and significant weight loss is only observed if there is a stream of moving air, that then sweeps gaseous PtO_2 away from the surface as soon as it is formed (Chaston 1964).

The studies presented so far referred to the investigation of noble metals surfaces behaviour in oxygen. In exhaust aftertreatment systems, supported noble metal catalysts are commonly used. Their behaviour in the presence of oxygen has also been explored.

As discussed in Section 2.1.2, Pt and Pd have good activity towards oxidation of HC, being of interest for exhaust aftertreatment systems and therefore further discussed in this section.

Gélin & Primet (2002) presents a review of oxidation of methane at low temperatures over supported noble metal catalysts, in which volatility was covered. They observed that the reactivity of these metals towards oxygen is quite different: Pd oxidises into PdO at approximately 300-400°C, being stable in air at atmospheric pressure until approximately 800°C. Above 800°C, metallic Pd is the stable form. Pt oxidises to PtO_2, which is unstable when compared to PdO, decomposing at approximately 400°C. As PtO_2 is a highly volatile species, this has been an important factor to explain the reconstruction of platinum surfaces exposed to oxygen atmosphere (Gélin & Primet 2002).

Further investigation of supported platinum catalysts has revealed that the size of the particle is relevant. By studying the oxidation of metallic Pt, McCabe et al. (1988) found that only the exposed Pt atoms are oxidised. Therefore, small supported Pt crystallites are more oxidised than large crystallites or bulk Pt samples due to larger surface-to-bulk atom ratios. The examination of the structure and chemical form of the oxide film that is formed did not lead to strong conclusions, but it seems that for small particles (radii<0.75 nm), the oxygen film is based on PtO_2. For large particles (radii>2nm), the oxygen film seems to be based on chemisorbed oxygen, since there is a decrease in the O-to-Pt ratio (McCabe et al. 1988).

Wang & Yeh (1998) also observed that the species of surface platinum oxide formed depends on the particle size of the dispersed platinum. Like the findings of McCabe et al. (1988), particles with a diameter smaller than 1.3 nm (radii<0.65nm) led to the formation of surface PtO_2 at 497°C (770K), with a heat of formation of -190 kJ/mol O_2. For particles with a diameter bigger than 2.0 nm (radii>1nm), surface PtO was formed, with a heat of formation of -169 kJ/mol.

Additionally, it was found that supported platinum samples with high dispersion exposed to temperatures as high as 597°C (870K) exhibited an insignificant weight loss. However, as dispersion decreased, the weight loss became substantial. This can be attributed to the fact that possibly in highly dispersed samples, the adhesive forces between the alumina support and platinum atoms are strong, making the changes in weight to be due to oxygen desorption. However, as dispersion gets lower, platinum oxide sublimation competes with oxygen desorption for weight loss (Wang & Yeh 1998).

Wang & Yeh (1998) further observed that the extent of oxidation of supported platinum particles varies according to four consecutive steps. At room or lower temperature, adsorption of oxygen on the surface occurs. Above 27°C (300K), the platinum surface goes through reconstruction to accommodate more oxygen. At about 477°C (750K), a stable surface layer of platinum oxides is formed. Above 527°C (800K) desorption of oxygen and platinum oxide occurs (Wang & Yeh 1998).

Regarding the thermodynamics of platinum oxides, not much is known, being a great part of the information available based on high-temperature (>1000°C) experiments, which brings significant errors when extrapolating to obtain enthalpies from equilibrium constants (Citir et al. 2008). Citir et al. (2008) determined the ionisation energies for PtO and PtO_2 by direct measurement, which led to improvements in the calculation of the enthalpies of formation of the gas-phase molecules. The gas-phase enthalpy of formation ($\Delta H^0_{f,0}$) of PtO and PtO_2, respectively, were estimated to be 396±12 kJ/mol and 218±11 kJ/mol.

Wang & Yeh (1998) presents in their study a summary of different heats of formation found for surface platinum oxides in the literature, varying from 222 to 134 kJ/mol for surface PtO_2. For gaseous PtO_2, Jehn (1984) also presents a summary of heats of formation found in diverse

literature. The reported values are 164.31 kJ/mol for temperatures between 1100-1550°C and 163.35 kJ/mol for temperatures between 630-1730°C.

In Table 2, a summary of the different heats of formation found in the literature for PtO_2 on its surface and gaseous form as well as for PtO are presented:

Table 2 Summary of the heats of formation for Pt-oxides from consulted literature.

Oxide	Heat of formation (kJ/mol)	Gibbs free energy of formation (kJ/mol)	Comments	Source
PtO_2 (surface)	190			Wang & Yeh (1998)
PtO_2 (gaseous)		164.31	1100-1550°C	Jehn (1984)
		163.35	630-1730°C	Jehn (1984)
	218±11			Citir et al. (2008)
PtO (gaseous)	396±12			Citir et al. (2008)
PtO (surface)	169			Wang & Yeh (1998)

2.4 Platinum oxidation: reaction mechanism and rate expressions

As discussed in Section 2.3, at high temperatures in the presence of oxygen or air, platinum and other PGM form volatile oxides.

Fryburg & Petrus (1961) studied oxidation of platinum using electrically heated ribbons and expressed the rate of oxidation of platinum at any given platinum temperature as:

$$\dot{R} = k_B p_{O2} P_e \tag{6}$$

Where $\dot{R}$ is the rate of oxidation in μg cm^{-2} h^{-1}, p_{O2} is the partial pressure of oxygen in mmHg, P_e is the escape probability (characteristic of the total pressure and temperature surrounding the gas) and k_B is the slope of the straight-line region of the curve obtained for rate of oxidation vs. pressure of oxygen.

To take into account the effect of temperature, an Arrhenius type equation was used:

$$k_B = A \exp\left(-\frac{E}{RT}\right) \tag{7}$$

Where A is a collision frequency, E an activation energy and T the temperature of the platinum. According to their study, the rate also depends on the temperature, since that affects the rate of collision of the oxygen molecules and the platinum surface, resulting in:

$$A = A_0 T_{O2}^{-1/2} \tag{8}$$

Where A_0 is a proportionality constant. The resulting oxidation rate expression was then proposed as:

$$\dot{R} = A_0 T_{O2}^{-1/2} \exp\left(-\frac{E}{RT}\right) p_{O2} P_e \tag{9}$$

The escape probability is a challenging factor to be determined (Fryburg & Petrus 1961); it depends on the relative dimensions of the sample and on the mean free path of the oxide molecules in the surrounding gas, which, in turn, depends on temperature. At a pressure of 1 atm, the escape probability was found to be 0.002, which means that 0.2% of the oxide that was formed was able to escape the surroundings of the sample, being the rest reflected back to the surface. When the pressure is sufficiently low, P_e=1 and the rate expression determined can be applied (Fryburg & Petrus 1961).

The investigation of oxidation of platinum made by Fryburg & Petrus (1961) using electrically heated ribbons in the temperature range of 900°C-1500°C and pressure range of 15μ-1 atm allowed for the determination of energy of activation E and proportionality constant A_0, summarised in Table 3.

Table 3 Activation energy and proportionality constant for Fryburg & Petrus (1961) platinum oxidation rate. Extracted from:Fryburg & Petrus (1961)

Parameter		Comments
Activation energy (E)	177.9 kJ/mol (42.5 kcal/mol)	-
Proportionality factor (A_0)	1.09E10	Polycrystalline, randomly oriented platinum
	6.75E9	(111) plane of platinum

Through their experiments, Fryburg & Petrus (1961) observed that back-reflection of the volatile PtO_2 by the surrounding gas to the surface creates an unusual pressure-dependence. At lower pressures, the rate of oxidation is directly proportional to pressure. At higher pressures, the oxidation rate still increases with pressure but differs from the linear relation. Back-reflection of PtO_2 makes that the oxide molecules that hit the hot platinum dissociate on the impact, redepositing platinum.

When the pressure is low, all the oxide escapes from the region of the ribbon and is then measured. At higher pressures, the mean free path decreases and collision with the surrounding gas is significant, resulting in the observed behaviour (Fryburg & Petrus 1961).

Bartlett (1967) stated that the overall oxidation reaction of PGM could be described by the following steps:

I. Transport of O_2 molecules to the surface
II. Dissociation of O_2 followed by adsorption of O atoms
III. Formation and evaporation of volatile oxides
IV. Transport of gaseous oxides away from the surface

Based on that, the rate of oxidation as a metal recession rate ($\dot{X}$) was expressed in cm/s. According to Bartlett (1967), diffusion rate and surface reaction rate need to be taken into account when developing $\dot{X}$, since both affect the oxidation rate.

The steady-state value of the platinum oxide vapour pressure at the surface ($p_{PtO2,S}$) is unknown and cannot be measured directly without causing disturbances in the boundary layer.

Therefore, a relation between the diffusion step and surface reaction step was established (Bartlett 1967):

$$\dot{X}_D = \dot{X}_S \tag{10}$$

Where $\dot{X}_D$ is the gaseous diffusion rate and $\dot{X}_S$ the surface reaction rate.

The diffusion rate through the boundary layer can be described by (Bartlett 1967):

$$\dot{X}_D = \left(\frac{M_{0Pt}}{\rho_{Pt}}\right) k_m \frac{(p_{PtO2,S} - p_{PtO2})}{p_t} \tag{11}$$

$\left(\frac{M_{0Pt}}{\rho_{Pt}}\right)$= ratio of equivalent weight to density for platinum required to convert molar oxidation rate to surface recession rate; k_m= mass transfer coefficient; p_{PtO2}= platinum oxide vapor pressure beyond the boundary layer = 0; p_t= total pressure.

When steady-state is reached at the surface (under fixed temperature, pressure, etc.), equilibrium involving the forward and backward reaction in O_2 + Pt (s) $\leftrightarrow$ PtO_2(g) results in net oxidation of platinum combined with migration of PtO_2 (g) from the surface. The surface oxidation rate is then (Bartlett 1967):

$$\dot{X}_S = \left(\frac{M_{0Pt}}{\rho_{Pt}}\right)(k_f p_{O2} - k_b p_{PtO2,S}) \tag{12}$$

Where k_f = reaction coefficient – forward reaction; k_b = reaction coefficient – backward reaction.

As the oxidation rate is slow and $p_{O2} \gg p_{PtO2,S}$, there is no perturbation in the oxygen pressure (Bartlett 1967).

Based on Fryburg & Petrus (1961)'s study that resulted in the determination of the activation energy for the oxidation reaction, Bartlett (1967) assumed that the PtO_2(g) molecules are dissociated by striking on the platinum surface, which corresponds to a condensation coefficient of unity. Thus, with the help of gas kinetics, the backward reaction rate constant can be defined as the surface collision of PtO_2 molecules (Bartlett 1967):

$$k_b = (2\pi MRT)^{-\frac{1}{2}} \tag{13}$$

Where M= molecular weight of PtO_2.

Knowing that the equilibrium constant (K) can be expressed by (Bartlett 1967) :

$$K = k_f / k_b \tag{14}$$

The expressions can be combined, resulting in (Bartlett 1967):

$$\dot{X} = \frac{\left(\frac{M_{0Pt}}{\rho_{Pt}}\right)(2\pi MRT)^{-\frac{1}{2}} K p_{O2}}{1 + \frac{(2\pi MRT)^{-\frac{1}{2}} p_t}{k_m}} \tag{15}$$

Where $\dot{X}$ = metal recession rate (cm/s);

The determined oxidation rate expression is valid at all pressures and temperatures in which volatile PtO_2 is produced, comprising the region where convective diffusion is rate determining (high pressure) and the region where surface reaction is rate determining (low pressure). It is also valid for static and flowing gases (Bartlett 1967).

Jehn (1981) investigated metal losses in polycrystalline platinum discs in the pressure range of 10^{-1}-10^{5} Pa at temperatures from 1300 to 1600°C. It was found that the weight loss is linear with time and that it increases both with pressure and temperature. Activation energies for the oxidation reaction were found to be of 140-180 kJ/mol in the lower temperature range. At higher temperatures, these values increased, however, no more exact details were given about how much. Furthermore, it was observed that at high temperatures and high pressures, the weight loss depends very slightly on the oxygen pressure and that at very low pressures, weight loss is mainly caused by evaporation of pure metal.

Jehn (1981) investigated the nature of the evaporating oxides by two methods. From equilibrium pressure measurements, only PtO_2 was detected; from mass spectrometric studies, PtO and PtO_3 were detected. At low pressures, the reaction between oxygen and platinum results in a steady-state scenario between oxygen sorption and oxide evaporation (Jehn 1981). Assuming PtO_2 is the only oxide that evaporates, Jehn (1981) proposed the platinum loss as being:

$$v_{Pt} = k_{PtO2}\theta_O^2 + k_{Pt} \tag{16}$$

Where k_{PtO2} and k_{Pt} are temperature-dependent rate constants and θ_0 is the oxygen surface coverage.

The oxygen flux for adsorption and desorption was defined as (Jehn 1981):

$$2k_{PtO2}\theta_O^2 = 2k_{O2}p_{O2} \tag{17}$$

Based on these expressions, Jehn (1981) stated that the rate of oxidation could be determined to take into consideration the thermally activated reaction probability and the number of collisions between O_2 and the Pt surface.

Jehn (1984) describes a general rate of oxidation of PGM according to:

$$M(s) + \frac{y}{2}O_2 \leftrightarrow MO_y(g) \tag{18}$$

Where M represents one of the PGM.

Jehn (1984), as Bartlett (1967) also states the importance of taking into consideration the transport of gaseous oxide through the gaseous boundary layer. The transport of species affects the oxidation of PGM when pressure is higher than 10^2 mbar when the backward reaction rate also is significant (Jehn 1984). When steady state is reached, the equilibrium between forward and backward reaction will result in a net oxidation of the metals (Jehn 1984).

Based on the overall oxidation reaction mechanism presented by Bartlett (1967), Jehn (1984) established that the fluxes of oxygen and oxides are determined by the partial pressures at the surface or equilibrium pressure ($p^{=}$), the pressures over the surface (p^{S}), the pressures in the reaction chamber (p^{*}) and rate constants of surface reaction (k) and mass transfer coefficient (k_m).

A representation of the different fluxes used for the determination of the oxidation rate is presented in Figure 2, extracted from Jehn (1984).

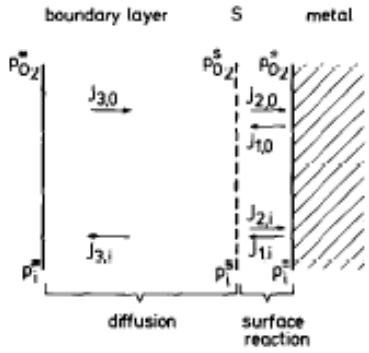

Figure 2 Different fluxes over the catalyst surface for Jehn (1984) oxidation rate expression. Extracted from Jehn (1984).

For adsorption, fluxes can be described as (Jehn 1984):

$$J_{2,O2} = k_{O2} p_{O2}^{S} \tag{19}$$

$$J_{2,MOy} = k_{MOy} p_{MOy}^{S} \tag{20}$$

For desorption (Jehn 1984):

$$J_{1,O2} = k_{O2} p_{O2}^{=} \tag{21}$$

$$J_{1,MOy} = k_{MOy} p_{MOy}^{=} \tag{22}$$

For diffusion (Jehn 1984):

$$J_{3,O2} = k_{m,O2}(p_{O2}^{*} - p_{O2}^{S}) \tag{23}$$

$$J_{3,MOy} = k_{MOy}(p_{MOy}^{*} - p_{MOy}^{S}) \tag{24}$$

As shown in Figure 2, a positive flux is established towards the surface. By balancing the fluxes over the boundary layer, the general equation is obtained (Jehn 1984):

$$J = J_3 = J_1 - J_2 = \frac{p^{*} - p^{=}}{\frac{1}{k} + \frac{1}{k_m}} \tag{25}$$

Where the dependence on p^S is eliminated.

When the process is surface-controlled at low pressures (<10^{-2} mbar), J becomes (Jehn 1984):

$$J = k(p^{*} - p^{=}) \tag{26}$$

When the process is diffusion controlled at high pressures (>10 mbar), J becomes (Jehn 1984):

$$J = k_m(p^{*} - p^{=}) \tag{27}$$

From the thermodynamic data, $p_{O2}^{=} \gg p_{MOy}^{=}$, so $p_{O2}^{=} \sim p_{O2}^{*}$. The equilibrium constant (K) of the reaction is given by (Jehn 1984):

$$p_{MOy} = K p_{O2}^{\frac{y}{2}} \tag{28}$$

Which leads to reaction rates for surface reaction controlled systems and diffusion-controlled reaction systems as being (Jehn 1984):

$$Z_{MOy} = k' p_{O2}^{=} = k' K p^{*\frac{y}{2}}_{O2} \quad (29)$$

$$Z_{MOy} = -k_m{}' p_{MOy}^{=} = k_m{}' K p^{*\frac{y}{2}}_{O2} \quad (30)$$

Where Z_{MOy} is the number of evaporating molecules and the coefficients k' and $k_m{}'$ include the factor for converting vapor pressure into number of molecules. k' also includes the accommodation coefficient, assumed to be one for oxide molecules (Jehn 1984).

Jehn (1984) observed that when the total pressure was high, the metal loss rates were lower than the extrapolated by the rates obtained from lower pressure values. As described by Bartlett (1967), this was attributed to backscattering of the evaporating molecules and metal atoms in the gaseous boundary layer. The evaporation rate of volatile oxides is constant at lower pressures and at higher pressures can have a decreasing, constant or increasing dependence on the total pressure (Jehn 1984).

Fryburg & Petrus (1961) estimated in their work, equilibrium constants for the reaction Pt(s) + $O_2 \leftrightarrow PtO_2$(g) at different temperatures based on collision efficiency. They compared the values obtained to equilibrium constants determined in other works. The values are summarised in Table 4, extracted from Fryburg & Petrus (1961).

Table 4 Equilibrium constants for Pt oxidation reaction. Extracted from Fryburg & Petrus (1961).

Equilibrium constants		Author
1200°C (1473K)	1500°C(1773K)	
1.7E-06	----	Schneider and Esch in Fryburg & Petrus (1961)
----	3E-05	Brewer and Elliot in Fryburg & Petrus (1961)
2.4E-06	2.3E-05	Alcock and Hooper in Fryburg & Petrus (1961)
2E-06	2.3E-05	Fryburg&Petrus (1961)

Bartlett (1967) also determined equilibrium constants for the same equilibrium reaction as Fryburg & Petrus (1961). The temperatures investigated were 1060, 1200 and 1400°C. The values are presented in Table 5.

Table 5 Equilibrium constants for platinum oxidation in oxygen (Bartlett 1967).

Temperature (°C)	K_{eq}
1060	5.9E-07
1200	2.5E-6
1400	1.3E-5

Llopis (1969) performed studies of the chemisorption of oxygen in platinum metals. It was found that, at room temperature, an initial portion of rapid increase in O_2 sorption occurred,

followed by a slow one. This behaviour can most likely be attributed to the fact that a close-packed layer of oxygen is formed by the rapid uptake of oxygen at room temperature. Then, this layer acts like a hinder for the succeeding gas sorption resulting in the slower sorption rate (Llopis 1969).

Furthermore, it was observed that under 400°C, rapid sorption of a certain amount of O_2 on platinum occurs independently of the temperature, which was attributed to the formation of a chemisorbed layer of oxygen over the surface, with four oxygen atoms for each Pt. Between 200 and 350°C, the oxides PtO and PtO_2 are formed, followed by PtO_2 at 400-450°C. Above 500°C equilibrium is established between PtO_2 and O_2. At temperatures higher than 900°C, all PGM except Pd, exhibit a linear rate of weight loss in air through the formation of volatile oxides (Llopis 1969).

Ritchie & Hunt (1969) investigated the pressure influence on surface controlled metal oxidation reactions. Their study showed that the oxidation rate is expected to be linear if the concentration of electrons on the surface is kept practically constant. Pressure change results in complex variation in reaction velocity, however, simplifications of the rate expressions are possible. At low pressures, if the rate determining step is dissociation of O_2 or one of the steps prior to that, the rate will be proportional to the pressure. In all other cases, the rate is proportional to the square root of the oxygen pressure (Ritchie & Hunt 1969).

In the region surrounding the Pt surface that is under oxidation, PtO_2 being formed diffuses away. In the cooler areas, Pt is then deposited. If the hot air carrying PtO_2 gets in contact with a much cooler surface, shock-cooling will occur, and PtO_2 will be deposited as a solid oxide, being this effect more pronounced the higher the temperature is (Llopis 1969).

2.5 Monolith catalytic reactors

Monolith supports were first used in large-scale application in the 1970s when catalytic converters were installed in new vehicles in the USA (Heck et al. 2001). The large open frontal area results in low resistance to flow leading to low pressure drop (Heck & Farrauto 2001; Cybulski & Moulijn 1994). In the exhaust system of an automobile, less resistance to flow means less power loss which is an important feature that contributed to outweigh the use of particulate bead catalysts in this segment. Moreover, due to its open structure, monolith supports do not face plugging in dust applications, i.e. diesel exhausts and in extreme cases, can be cleaned with certain ease (Heck et al. 2001).

Another important feature of monolith supports is related to the conversion. In a warmed-up vehicle, the rate of conversion is, generally, limited by bulk mass transfer (Heck et al. 2001). Monoliths have a high geometric area, which favours high conversion in those conditions. Besides that, the reduced weight favours conversion in the sense that it becomes warm faster (Heck et al. 2001).

The operating conditions in exhaust catalytic converters for vehicles can be severe, with temperatures over 1000°C and thermal shock (Heck et al. 2001), which requires the use of a suitable material. Ceramic materials withstand high temperatures (melting point of 1465°C), are resistant to oxidation and to thermal shock and have been extensively used by automobile manufacturers since the 1980s (Heck et al. 2001). Cordierite (14% MgO, 35% Al_2O_3, 51% SiO_2), for instance, is commonly used for exhaust applications, offering a good mechanical strength (Heck et al. 2001; Cybulski & Moulijn 1994).

When a monolith support is covered with a thin catalytic layer, a monolithic catalyst is formed (Cybulski & Moulijn 1994). Monolithic catalysts are known to have a lower internal diffusion resistance when compared to i.e. packed beds, and even the external mass transfer resistance in gaseous systems is reduced (Cybulski & Moulijn 1994). They are commonly prepared via washcoating, in which a high-surface material is deposited onto the monolith support, being γ-alumina the most used washcoat material (Cybulski & Moulijn 1994). Figure 3 shows the typical structure of coating used in emission control applications in vehicles (Cybulski & Moulijn 1994). As can be seen, the active material (in this case Pt) was incorporated to the washcoat.

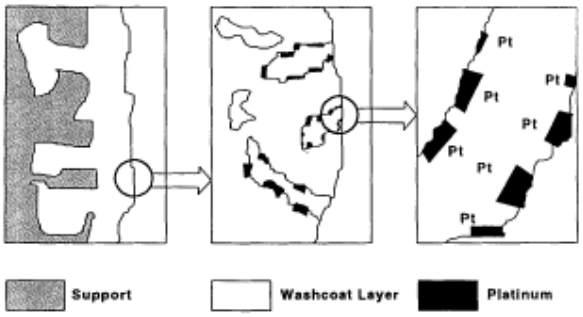

Figure 3. Coat structure for typical emission control application in vehicles. Extracted from Cybulski & Moulijn (1994).

Conventional fixed-bed reactors tend to present high pressure drop and maldistribution such as channel formation. Structured catalysts such as monolithic catalysts do not present those disadvantages and have therefore been used in diverse applications (Cybulski & Moulijn 1994).

Flow reactors are commonly used for investigation of catalytic reactions in laboratory. Generally, mass-flow controllers are used to control the inlet gas flow, and a system such as gas chromatograph or FTIR is used to analyse the outlet gas flow. This allows for measuring the catalytic reaction rate, which is useful for performance comparison (Ross 2012).

2.6 Characterization techniques

Chemical and physical techniques can be used in the study of catalysis to characterise catalysts and obtain information that can lead to a better understanding of the catalytic phenomenon. In this study, NH_3 and CO oxidation were used as tools for evaluating activity. Also relevant for catalyst characterization, were the techniques ICP-MS, XRD and electron microscopy. A brief presentation and relevant details of these techniques are presented throughout this section.

2.6.1 NH_3 oxidation

Oxidation catalysts containing small amounts of Pt can effectively convert NH_3, with a low selectivity to N_2. For instance, Pt/Al_2O_3 catalysts are known to produce large amounts of NOx and N_2O (Kamasamudram et al. 2011).

PGM are used in nitric acid production processes to oxidise NH_3 to NOx (Kamasamudram et al. 2011). Therefore, high selectivity to NOx is expected even though N_2 is the most thermodynamically favoured product of NH_3 oxidation (Kamasamudram et al. 2011). Figure 4 shows the feasible pathways for NH_3 oxidation.

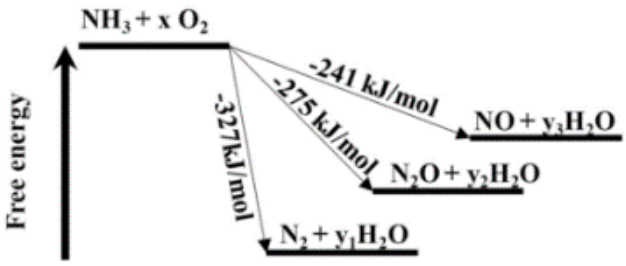

Figure 4 Feasible pathways for NH_3 oxidation (Extracted from Kamasamudram et al. (2011)

The simplified reaction mechanism over a metal-containing-catalyst surface is presented below, where * represents an empty catalyst site (Kamasamudram et al. 2011):

$$NH_3 + * \rightarrow N^* \text{ (or } NHx^*) + H_2O \quad (31)$$

$$O_2 + 2^* \rightarrow O^* + O^* \quad (32)$$

$$N^* + O^* \rightarrow NO^* \text{ (or NO gas phase)} + * \quad (33)$$

$$N^* + NO^* \rightarrow N_2O + 2^* \quad (34)$$

$$NHx^* + NO^* \rightarrow N_2 + 2^* + H_2O \quad (35)$$

The rates of theses reactions depend on the reaction temperature, feed gas composition as well as on catalyst properties (Kamasamudram et al. 2011).

Kamasamudram et al. 2011 have found that catalysts containing higher PGM content present higher selectivity to NOx. N_2O is commonly obtained as a byproduct of NH_3 oxidation on PGM, with a selectivity peak at temperatures close to 250°C. However, N_2O formation is almost inexistent at temperatures around 450°C. Regarding selectivity to N_2, it was observed in the same study to be almost inexistent at temperatures above approximately 300°C for catalysts with high PGM content.

2.6.2 CO oxidation

CO oxidation over PGM has been widely investigated in surface chemistry (Bobaru 2006).

$$CO + ½\ O_2 \rightarrow CO_2 \quad (36)$$

Investigation of CO oxidation over Pt has revealed that the oxidation rate starts to be observed at around 100°C (373 K) and reaches maximum levels at around 185°C (473K) (Anderson 1992).

Manasilp & Gulari (2002) investigated the effect of Pt loading on CO oxidation, by having Al_2O_3 supported Pt catalysts with 1 and 2 wt% Pt loading as part of their study. CO oxidation levels were higher for the catalysts containing a higher Pt loading.

Moreover, CO oxidation over Pt has been reported to be insensitive to structure and also to not depend on particle size over a wide interval of dispersion. However, for extremely highly dispersed catalysts some structure sensitivity can be observed (Anderson 1992).

Different mechanisms can be attributed to CO oxidation over a metal surface, being Langmuir-Hinshelwood's widely accepted (Bobaru 2006).

It has been observed that reactions occurring in conditions far from equilibrium can exhibit oscillations and instabilities. At low CO pressure, the rate of CO oxidation is limited by adsorption of molecules, increasing linearly with increasing CO pressure. However, as the concentration of CO molecules starts to increase, it inhibits the adsorption of O_2, resulting in a

reduction in the oxidation rate, forming a zone of low reactivity. In between the high reactive and low reactivity regions, there is a transition region where oscillations in the reaction rate can occur (Bobaru 2006).

2.6.3 Electron Microscopy – SEM and TEM

Heterogeneous catalysts have a complex structure, highly divided that is difficult to characterise. Different types of electron microscopy allow, for example, the direct observation of the catalyst morphology at a resolution range of 10^{-4} - 10^{-10} m and even the investigation of the local composition of the sample at a resolution of 1 nm, by combining X-ray analysers (Imelik & Vedrine 1994). Those factors contribute to making electron microscopy a common technique for characterising catalysts (Imelik & Vedrine 1994).

When a sample is exposed to an electron beam, different signals are produced, being some of them transmitted, and some reflected (Imelik & Vedrine 1994; Egerton 2016). Both types can be used to produce an image. Among the reflected signals are photons; the de-excitation of atoms leads to the formation of photons in a scale range from X-ray to visible, which makes X-ray emission spectroscopy, for instance, an important instrument for qualitative and quantitative analysis of the sample (Imelik & Vedrine 1994).

A scanning electron microscope (SEM) uses backscattered electrons and secondary electrons, which are reflected signals, to produce an image (Imelik & Vedrine 1994). As the name suggests, this technique makes use of an electron beam that scans the sample horizontally in two perpendicular directions (i.e. x and y). Modern SEM can provide images with a resolution between 1 and 10 nm (Egerton 2016). The combination of the imaging function with an analytical function such as Energy Dispersive X-Ray Emission (EDX) provides an important tool in catalyst characterization. The typical detection limit for EDX is approximately 0.1 wt% (Kuisma-Kursula 2000).

A transmission electron microscope (TEM) uses transmitted electrons to produce an image (Imelik & Vedrine 1994). In contrast to SEM, the TEM makes use of a stationary electron beam that penetrates a thin layer of the sample (Egerton 2016). If the sample is not thin enough, the electrons will become too scattered and can even be absorbed instead of transmitted, creating problems for imaging. That is why sample preparation is critical in TEM applications. A TEM can provide magnified images in the range of 10^3 to 10^6 (Imelik & Vedrine 1994).

2.6.4 Inductively Coupled Plasma Mass Spectrometry (ICP-MS)

Mass spectrometry makes use of molecular ionisation to mass discrimination (Imelik & Vedrine 1994). This process is irreversible and therefore destructive. The molecules are ionised and the mass spectrometer basically measures the ratio between the mass and the charge of the ion formed (Imelik & Vedrine 1994). Besides the quantitative measurement of different ions, the mass spectrometer also is responsible for ionising the molecules and separating them according to the mass/charge ratio (Imelik & Vedrine 1994).

ICP-MS, specifically, provides extremely low detection limits, in the part per trillion range but is also suitable to detect parts per million (Thomas 2013). This particularity makes it attractive as a trace metal detection technique since it is more flexible if compared to other techniques such as ETA or FAA that are traditionally used for detecting higher concentrations (Thomas 2013). For Pt, the detection limit estimated to be 0.00005 wt% (Chen et al. 2013).

In ICP-MS, a plasma torch, which is placed horizontally, is used to generate positively charged ions (Thomas 2013). The ions are then directed into the mass spectrometer through an interface region maintained at vacuum conditions. Once they pass electrostatic lenses, called ion optics, the ions are directed into the mass separation device (Thomas 2013). The ion optics avoid that photons, particulates and neutral species reach the detector, only allowing that the ion beam passes to the mass spectrometer, where separation occurs (Thomas 2013). An ion detector then converts the ions into an electrical signal that is processed by a data-handling system and converted into analyte concentration according to ICP-MS calibration standards (Thomas 2013).

2.7 Modelling software

The commercial software AVL BOOST™, version 2013, was used to perform the kinetic modelling developed in this work.

AVL BOOST™ is a software that can be used for the simulation of internal combustion engines. Through its models, prediction of engine performance, emissions and acoustics can be made accurately (AVL 2017).

Of interest for the execution of this work is the Exhaust Gas Aftertreatment simulation functionality. The main details and models solved under this functionality are described below (AVL 2013).

The catalytic converter is of the honeycomb-type. It is assumed that the differences between channels are negligible. Therefore, the one single channel model can be appropriately used. As the name suggests, in this model the whole catalytic converter is represented by one single channel.

The effects acting on the channel are: in the gas phase, convection, diffusion and conduction; in the washcoat, diffusion and catalytic conversion; through the boundary layer, effects of mass and energy transfer; in the solid phase, conduction.

Since no radial gradients are considered in the channel, transient and 1D conservation equations are enough to model the thermodynamics and fluid dynamics of the system.

The continuity equation of the gas phase is described as:

$$\frac{\partial \rho_g}{\partial t} = \frac{\partial \rho_g v_g}{\partial x} \tag{37}$$

ρ_g= density of gas phase; t = time; v_g= interstitial gas velocity; x= spatial coordinate in axial direction.

The momentum conservation equation is described as:

$$\frac{\partial p_g}{\partial x} = -D_a v_g \tag{38}$$

p_g = pressure of the system; D_a= Darcy constant.

The species conservation is described as:

$$\varepsilon_g \frac{\partial \rho_g \ \omega_{k,g}}{\partial t} = \varepsilon_g \frac{\partial \rho_g \, \omega_{k,g} \, v_g}{\partial z} + \varepsilon_g \frac{\partial}{\partial z}\left(\rho_g D_{eff} v_g \frac{\partial \omega_{k,g}}{\partial z}\right) + M_{k,g} \sum_i^I \vartheta_{i,k} \, \dot{r_k} \tag{39}$$

$\omega_{k,g}$= mass fraction of species k; D_{eff}= effective diffusion coefficient; $\dot{r_k}$ = general reaction term; $\vartheta_{i,k}$= stoichiometric coefficients; ε_g= volume fraction of gas phase.

As chemical reactions occur on the surface of a catalyst, the bulk concentration of the species and the concentration of species right above the surface are different. To take that into consideration, by assuming quasi-steady-state conditions, the molar surface concentration is described as:

$$GSA\ k_{m,k}(C_k^S - C_k^B) = \sum_k^K \dot{r_k} \tag{40}$$

C_k^L = molar surface concentration of species k; $c_{k,g}^B$= molar concentration of species k in the bulk; $k_{m,k}$ = mass transfer coefficient of the species k; $GSA = 4\ \frac{d_{hyd}}{\sqrt{\frac{1}{CPSM}}}$; d_{hyd}= hydraulic diameter; CPSM= cell density.

The coverage of component k on the surface is described by:

$$\frac{\partial \theta_k}{\partial t}(\Theta\ GSA) = \dot{r_k} \tag{41}$$

$(\Theta\ GSA)$ = measure for the entire storage capacity; Θ= site density;

Heat transfer was not solved in the study performed at this work, and therefore those equations were not described in this section. They can be found on AVL BOOST Aftertreatment Users guide.

3 Methodology

The work performed in this Master's thesis project consisted of two main parts: experiments and kinetic modelling.

The experimental part consisted of the investigation of Pt migration from model DOC supported Pt/Al_2O_3 catalysts, produced at Chalmers, by exposure to high temperatures in the presence of a "capturing monolith", located downstream from the model DOC. The effects of different temperatures, durations of exposure to a high temperature, oxygen concentrations and Pd doping were studied. Also, a commercial DOC, provided by Cummins Inc, was tested.

Based on the experimental results obtained, a kinetic model of the simplified kinetics of Pt evaporation was developed using the commercial software AVL BOOST, version 2013.

This chapter is divided into two main sections: "Experiments" and "Kinetic model".

3.1 Experiments

The experimental work consisted of samples preparation, flow reactor experiments and physical characterization of tested samples. The methodology used in each of them is described in the subsections 3.1.1, 3.1.2 and 3.1.3, respectively. The physical characterizations were done by the company ALS, however, the samples were prepared for characterization at Chalmers.

3.1.1 Samples preparation

3.1.1.1 Catalytic material

The catalytic material produced consisted of Pt/Al_2O_3 and $Pt/Pd/Al_2O_3$, both produced via incipient wetness impregnation. The Pt content of the Pt/Al_2O_3 catalyst was 2 %wt. When it comes to the $Pt/Pd/Al_2O_3$ sample, the number of moles of Pt was calculated to be the same as the one in the Pt/Al_2O_3 sample, and the amount of Pd, such that Pd and Pt were in a 20:80 weight percent ratio. This resulted in 2% Pt/0.5% Pd/Al_2O_3.

The first step in catalyst production was the characterization of the alumina support (Sasol Puralox Nga150) by BET to obtain the pore volume of the material (0.524 mL/g). This allowed for calculating the amount of precursor necessary to impregnate the alumina support to achieve the desired Pt content. The Pt precursor used was a diamminedinitritoplatinum (II) solution in NH_4OH from Sigma-Aldrich.

For the preparation of the Pt/Al_2O_3 catalyst, the stepwise incipient wetness impregnation procedure was required, being two impregnation steps necessary. In each step, the precursor was dissolved in deionized water, producing a solution with the exact volume necessary to completely fill the pores of the alumina support. Between the steps, the material was dried in the oven at 100°C during 19h. Once the second step of impregnation was completed, the material was calcined in the oven at 500°C during 2h with a ramp of 5°C/min. The total amount of Pt/Al_2O_3 catalyst obtained was approximately 9.1 g and was sufficient to perform all sets of experiments presented in this study.

Likewise, for the preparation of the $Pt/Pd/Al_2O_3$ catalyst, the stepwise incipient wetness impregnation method was used. First, the overall procedure described for the production of Pt/Al_2O_3 catalyst was repeated. Once the material was produced, impregnation with Pd was done via incipient wetness impregnation. However, only one step was required at this stage. The precursor used was a tetraamminepalladium (II) nitrate solution. After Pd impregnation,

the material was dried in the oven at 100°C overnight. Calcination was then performed during 2h at 500°C, with a ramp of 5°C/min.

3.1.1.2 Monolith preparation

The monoliths were cut out of a commercial honeycomb structure made of cordierite containing 400 cpsi. They were cut to a length of 2 cm and a diameter of 1.1 cm, according to the pattern presented in Figure 5, resulting in a total of 89 channels per monolith sample.

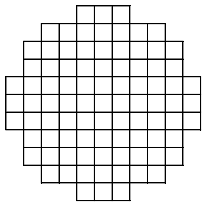

Figure 5. Monolith pattern

After the cutting process, all monoliths were submitted to calcination at 500°C during 2 hours, with a ramp of 5°C/min.

3.1.1.3 Washcoating

Once the catalysts and the monoliths were prepared, washcoating of the monoliths was performed.

The aimed amount of washcoat per monolith of model DOC was of approximately 250 mg. The solution used for washcoating was prepared with a ratio of 20:80 solids:liquid, where "solids" consisted of catalyst+binder and "liquid", of ethanol and water. The binder used for the monoliths was Disperal P2, and the proportion between catalyst and binder was 95:5.

The water and ethanol were mixed in a ratio of 50:50 in a beaker, to which the solids were added, creating a slurry that was constantly agitated with the help of a magnetic agitator. With a plastic pipette, the slurry was dropped onto the monolith channels. After the excess had been taken away, the sample was dried with a hot gun at 90°C during 2 min, assuring that the channels were not obstructed. The sample was weighted, and the procedure was repeated until the desired final washcoat weight was achieved. The sample was then calcined with a hot gun at 500°C during 2 min and after that, in the oven at 500ºC for 2 hours with a ramp of 5°C/min. The final washcoat amount obtained after calcination showed a variation of ± 7% from the desired value of 250 mg.

Capturing monoliths were placed downstream of the model DOC, as further detailed in Section 3.1.2. Those were washcoated with Al_2O_3 to create an improved surface area to capture the evaporated Pt. This was done by preparing a slurry with a ratio of 5:95 binder to "liquid". The binder used was Disperal P2, and the "liquid" consisted of water and ethanol in a ratio of 50:50. With the help of a plastic pipette, the slurry was dropped onto the monolith channels. After the excess had been taken away, the sample was dried with a hot gun at 90°C during 2 min and weighted. As for the catalyst washcoating, the process was repeated until the desired weight was achieved. The monolith was then calcined with the hot gun at 500°C for 2 min and after that, in the oven at 500°C for 2 hours with a ramp of 5ºC/min.

The amount of alumina washcoat in the capturing monoliths was either of about 20 mg or of approximately 80 mg. The amount of alumina washcoat was increased from 20 to 80 mg to investigate if this factor was influencing the capture of Pt.

The exact amount of washcoat in the model DOC and capturing monoliths are specified in Table 40 and Table 41, presented in the Appendix (A.1), where they are also named. Also in the Appendix (A.1), the deviation of the amount of washcoat obtained in relation to the desired value is presented for each produced sample (Table 42).

Mistakenly, Sasol Puralox Nga150 was used as a binder instead of Disperal P2 for the model DOC P6-P9 (see Table 40 – Appendix A.1), but as boehmite transforms to alumina during calcination and the process examined is most likely not limited by mass transfer, this was not seen as a potential problem.

The tested commercial DOC monolith was cut from a honeycomb provided by Cummins Inc. It was calcined in the oven at 500ºC for 2 hours with a ramp of 5ºC/min before being used in the experiments.

3.1.2 Flow reactor experiments

The flow reactor experiments consisted of evaporation trials, in which the DOCs were exposed to temperatures that led to Pt volatilization and oxidation trials, in which activity for NH_3 and CO oxidation were tested. For both types of trials, the experimental reactor setup comprised a quartz tube, heating coil, thermocouples, monoliths and quartz wool, used for insulation and monolith wrapping. The monoliths were wrapped in quartz wool when placed horizontally into the reactor tube to avoid that gas flowed between the sample and the tube. The inlet gases used in the feed were injected and regulated by Bronkhorst mass flow controllers (MFCs), and water vapour was produced by a Bronkhorst controlled Evaporation and Mixing (CEM) system.

Each evaporation trial made use of a DOC and a capturing monolith. The DOC was placed upstream from the capturing monolith, and a heating coil was used to control the temperature in the region where the DOC was positioned. The capturing monolith was placed outside of the heating zone, at a distance that ensured that temperatures lower than 400°C were achieved in the centre of the monolith.

Three thermocouples were used in the evaporation trials: one for measuring the gas temperature, with its end positioned about 1 cm from the DOC front (the side facing the reactor inlet); one for measuring the temperature in the centre of the DOC; and one for measuring the temperature in the capturing monolith. The thermocouple used for measuring the gas temperature was the one used for regulating the temperature according to the set point. The thermocouple used for measuring the temperature in the capturing monolith was not connected to a data acquisition system, so the temperature was manually registered when it had been observed that all temperatures in the system were stable.

The oxidation experiments made use of the capturing monoliths that had been used in the evaporation trials, or “contaminated” capturing monoliths. In this system, two thermocouples were used, one for measuring the gas temperature, positioned in the same way as described for the DOC and another one for measuring the temperature in the centre of the “contaminated” monolith. A heating coil was used for regulating the temperature based on the measurements of the gas temperature thermocouple.

The correct positioning of the “contaminated” monolith was an important feature on the oxidation trials: the monolith side facing the DOC during evaporation trials, or monolith front, was positioned facing the reactor inlet during the oxidation trials. In other words, its positioning when it comes to back and front side was kept unchanged.

The outlet gases from the oxidation trials were analysed using an MKS Multigas 2030 FTIR spectrometer. The concentrations of NH_3, NO, NO_2, N_2O, CO and H_2O were monitored. The outlet gases from the evaporation trials were sent directly to the exhaust system of the laboratory to avoid a possible metal contamination of the analysis equipment.

Different quartz tubes were used in the evaporation and oxidation trials, to avoid that a possible metal contamination of the tube resulted in misleading results. Also, before starting the oxidation trials, empty tube tests were performed to ensure that no contamination was present in the reactor system.

All trials were performed with a total volume flow of 1200 mL/min and a space velocity of 37882 h^{-1}. Argon was used as inert balance in all cases.

The overall reactor setup is presented in Figure 6. The gases were injected from the left side. The quartz tube, with the monoliths, and the heating coil are covered by the insulation. The heating coil was connected to the power source through the red wires that can be observed above the insulated reactor tube.

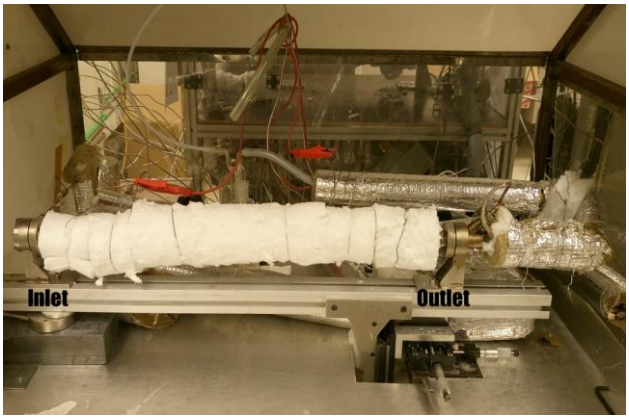

Figure 6 Overall reactor setup.

The Pt evaporation behaviour was investigated under different temperatures, different O_2 concentrations and different time durations. In Table 6, the different conditions investigated are presented.

Table 6 Summary of the experimental conditions investigated in the evaporation trials.

Temperature (°C)	O_2 concentration (%)	Time duration (h)
550	8	15
625	8	15
700	8	15
700	5	15
700	2	15
700	8	5
700	8	10
775	8	15
850	8	15

In Figure 7, the configuration adopted in the evaporation experiments, without insulation, is presented.

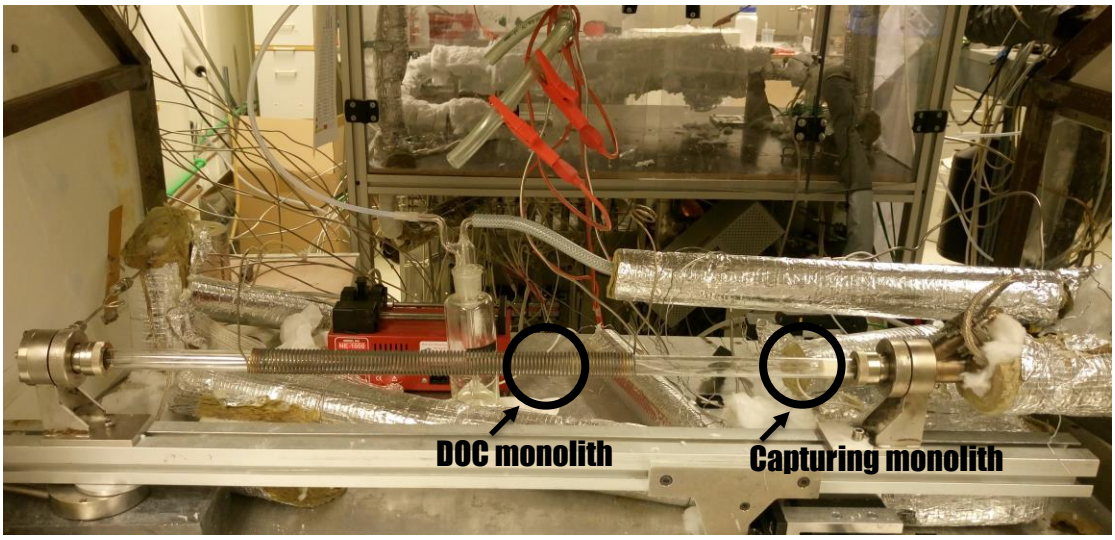

Figure 7 Configuration of the reactor system for evaporation experiments.

Regarding the experimental protocol, all evaporation trials were divided into lean pre-treatment, degreening and evaporation steps. The oxidation trials were divided into surface cleaning, NH_3 oxidation and CO oxidation steps, with surface cleaning always being repeated prior to CO oxidation. The detailed specifications of each step are presented in Table 7. Three different types of pre-treatment were tested, being abbreviated further in the report as "H_2", "C_3H_6" and "C_3H_6+O_2".

Table 7 Detailed experiments conditions.

<table>
<tr><th>Oxidation</th><th colspan="2">Evaporation</th></tr>
<tr><td>Surface cleaning</td><td colspan="2">Lean pre-treatment</td></tr>
<tr><td>8% O_2, 5% H_2O; 500°C, 20 min</td><td>H_2</td><td>1% H_2;
500°C, 40 min</td></tr>
<tr><td>NH3 oxidation</td><td colspan="2" rowspan="2"></td></tr>
<tr><td>400 ppm NH_3, 8% O_2, 5% H_2O; 100-500°C;
20 min + ramp;
Ramp: 10°C/min;</td></tr>
<tr><td>CO oxidation</td><td>C_3H_6</td><td>1% C_3H_6, 5% H_2O;
500°C, 40 min</td></tr>
<tr><td rowspan="2">400 ppm CO, 8% O2, 5% H2O; 100-500°C;
20 min + ramp;
Ramp: 10°C/min</td><td>C_3H_6+O_2</td><td>300 ppm C_3H_6, 8% O_2, 5% H_2O;
500°C, 40 min</td></tr>
<tr><td>Degreening</td><td>400 ppm NO; 8% O2; 5% H2O; 500°C; 30 min</td></tr>
<tr><td></td><td>Evaporation</td><td>8%O2, 5% H_2O; T(°C), %O2 and duration (h) varied according to trial; Ramp: 20°C/min</td></tr>
</table>

In Figure 8, a representation of the evaporation trials protocol, with the steps presented in Table 7, is shown. All evaporation trials followed this protocol. In "Results and Discussion", the pre-treatment type used for each experiment is specified.

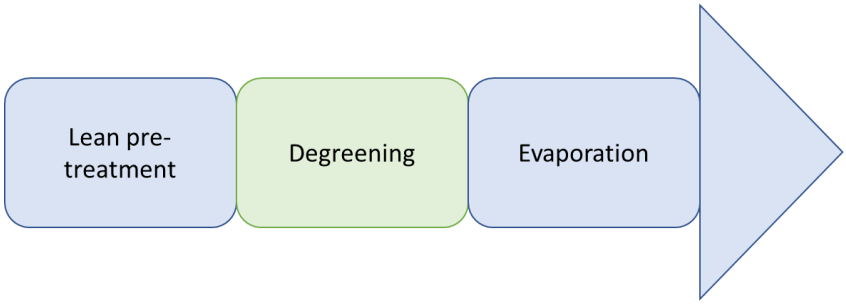

Figure 8 Evaporation trials protocol.

In Figure 9 and Figure 10, the oxidation trials protocols are presented schematically. Some "contaminated" capturing monolith samples were submitted to "One NH_3 oxidation" (protocol presented in Figure 9), but most of them were submitted to "Two NH_3 oxidations" (protocol presented in Figure 10). The oxidation trial protocol to which the sample in discussion was submitted to is specified in "Results and Discussion".

Independently of the protocol, the gas concentrations were measured by FTIR during all oxidation steps.

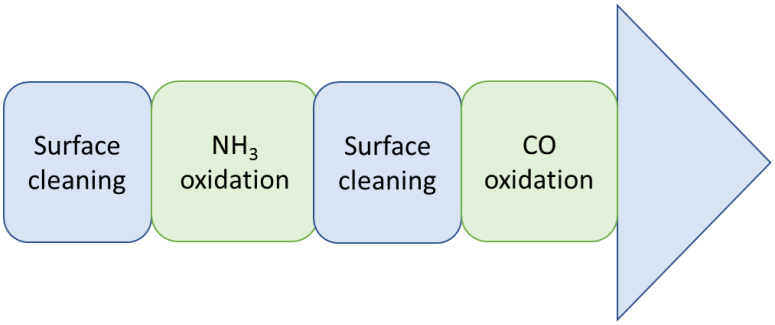

Figure 9 Oxidation trials protocol – "One NH_3 oxidation".

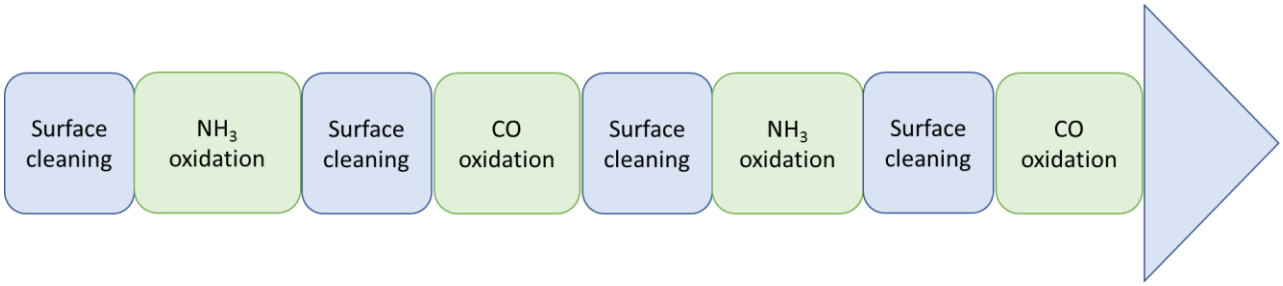

Figure 10 Oxidation trials protocol "Two NH_3 oxidations".

3.1.3 Physical characterization techniques

The low amount of Pt that migrates from the DOC and is captured by the capturing monolith limits the techniques that can be used for physical characterization of the samples.

The applicability of SEM/EDX analysis was tested on one "contaminated" capturing monolith, but the technique did not detect the Pt levels present in that sample, so no other capturing monoliths were submitted to this characterization technique. Further details are presented in Section 4.1.7.

ICP-MS, on the other hand, was able to detect the Pt levels in the "contaminated" capturing monoliths. The samples were prepared to be sent for ICP-MS analysis in two different ways. Some of the monoliths were cut transversally in three sections, being "front" (the side facing the DOC during evaporation trial) and "back" sent for analysis. The middle section was stored. This configuration allowed for studying the differences in Pt deposition in the axial direction, as had previously been observed in other studies of Pt migration from DOC, discussed in Section 2.2.

To be able to develop the kinetic model, information about the total amount of Pt in the "contaminated" capturing monolith was necessary. Thus, the capturing monoliths employed in experiments used for the development of the kinetic model were cut in the longitudinal direction, being one-half sent to ICP-MS and the other one stored for possible future use.

Figure 11 illustrates the longitudinal and transversal cuts performed on the monoliths.

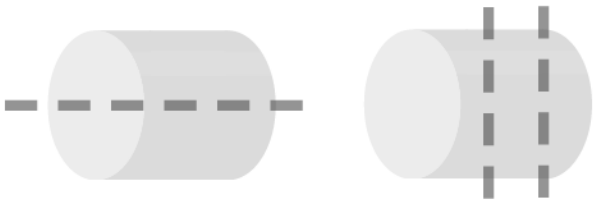

Figure 11 Representation of the longitudinal and transversal cuts performed on the monoliths during preparation for ICP-MS analysis.

3.2 Kinetic modelling

The model of the simplified kinetics of Pt evaporation was developed according to:

$$Pt(s) + O_2 \leftrightarrow PtO_2(g) \tag{42}$$

Bartlett (1967) developed a metal recession rate based on the same reaction as presented in Equation 42. Jehn (1984) also used an equivalent global reaction expression for oxidation of PGM to develop a general rate of oxidation (refer to Section 2.4 for more details). These authors investigated Pt evaporation from metal ribbons and surfaces in furnaces. No studies on kinetic modelling of Pt evaporation from DOC were found to the date when this work was written.

A general reaction rate expression was proposed as:

$$\dot{r} = k_1 Z_{Pt} {y_{O2}}^{\alpha} - k_2 y_{PtO2} \tag{43}$$

Where $\dot{r}$ = rate of Pt evaporation (kmol/m²s); k_1 = reaction constant, forward reaction (kmol/m²s); Z_{Pt} = Pt loading ratio; y_{O2} = mole fraction of O_2 in the gas phase; k_2 = reaction constant, backward reaction (kmol/m²s); y_{PtO2} = mole fraction of PtO_2 in the gas phase; α = reaction order with respect to O_2.

To account for the effects of temperature, an Arrhenius type equation was used for the reaction constants, leading to the following expression:

$$\dot{r} = \left(K_1 e^{-\frac{E_1}{RT}}\right) Z_{Pt} {y_{O2}}^{\alpha} - \left(K_2 e^{-\frac{E_2}{RT}}\right) y_{PtO2} \quad (44)$$

Where K_1, K_2 = pre-exponential factors (kmol/m²s); E_1, E_2 = activation energies (J/mol); R = gas constant = 8.314 J/molK.

Equation 44 was implemented on the commercial software AVL BOOST. Through BOOST, the parameters K_1, K_2, E_1, E_2 and α were varied, and the amount of PtO_2 produced was evaluated and compared to experimental data.

The simulations on BOOST were made using a catalytic converter model, as presented in Figure 12, which consisted of two "Aftertreatment Boundary Conditions", being one the conditions at the inlet and the other, at the outlet, and a "Catalyst".

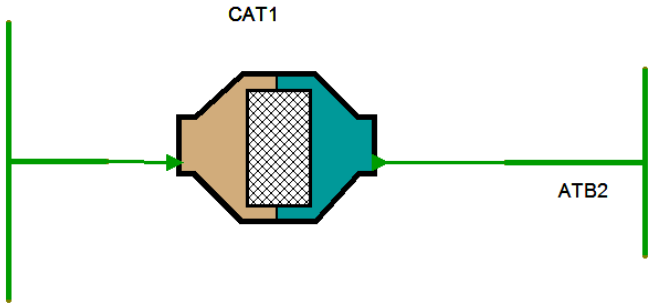

Figure 12 Catalytic converter model from AVL BOOST.

At the inlet, the following specifications were made:

- Volume flow: 1200 mL/min
- Temperature of the solid phase (°C)
- Mole fraction of inlet species

The temperature was specified via external input files extracted from the MFC data-files, computed during the evaporation experiments. The MFC data was collected at every second, so the temperature input file to BOOST consisted of a table of temperature vs. time over the duration of the evaporation step of the experimental trials, which varied from 5-15h according to the trial. The input file was updated for each simulation case file. As heat balance was not solved, the temperature used in the input file was the temperature measured in the catalyst during the experiments.

The mole fractions were specified over the same time range as the temperature. The flow consisted of O_2 (2%mol, 5%mol or 8%mol), H_2O (5%mol) and Ar (as balance). These values were also updated for each simulation case file.

As no detailed information about the outlet conditions was available, adiabatic backflow conditions were selected on BOOST, which implies that no gradients in temperature and species were assumed. The outlet pressure was specified as atmospheric pressure, 101325 Pa.

When it comes to the catalyst unit, specifications regarding the geometry, fluid dynamics, thermodynamics and conversion reactions were made, which can be verified in the Appendix (A.3). The monolith volume was set to 0.2 dm³ and the length, to 2 cm to correspond to the experimental conditions. As the same type of catalyst and monolith were used in all experiments, these specifications were only made once and were valid for all simulation cases.

User defined reactions can be implemented on BOOST by using the AST User Coding Interface. The reaction rate defined in Equation 44 was implemented through this tool. Surface sites and the species that are involved in the reaction mechanism need to be defined. Details about the specifications made can be verified in the Appendix (A.3).

It was assumed that the washcoat surface sites were either Pt sites or empty sites. Initially, before evaporation effects occurred, all sites were assumed to be Pt sites. As Pt migrated from the surface, empty sites were created. To ensure mass conservation, BOOST recommends the empty site to be specified as an individual surface site species and, also, that it should be used in the reaction stoichiometry. "Z_void" was created for that purpose (Appendix A.3). The storage capacity of Pt, most commonly known as site density, was set as 1.7 x 10^{-5} mol/m² (Rankovic et al. 2010).

From the simulations, the cumulative mass flux of PtO_2(g), in kg, was obtained. This analysis result is automatically calculated by BOOST and corresponds to the integration of the species flux from the beginning of the simulation to the current time point, at the inlet or outlet. For this study, as further detailed, the end of the simulation and the outlet were of interest. Equation 45 describes the cumulative mass flux (CMF) of species I, calculated by BOOST as specified in FIRE BOOST Aftertreatment Users Guide: BOOST Aftertreatment Input Data (AVL 2013):

$$CMF_i = \int_{t0}^{tcurrent} w_i \rho_{gas} v_{gas} \tag{45}$$

The cumulative mass flux of PtO_2 at the outlet of the simulated system, at the end of simulation time, was used to evaluate how well the tested parameters adjusted to the experimental data.

Quantitative experimental data was available in the form of ICP-analysis data of the different capturing monoliths. This data corresponded to the amount of Pt captured by the capturing monolith over the duration of the evaporation trials.

For developing the kinetic model, it was assumed that all the Pt that evaporated from the DOC was captured in the capturing monolith. So, from the results of ICP that provided the amount of Pt in mg/kg sample, the number of mols of Pt in each capturing monolith was calculated. Based on that, the calculation of the equivalent mass of PtO_2 was done, which gave an entity that could be compared to the results obtained from BOOST. The routine done for obtaining the mass of PtO_2 from the ICP results is summarised below:

$$n_{Pt,i} = \frac{ICP_i \, m_{monolith,i}}{M_{Pt}} \tag{46}$$

Where $n_{Pt,i}$= number of mols of Pt; ICP_i = results from ICP of sample i (g/kg); $m_{monolith}$ = mass of the corresponding capturing monolith (kg); M_{Pt} = molar mass of Pt = 195.078 g/mol.

From Equation 46, assuming that all PtO_2 was deposited on the capturing monolith as Pt, $n_{Pt,i}$ = $n_{PtO2,i}$. So,

$$m_{PtO2,i} = n_{Pt,i} \, M_{PtO2} \tag{47}$$

Where $m_{PtO2,i}$= mass of PtO_2 that evaporated from the DOC; M_{PtO2} = molar mass of PtO_2 = 227.08 g/mol.

The strategy adopted to find the parameters that adjusted to the experimental data was to start with the simulations that corresponded to the experiments in which duration was varied,

temperature was kept at 700°C and O_2 concentration at 8%. Once a good fit was achieved, those parameters were used as starting point for the simulations fitting to the experiments in which temperature was varied, duration was kept at 15h and O_2 concentration at 8%. The process required a back and forth approach between the simulations with varying duration and varying temperature until an adequate fit to both was achieved with the same set of parameters. Those parameters were then used for simulations of experiments in which O_2 concentration was varied, temperature kept at 700°C and duration of 15h. The results obtained from the simulations were compared to the experimental ones.

4 Results and Discussion

In this section, the results achieved in this study are presented and discussed.

First, the experimental results are covered, being presented according to the effect on Pt migration that was investigated: temperature, duration, oxygen concentration and Pd doping. Besides those, separated sections were dedicated to other topics of interest to this work, i.e. investigation of the Commercial DOC provided by Cummins Inc., reproducibility of experiments.

Following the experimental results, the results and discussion related to the development of the kinetic model are presented.

4.1 Experimental part

The experiments were numbered according to Table 8 to ease the presentation and analysis of results. Important information relevant for understanding was also summarized for each experiment, such as temperature, O_2 concentration and type of lean pre-treatment used at the evaporation experiments, duration of those experiments, if surface cleaning with O_2 was performed prior to the oxidation experiments and number of NH_3 oxidations performed on the sample, since as presented in the Appendix (Section A.2), it was observed that this parameter affects the amount of NH_3 converted. Important to know is that, for all cases, NH_3 oxidation is followed by CO oxidation, as detailed in Section 3.1.2. So, if two NH_3 oxidations were performed, it implies that the sequence NH_3 oxidation – CO oxidation – NH_3 oxidation – CO oxidation was done.

The numbers were used to differ between evaporation experiments. Each pair Pt/Al_2O_3 – capturing monolith was only used once, that is, in one evaporation experiment.

If the capturing monolith sample was used in more than one NH_3 oxidation in total, "A" and "B" were used to designate the number of NH_3 oxidation experiments to which the sample had been exposed to at that point. "A" was used for one NH_3 oxidation and "B" for two. If no letter was used combined with the number, it implies that only one NH_3 oxidation, in total, was performed on the sample and therefore the results presented correspond to one NH_3 oxidation.

Details about the different pre-treatments and surface cleaning were presented in Section 3.1.2. Information about the washcoat content of capturing monoliths and Pt/Al_2O_3 samples are found in the Appendix (Section A.1).

Empty tube tests prior to the oxidation experiments were performed to ensure that no contamination that could lead to misleading oxidation results occurred. Also, an NH_3 oxidation experiment with a "non-contaminated" capturing monolith that was not subjected to DOC evaporation was performed to ensure that NH_3 and CO oxidation could indeed be attributed to Pt contamination. The result of this test is presented in the Appendix (Section A.2).

Table 8 Summary of the experiments with model Pt/Al2O3

Exp. #	T (°C)	%O_2	t (h)	# of NH_3 oxidation	Lean pre-treatment type	Surface cleaning	Capturing monolith sample	Pt/Al_2O_3 sample
1A	700	8	15	1	H_2	No	C2	P2
1B	700	8	15	2	H_2	Yes		
2A	775	8	15	1	H_2	No	C3	P4
2B	775	8	15	2	H_2	Yes		
3A	850	8	15	1	H_2	No	C1	P1
3B	850	8	15	2	H_2	Yes		
4	850	8	15	1	H_2	Yes	C4	P5
5	550	8	15	1	C_3H_6	Yes	C5	P3
6	625	8	15	1	C_3H_6	Yes	C9	P9
7	700	8	15	1	C_3H_6	Yes	C8	P8
8	775	8	15	1	C_3H_6	Yes	C7	P7
9	850	8	15	1	C_3H_6	Yes	C6	P6
10A	550	8	15	1	$C_3H_6 + O_2$	Yes	C14	P13
10B	550	8	15	2	$C_3H_6 + O_2$	Yes		
11A	700	8	15	1	$C_3H_6 + O_2$	Yes	C18	P17
11B	700	8	15	2	$C_3H_6 + O_2$	Yes		
12A	850	8	15	1	$C_3H_6 + O_2$	Yes	C15	P14
12B	850	8	15	2	$C_3H_6 + O_2$	Yes		
13A	700	8	5	1	$C_3H_6 + O_2$	Yes	C10	P10
13B	700	8	5	2	$C_3H_6 + O_2$	Yes		
14A	700	8	10	1	$C_3H_6 + O_2$	Yes	C11	P11
14B	700	8	10	2	$C_3H_6 + O_2$	Yes		
15A	700	2	15	1	$C_3H_6 + O_2$	Yes	C16	P15
15B	700	2	15	2	$C_3H_6 + O_2$	Yes		
16A	700	5	15	1	$C_3H_6 + O_2$	Yes	C17	P16
16B	700	5	15	2	$C_3H_6 + O_2$	Yes		
17A	700	8	15	1	$C_3H_6 + O_2$	Yes	C13	P12
17B	700	8	15	2	$C_3H_6 + O_2$	Yes		

The reactor system used for the experiments was available according to a booking system, in which a limited amount of time could be used on each booking. The oxidation experiments corresponding to the evaporating trials performed at a specific booking were always carried

out during the same booking period to reduce variability due to uncontrollable experimental factors among the different bookings. The experiments carried out at each booking were:

- Booking 1: Experiments 1-4;
- Booking 2: Experiments 5-9;
- Booking 3: Experiments 10-12, 15 and 16;
- Booking 4: Experiments 13-14 and 17.

4.1.1 Effect of temperature

4.1.1.1 Flow reactor experiments

In total, the effect of seven evaporation temperatures was investigated: 550°C, 625°C, 700°C, 775°C, 850°C. This interval was defined based on the literature that states that when active regeneration of the DPF occurs, the DOC can be exposed to temperatures of up to 850°C (Cavataio et al., 2009). Elemental carbon that is deposited on the DPF is oxidised at 600°C (Khair 2003). So, at least a temperature as high as 600°C is required at the DPF when active regeneration is performed, which implies the DOC can be exposed to even higher temperatures. It was of interest though to investigate at which levels Pt migration became significant, and therefore slightly lower temperature values were also explored.

All evaporation experiments aiming to study the effect of temperature in Pt migration had a duration of 15h and were carried out with an oxygen concentration of 8%, in the presence of 5% water vapour.

Experiments 1-4, performed with H_2 pre-treatment, explored the 700-850°C temperature range. Those experiments were done at the beginning of this work and can be seen as an initial screening regarding the interval of temperatures that were to be investigated. The absence of surface cleaning prior to oxidation (Experiments 1A, 2A, and 3A) was due to an error in procedure but led to the possibility of observation of the effect of this step, as presented in the Appendix (Section A.2).

In Table 9, the reactor and DOC temperatures, as well as the observed capturing monolith temperatures, are presented for each experiment.

Table 9 Temperature values for the DOC, capturing monolith and reactor (Experiments 1-4).

	Temperature (°C)		
Experiment	Reactor	Capturing monolith	DOC
1	700	323	700
2	775	350	777
3	850	317	853
4	850	346	859

The behaviour of NH_3 oxidation as a function of temperature for samples exposed to evaporation at 850°C and 775°C are presented in Figure 13. Experiment 1B was omitted due to unreasonable behaviour. “MFC” represents the amount of NH_3 injected into the system, equivalent to 400 ppm.

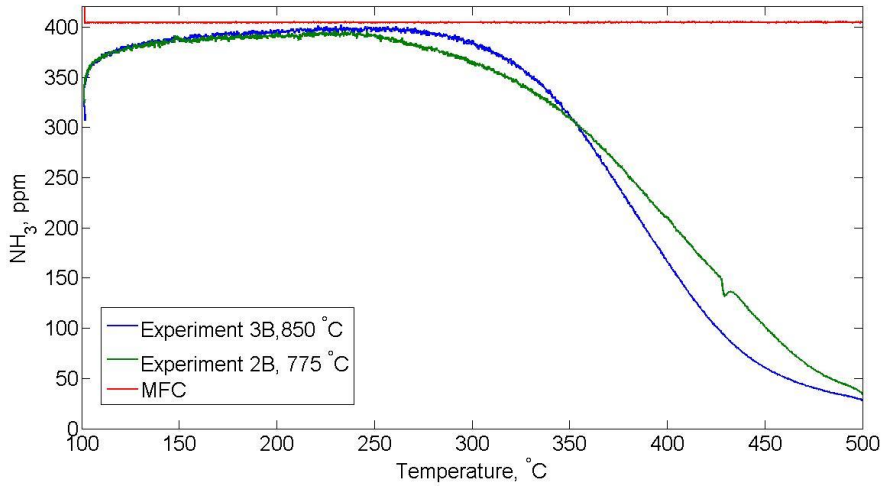

Figure 13 Effect of evaporation temperature on NH_3 oxidation; pre-treatment: H_2; # of NH_3 oxidations: 2 (refer to Table 8 for further details).

As temperature increases, signs of NH_3 oxidation start to be observed. It is known that above around 200°C, NH_3 oxidation starts to prevail in SCR systems over Pt catalysts (Bartholomew & Farrauto 2010). From Figure 13, deflections in the curve towards NH_3 consumption are noticed at about 250°C for both experiments, indicating the presence of Pt.

Experiment 3B (850°C) and Experiment 2B (775°C) exhibit similar levels of NH_3 consumption, being difficult to state if there was a difference in consumption visually.

Integration of the NH_3 consumption over time during the temperature ramp was performed for all experiments discussed in this thesis work to obtain the total amount of NH_3 consumed, in mols. It was chosen to perform the integration during the time corresponding to the temperature range 200°C-480°C to avoid numerical errors experienced when NH_3 consumption was zero and to ensure that integration was done over exactly the same temperature range for all experiments. The results of the integration performed for Experiments 2B and 3B are presented in Table 10.

Table 10 NH_3 consumption from the integration of NH_3 concentration vs. time (200°C-480°C, Experiments 2B and 3B).

Experiment	Evaporation Temp. (°C)	NH_3 consumption ($x10^{-4}$ mols)
2B	775	1.7
3B	850	1.9

The difference in NH_3 consumption was low, but as observed in other studies, the Pt contamination level by Pt migration is very low, in the order of 10^{-4} wt% (Jen et al. 2008; Chen et al. 2013). With that in mind, it is not that surprising that such subtle differences were observed.

In Figure 14, the behaviour of CO oxidation as a function of temperature is presented. "MFC" represents the amount of CO injected into the system, equivalent to 400 ppm.

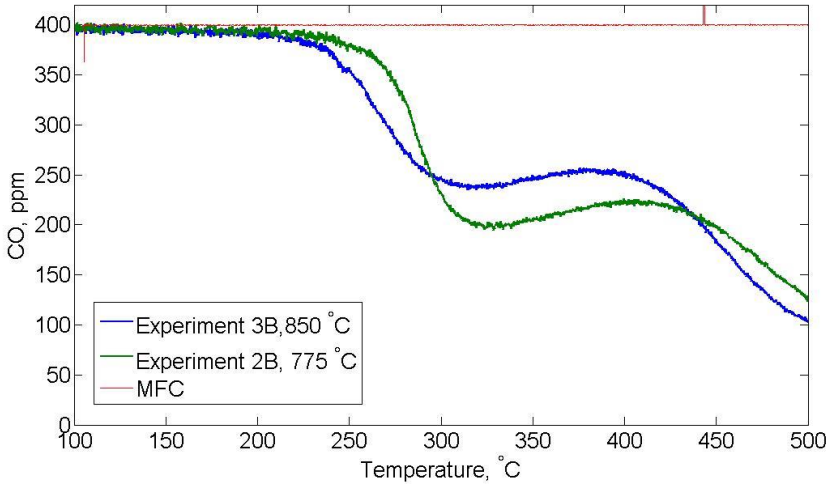

Figure 14 Effect of evaporation temperature on CO oxidation; pre-treatment: H_2; # of NH_3 oxidations: 2 (refer to Table 8 for further details).

The extent of CO oxidation of Experiments 2B and 3B is observed to be similar, as well as the non-monotonous behaviour with the curve going through both a minimum and a maximum. This behaviour was only observed in Experiments 1-3, though so it is likely that some unknown experimental factor affected these specific experiments.

As with NH_3, integration of CO consumption over time during the duration of the temperature ramp was performed for all experiments to obtain the total amount of CO consumed, in mols. For the same reasons exposed there, it was chosen to perform the integration during the time corresponding to the temperature range 150°C-475°C. The results for Experiments 2B and 3B are presented in Table 11. The results reveal practically the same CO consumption for both samples.

Table 11 CO consumption from the integration of CO concentration vs. time (150°C-475°C, Experiments 2B and 3B).

Experiment	Evaporation Temp. (°C)	CO consumption ($x10^{-4}$ mol)
2B	775	1.9
3B	850	2.0

Experiments 5-9 were carried out with C_3H_6 as reducing agent in the lean pre-treatment step since DOCs used in real applications are not exposed to H_2; HCs, on the other hand, are present in the exhaust system.

Despite Experiment 1B being omitted due to unreasonable behaviour and Experiment 1A being performed without surface cleaning, both showed that Pt evaporation is still very significant at 700°C, which motivated the expansion of the investigated evaporation temperature range to 550°C-850°C.

In Table 12, the reactor and DOC temperatures, as well as the observed capturing monolith temperatures, are presented for each experiment.

Table 12 Temperature values for the DOC, capturing monolith and reactor (Experiments 5-9).

	Temperature (°C)		
Experiment	Reactor	Capturing monolith	DOC
5	550	297	562
6	625	277	636
7	700	309	707
8	775	298	782
9	850	325	855

The results obtained for NH_3 oxidation are presented in Figure 15.

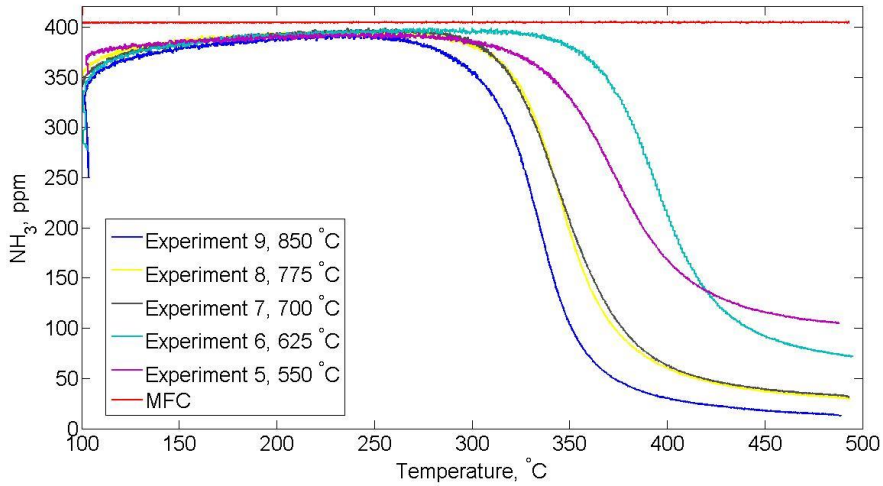

Figure 15 Effect of evaporation temperature on NH_3 oxidation; pre-treatment:C_3H_6; # of NH_3 oxidations: 1 (refer to Table 8 for further details).

From Figure 15, it is observed that two groups of curves were formed when it comes to the temperature in which the signs of NH_3 oxidation start to become evident. "Group 1", comprising Experiments 7, 8 and 9 exhibits the first signs of NH_3 oxidation at about 300-320°C. For "Group 2" (Experiments 5 and 6), this occurs at about 350-370°C. No clear correlation regarding experiments conditions i.e. temperature of the capturing monoliths, loading of catalyst, etc. were found to explain the "grouping" of these experiments.

One possibility is that Pt was deposited in different forms over the capturing monolith surface. It has been reported in the literature (Chaston 1964), in studies of Pt evaporation on furnaces, that when the gas flow carrying Pt comes in contact with a much cooler surface, shock-cooling is observed, resulting in deposits of PtO_2. On the other hand, if it occurs gradually, by diffusion, Pt as a metal is deposited. The temperature gradient between DOC and capturing monolith in "Group 1" is somewhat higher than of that in "Group 2", which could be an indicative of Pt depositing in different forms, leading to different NH_3 oxidation behaviour. However, differences in temperature observed in furnaces are much higher than those in the experiments carried out in this work so it is uncertain that this phenomenon would occur. No investigation of the form in which Pt is present on the capturing monolith surface was carried out and is kept as a suggestion for future studies. However, a challenging aspect is the ultra-low amounts of Pt, which limits the characterization techniques available.

"Group 1", if compared to "Group 2", resulted in higher levels of NH_3 oxidation, as expected due to the higher evaporation temperature range to which the capturing monoliths had been exposed to, indicating that higher levels of Pt migrated from the DOC surface. Experiment 9, which corresponded to the highest tested temperature, clearly had a higher level of NH_3 oxidation, indicating the presence of higher amounts of Pt, as expected. Experiments 7 and 8 exhibited practically equal behaviour, though.

Among the curves in "Group 2", Experiment 5 apparently had a higher NH_3 consumption than Experiment 6, going against the expected. As exposed in Section 3.1.1, the model DOC P6-P9, used in Experiments 5, 7, 8 and 9, were mistakenly prepared with Sasol Puralox Nga150 as a "binder" instead of Disperal P2. Experiment 6 was performed with DOC P3, which was prepared with Disperal P2, which might have caused the observed difference in behaviour for that particular curve.

Integration of the NH_3 consumption over time during the interval of the temperature ramp was performed, being the results presented in Table 13.

Table 13 NH_3 consumption from the integration of NH_3 concentration vs. time (200°C-480°C, Experiments 5-9).

Experiment	Evaporation Temp. (°C)	NH_3 consumption ($x10^{-4}$ mol)
5	550	1.7
6	625	1.5
7	700	2.5
8	775	2.5
9	850	2.9

From Table 13, the distinction made as "Group 1" and "Group 2" is supported; samples exposed to higher evaporation temperatures (Experiments 7-9) resulted in bigger consumption of NH_3 than those exposed to lower temperatures (Experiments 5-6), indicating the presence of higher amounts of Pt.

Jen et al. 2008 observed a similar trend in laboratory duplication of Pt contamination experiments. The temperatures tested were 670, 750 and 850°C and NOx conversion at 850°C was the most affected, resulting even in NOx remake due to NH_3 oxidation to NOx.

For this set of experiments, the formation of NO, N_2O, and NO_2 was also investigated. The results are presented in Figure 16, Figure 17 and Figure 18, respectively.

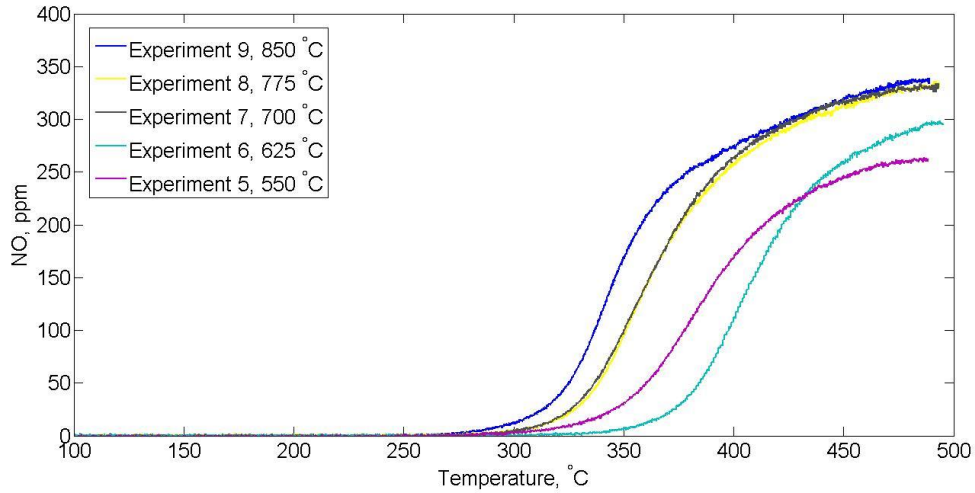

Figure 16 Effect of evaporation temperature on NO formation; pre-treatment:C_3H_6; # of NH_3 oxidations: 1 (refer to Table 8 for further details).

Figure 16 shows that NO starts to be formed at around the same temperature in which NH_3 oxidation was observed to begin, following the "Group 1" and "Group 2"- division, as expected. Remembering that the NH_3 fed into the system was at a concentration of 400 ppm, it is seen that high amounts of NO are formed, reaching values close to 350 ppm when oxidation of NH_3 was at its greatest levels, at high temperatures. NH_3 oxidation over PGM catalysts is known to give high selectivity towards NOx (Kamasamudram et al. 2011), which supports the observed behaviour.

At higher temperatures, the amount of NO formed by Experiments 7, 8 and 9 is practically the same. However, the amount of NH_3 oxidised in Experiment 9 is higher. Taking into consideration Figure 17, which shows the N_2O formation behaviour, this is understood. It is seen that Experiment 9 led to higher levels of production of N_2O when compared to the other experiments, reaching about 25 ppm at 400°C. So, the NO formation decreased to give place to the N_2O formation at high temperatures for Experiment 9.

Experiment 8 led to slightly higher levels of N_2O formation when compared to Experiment 7. This scenario is an indicative that exposure to higher evaporation temperatures leads to an increase in selectivity of NH_3 oxidation towards N_2O. Still, the amount of N_2O formed is very low, being less than 30 ppm for all cases.

Cavataio et al. (2009) observed the formation of N_2O in cases of Pt contamination of SCR samples. For FeSCR samples containing 0.001 %wt of Pt, up to 25 ppm of N_2O were generated. This seems reasonable with respect to the observations made in Figure 17.

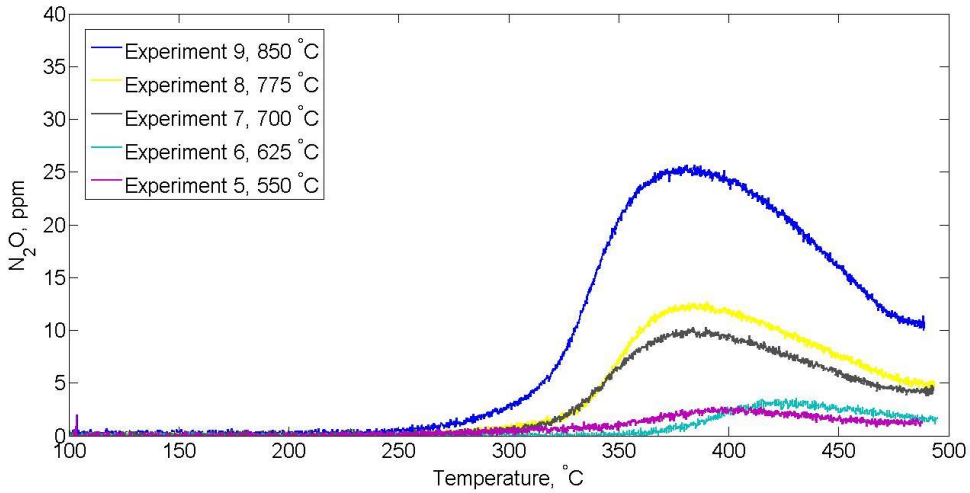

Figure 17 Effect of evaporation temperature on N_2O formation; pre-treatment:C_3H_6; # of NH_3 oxidations: 1 (refer to Table 8 for further details).

In Figure 18, the formation of NO_2 is presented. Experiment 9 resulted in the higher formation of NO_2 at high temperature, indicating that the observed NO "decrease" was also due to the NO_2 formation. In general, the amount of NO_2 formed is very low, being below 9 ppm for all cases.

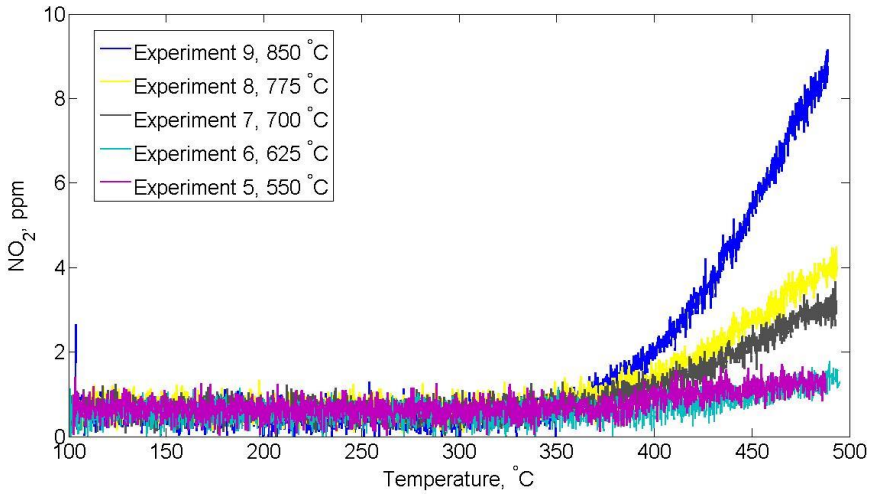

Figure 18 Effect of evaporation temperature on NO_2 formation; pre-treatment:C_3H_6; # of NH_3 oxidations: 1 (refer to Table 8 for further details).

The results for CO oxidation are presented in Figure 19. As for NH_3 oxidation, the same two groups of curves were observed. Experiment 9 presented a clearly higher CO consumption. Experiments 7 and 8 presented similar results, as observed for NH_3 oxidation. The relation between the curves in "Group 2" is unclear, but both had a lower CO consumption if compared to "Group 1", supporting the results of NH_3 oxidation.

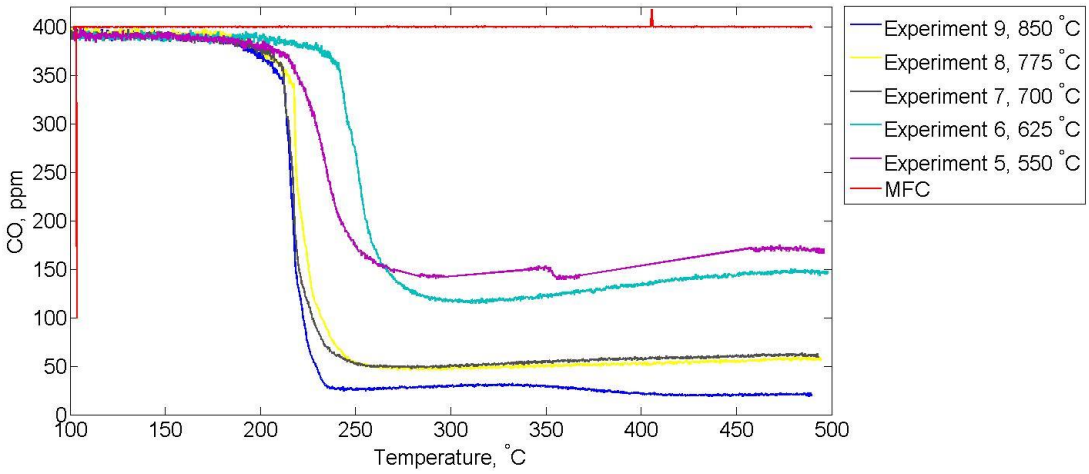

Figure 19 Effect of evaporation temperature on CO oxidation; pre-treatment:C_3H_6; # of NH_3 oxidations: 1 (refer to Table 8 for further details).

The results of the integration of CO consumption over time during the duration of the temperature ramp are presented in Table 14. Experiments 5 and 6 had practically the same consumption of CO, which was not expected due to the difference in temperature among these experiments but which confirms the observed in NH_3 oxidation. Looking into the extreme cases (550°C and 850°C) and the intermediate one (700°C), there is a clear trend of increasing oxidation with increasing temperature, indicating higher Pt evaporation.

Table 14 CO consumption from the integration of CO concentration vs. time (150°C-475°C, Experiments 5-9).

Experiment	Evaporation Temp. (°C)	CO consumption (x10^{-4} mol)
5	550	3.3
6	625	3.2
7	700	4.8
8	775	4.8
9	850	5.3

Experiments 10-12, pre-treated with C_3H_6+O_2, were performed at the temperatures 550°C, 700°C and 850°C since the differences observed for 625°C and 775°C experiments were not that high and did not lead to a significant trend.

Important to have in mind is that for this set of experiments, the amount of washcoat on the capturing monolith was increased from 20 mg to 80 mg, approximately, to see if that would affect the amount of Pt captured.

As Experiments 5-9 were submitted to only one NH_3 oxidation trial, and the pre-treatment conditions of this set of experiments were more similar to Experiments 10-12, if compared to Experiments 1-4, the results from Experiments 10A, 11A, and 12A, in which one NH_3 oxidation trial was performed, were chosen to be presented in this section. The results obtained for Experiments 10B, 11B and 12B are presented in the Appendix (Section A.2).

In Table 15, the reactor and DOC temperatures, as well as the observed capturing monolith temperatures, are presented for all the experiments.

Table 15 Temperature values for the DOC, capturing monolith and reactor (Experiments 10-12).

	Temperature (°C)		
Experiment	Reactor	Capturing monolith	DOC
10	550	233	536
11	700	301	683
12	850	368	833

In Figure 20, a very clear relation between increasing evaporation temperature and increasing NH_3 oxidation is observed. The rate of oxidation for Experiment 10A is very slow, being almost linear, differing considerably from the behaviour of the other curves and from Experiment 5 (Figure 15), where evaporation was also carried out at 550°C.

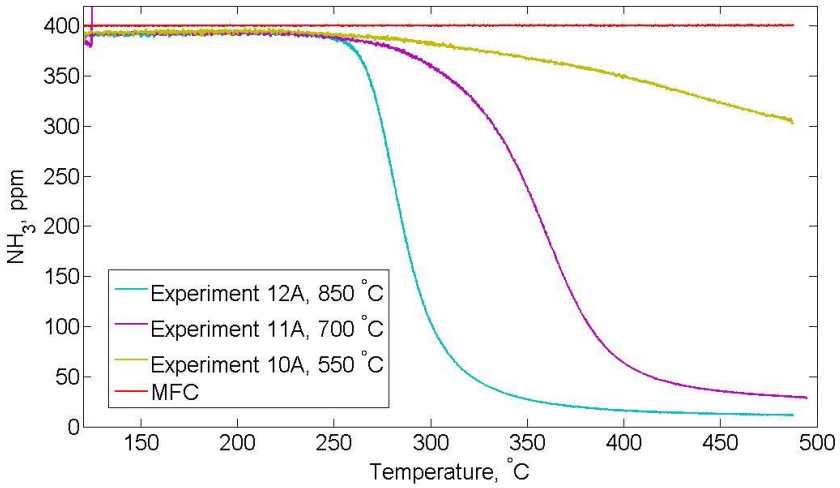

Figure 20 Effect of evaporation temperature on NH_3 formation; pre-treatment:C_3H_6+O_2; # of NH_3 oxidations: 1 (refer to Table 8 for further details).

Integration of NH_3 concentration over time during the interval of the temperature ramp for Experiments 10A-12A is presented in Table 16, confirming the trend observed in Figure 20 where increasing evaporation temperature leads to increasing NH_3 oxidation.

Table 16 NH_3 consumption from the integration of NH_3 concentration vs. time (200°C-480°C, Experiments 10A-12A).

Experiment	Evaporation Temp. (°C)	NH_3 consumption (x10^{-4} mol)
10A	550	0.4
11A	700	2.6
12A	850	3.1

As the order of magnitude of NH_3 consumption presented in Table 16, in which the capturing monoliths were washcoated with 80 mg Al_2O_3, is the same as for the remaining experiments previously discussed in this section, in which the Al_2O_3 washcoat amount was of 20 mg, it can be concluded that this factor did not act like a limiting one to Pt capturing.

Figure 21, Figure 22 and Figure 23 show the formation of NO, N_2O and NO_2 for this set of experiments, respectively.

High selectivity towards NO formation was once more observed. The behaviour seen in Figure 21 agrees with the one in Figure 20: Levels of NO formed followed the extent of NH_3 oxidation observed.

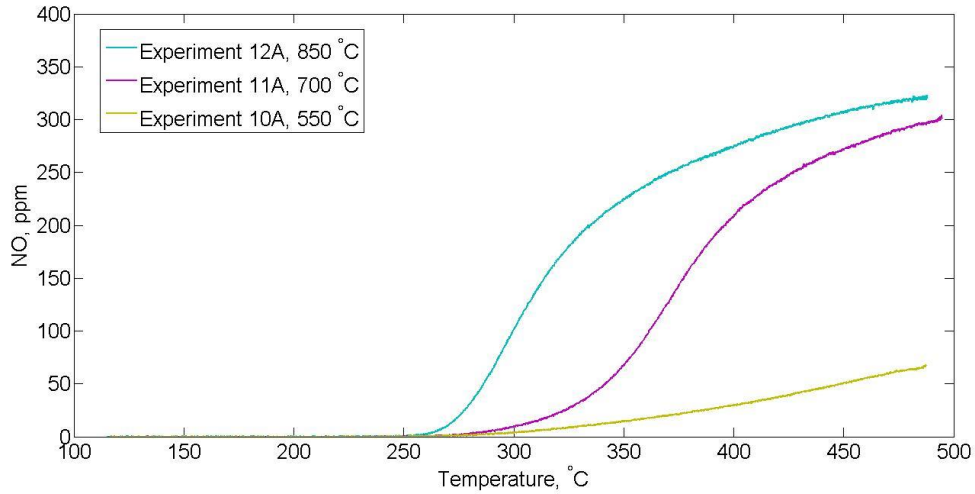

Figure 21 Effect of evaporation temperature on NO formation; pre-treatment:C_3H_6+O_2; # of NH_3 oxidations: 1 (refer to Table 8 for further details).

The amount of N_2O, as seen in Figure 22, is produced at low levels, reaching a maximum of about 37 ppm for the highest evaporation temperature. The behaviour is similar to the one observed and discussed for Experiments 5-9.

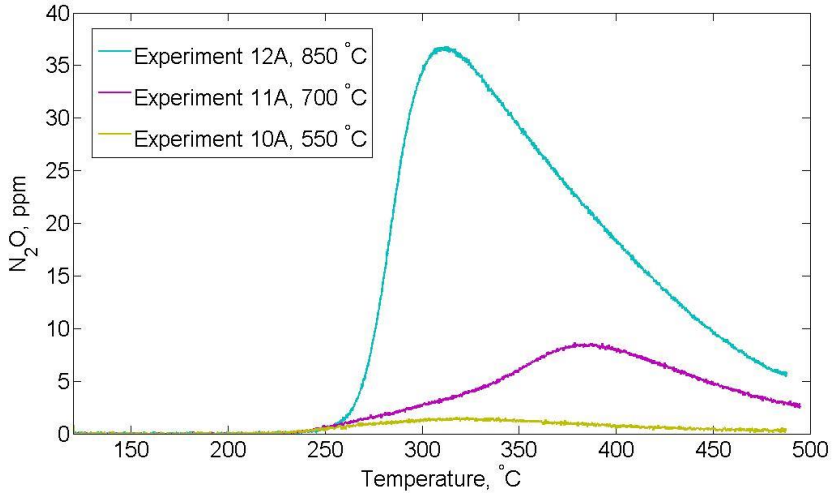

Figure 22 Effect of evaporation temperature on N_2O formation; pre-treatment:C_3H_6+O_2; # of NH_3 oxidations: 1 (refer to Table 8 for further details).

NO_2 formation, presented in Figure 23, also follows the same trend discussed for Experiments 5-9. Very low amounts of NO_2 are formed (under 10 ppm), and higher evaporation temperature resulted in a higher production of NO_2.

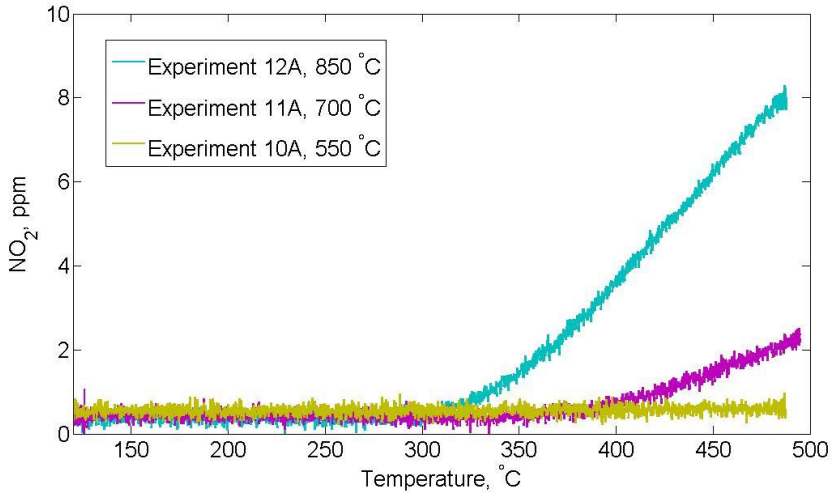

Figure 23 Effect of evaporation temperature on NO_2 formation; pre-treatment:C_3H_6+O_2; # of NH_3 oxidations: 1 (refer to Table 8 for further details).

The results for CO oxidation are presented in Figure 24. As for NH_3 oxidation, a clear distinction between the different samples could be made according to the evaporation temperature to which they were exposed.

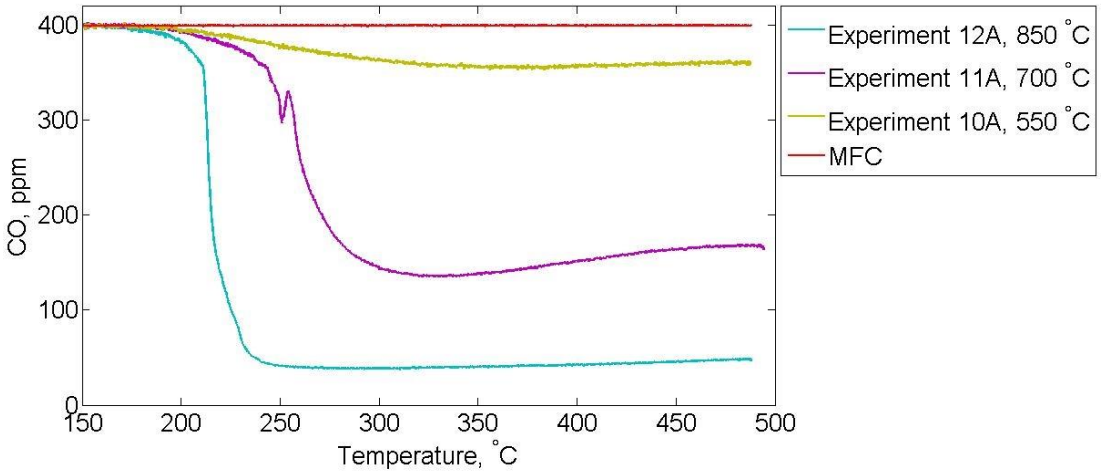

Figure 24 Effect of evaporation temperature on CO oxidation; pre-treatment:C_3H_6+O_2; # of NH_3 oxidations: 1 (refer to Table 8 for further details).

The results of integration of CO consumption over time during the duration of the temperature ramp are presented in Table 17.

Table 17 CO consumption from the integration of CO concentration vs. time (150°C-475°C, Experiments 10A-12A).

Experiment	Evaporation Temp. (°C)	CO consumption (x10^{-4} mol)
10A	550	0.5
11A	700	3.5
12A	850	5.3

4.1.1.2 ICP-MS analysis

ICP-MS analysis of samples C9 (Experiment 6, 625°C), C6 (Experiment 9, 850°C), C14 (Experiments 10, 550°C), C18 (Experiments 11, 700°C) and C15 (Experiments 12, 850°C) were performed to quantify the amount of Pt capture and investigate its distribution along the monolith.

C9 and C6 were divided into three sections in the transversal direction: front, middle and back. Front (side of the monolith facing the DOC during the evaporation experiments) and back (side of the monolith facing the reactor outlet) were sent for analysis. The results are presented in Table 18.

Table 18. ICP analysis results for monoliths C9 and C6.

	C9 - 625°C		C6 - 850°C	
	Front	Back	Front	Back
Pt (%wt)	1.3E-04±0.2E-04	5.0E-06±0.7E-04	1.4E-03±0.1E-03	7.4E-06±1.1E-06

From Table 18, three important factors can be observed. Firstly, there is a higher accumulation of Pt in the front part of the catalyst. This confirms the results obtained in other studies (Chen et al. 2013). Secondly, the amount of Pt that migrates from the DOC at 850°C is about one order of magnitude higher than the amount that migrates at 625°C, deposited in the front. Thirdly, the amount of Pt in the back parts is extremely low, which indicates that no significant amount of Pt is being carried out of the reactor.

In the study carried out by Chen et al. (2013) with SCR catalysts obtained from field-returned aftertreatment systems, Pt elemental analysis by ICP-MS was also performed. The results showed an amount of Pt of 4.2E-04 %wt on the front side of a sample treated for 2 hours at 600°C and for 6h at 700°C. The back side of the same sample presented values lower than 5.0E-05 %wt. The results presented in Table 18 showed values on the same order of magnitude for the front side of the capturing monolith submitted to the evaporation trial at 625°C.

Jen et al. (2008) also studied the effect of Pt migration on SCR catalysts. By using an estimation method based on ethylene hydrogenation, the amount of Pt found in the samples was between 5E-04 and 1E-03 %wt. The samples were aged in a diesel aftertreatment system, where the bed temperature of the DOC reached temperature values as high as 800°C during DPF regeneration cycles, and the SCR itself was submitted to temperatures ranging from 200 to 670°C several times. The amount obtained for the '850°C front' sample lies in the higher range of the Pt amounts detected by Jen et al. 2008, which seems reasonable since the temperature to which the DOC was exposed (850°C) was higher than the one tested by them.

The amount of Pt found in sample 850°C front supports the N_2O formation observations, in which a peak of approximately 25 ppm was observed (Figure 17). As previously mentioned in this section, Cavataio et al. (2009) observed a formation of up to 25 ppm N_2O for an SCR sample contaminated with 1E-03 wt% Pt, which matches the results for N_2O formation/Pt amount of this specific sample.

Monoliths C14, C15, and C18 were divided into two longitudinal sections, being one of those from each monolith sent to analysis. The results are presented in Table 19.

Table 19. ICP analysis results for monoliths C14, C15 and C18.

	C14 - 550°C	C18 - 700°C	C15 - 850°C
Pt (%wt)	1.2E-05±0.2E-05	6.6E-05±1.0E-05	2.08E-04±0.3E-04

The results from Table 19 show a clear increase in Pt content with increasing evaporation temperature, supporting the findings from NH_3 and CO oxidation experiments. A plot was made with those results, as seen in Figure 25.

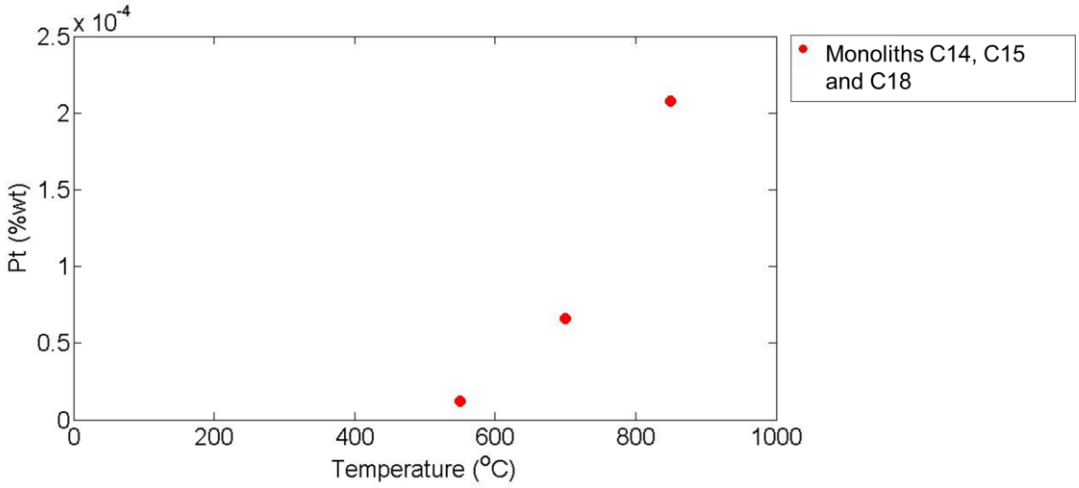

Figure 25 Pt content (%wt) vs. evaporation temperature.

Figure 25 goes in agreement with the observations made regarding the non-linear relation between increasing temperature and increasing evaporation rate of Pt from metal surfaces exposed to high temperatures (Jehn 1981; Fryburg & Petrus 1961).

Despite the experiment conditions when it comes to lean pre-treatment prior to evaporation being different among the here presented results, important conclusions could be drawn regarding the effect of temperature on Pt migration from model DOC samples.

A clear relation between increasing temperature and increasing amount of captured Pt was, in general, observed, implying higher Pt evaporation rates on the DOC as temperature increases. This behaviour was already observed in studies of Pt evaporation from metal surfaces at high temperatures (>1000°C) (Jehn 1981; Fryburg & Petrus 1961). Also, studies of SCR catalysts located downstream of DOCs had revealed that exposure to higher evaporation temperatures resulted in a higher loss in performance in NOx conversion, which was attributed to higher levels of contamination by PGM (Cavataio et al. 2009; Jen et al. 2008).

4.1.2 Effect of time

4.1.2.1 Flow reactor experiments

To study the effect of time on Pt migration, the investigation of three different evaporation durations was done: 5h, 10h, and 15h. The evaporation temperature was kept at 700°C and the oxygen concentration at 8% in all trials. Experiments 13 (5h), 14 (10h) and 17 (15h) correspond to those used for the investigation of this parameter. In Experiments 13B, 14B and 17B, two NH_3 oxidations were performed whereas, in Experiments 13A, 14A and 17A, one was done.

Experiments 14A and 17B experienced experimental adversities during execution and could not be used for analysis. Therefore, a simultaneous comparison of the NH_3 and CO oxidation effects over the three studied time durations under the same conditions regarding the number of NH_3 oxidations was not possible. Thus, they were analysed as pairs of experiments, being "Pair 1" Experiments 13B (5h, two NH_3 oxidations) and 14B (10h, two NH_3 oxidations) and "Pair 2" Experiments 13A (5h, one NH_3 oxidation) and 17A (15h, one NH_3 oxidation).

In Table 20, the reactor and DOC temperatures, as well as the observed capturing monolith temperatures, are presented.

Table 20 Temperature values for the DOC, capturing monolith and reactor (Experiments 13,14 and 17).

	Temperature (°C)		
Experiment	Reactor	Capturing monolith	DOC
13	700	388	695
14	700	360	686
17	700	384	695

The results for NH_3 oxidation for "Pair 1" and "Pair 2" are presented in Figure 26. From studies of Pt evaporation from metal surfaces at high temperatures, the rate of evaporation is expected to increase linearly with time (Jehn 1981; Fryburg & Petrus 1961). It is important to note though, that these results are for Pt metals not supported particles.

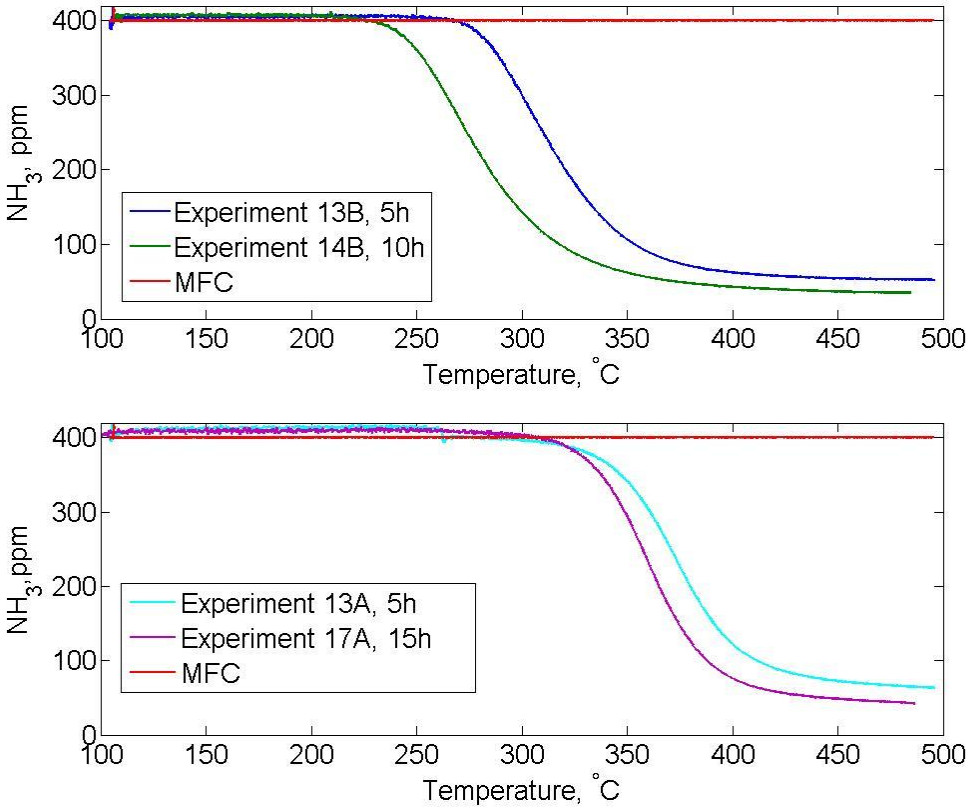

Figure 26 Effect of time duration on NH_3 consumption; pre-treatment:C_3H_6+O_2; # of NH_3 oxidations:13B and 14B=2, 13A and 17A=1 (refer to Table 8 for further details).

In both plots, it can be observed that samples submitted to evaporation under longer periods of time exhibited higher NH_3 conversion, indicating that higher amounts of Pt migrated from the DOC to the capturing monolith. The difference in consumption from Experiments 13B and 14B was somewhat higher than that between Experiments 13A and 17A.

Integration of NH_3 consumption over time for Experiments 13, 14B and 17A are presented in Table 21.

Table 21 NH_3 consumption from the integration of NH_3 concentration vs. time (200°C-480°C, Experiments 13, 14B and 17A).

	Experiment	Time duration (h)	NH_3 consumption ($x10^{-4}$ mol)
Pair 1	13B	5	3.1
	14B	10	4.1
Pair 2	13A	5	2.2
	17A	15	2.4

It can be seen that Experiment 14B (10h) had a higher NH_3 consumption than Experiment 13B (5h). Also, Experiment 17A (15h) had a slightly higher NH_3 consumption than Experiment 13A (5h), but the results were very close. The absolute values of NH_3 consumption of "Pair 1" and "Pair 2" cannot be compared due to a different number of NH_3 oxidations performed at the samples. However, unexpectedly, it is seen that for Pair 1, the difference in consumption of NH_3 is bigger than for Pair 2 even though the difference in duration is bigger for Pair 2. Pt migration is expected to increase linearly. However, with time the Pt particles will also sinter and large particles are more resistant to Pt oxide formation. This means that the large Pt particles also most likely have less evaporation. Ideally, these experiments should have been repeated. However, time constraints did not allow that.

Figure 27 exhibits the NO formation for all four experiments. NO was the main product of the NH_3 oxidation, as expected since selectivity towards this reaction is high when NH_3 oxidation is catalysed by PGM (Kamasamudram et al. 2011).

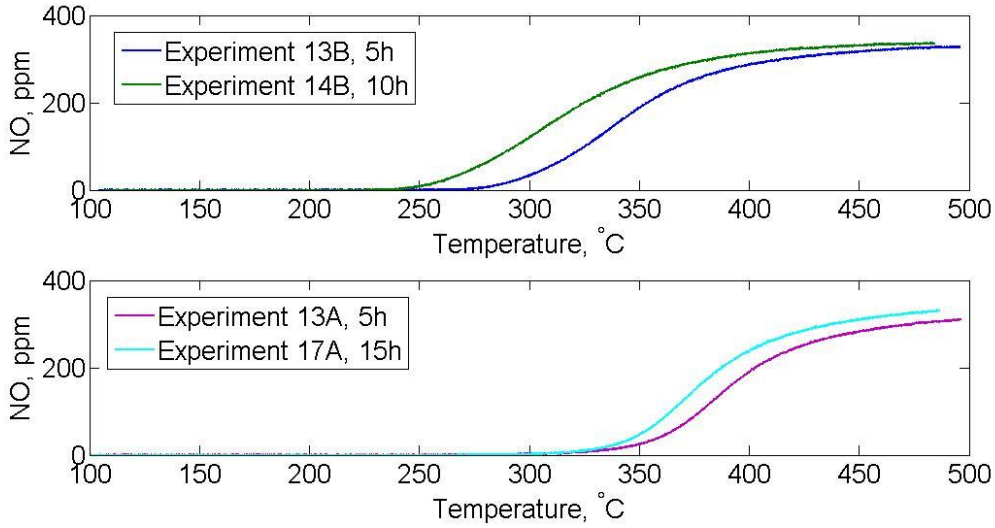

Figure 27 Effect of time duration on NO formation; pre-treatment:C_3H_6+O_2; # of NH_3 oxidations: Experiments 13B and 14B = 2, Experiments 13A and 17A=1 (refer to Table 8 for further details).

From Figure 28, it is observed that the levels of N_2O formation are below 20 ppm and that the experiments submitted to two NH_3 oxidations (13B and 14B) led to higher selectivity towards N_2O when compared to the experiments that were submitted to one NH_3 oxidation (13A and 17A). Also, N_2O reached its peak in formation at lower temperatures. These changes most likely indicate the presence of active species in different forms on the monoliths surfaces. As no "strange" elements were introduced into the system from one NH_3 oxidation to the other, the observed behaviour suggests that a restructuring of the active species on the surface occurred.

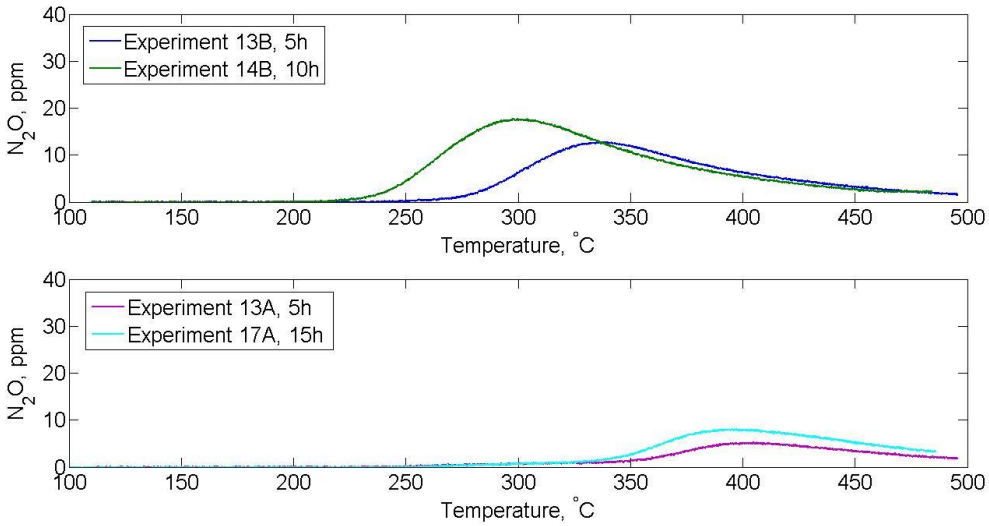

Figure 28 Effect of time duration on N_2O formation; pre-treatment:C_3H_6+O_2; # of NH_3 oxidations: Experiments 13B and 14B = 2, Experiments 13A and 17A=1 (refer to Table 8 for further details).

Formation of NO_2 was below 5 ppm for all experiments, and the results were therefore omitted in this section.

CO oxidation showed a very similar behaviour regardless the number of NH_3 oxidations to which the sample had been submitted, as can be verified on the Appendix (A.2) for the 5h duration cases (Figure 61). Therefore, Experiment 14B, 13A and 17A were combined into Figure 29 for observation of the effect of different evaporation durations on CO oxidation.

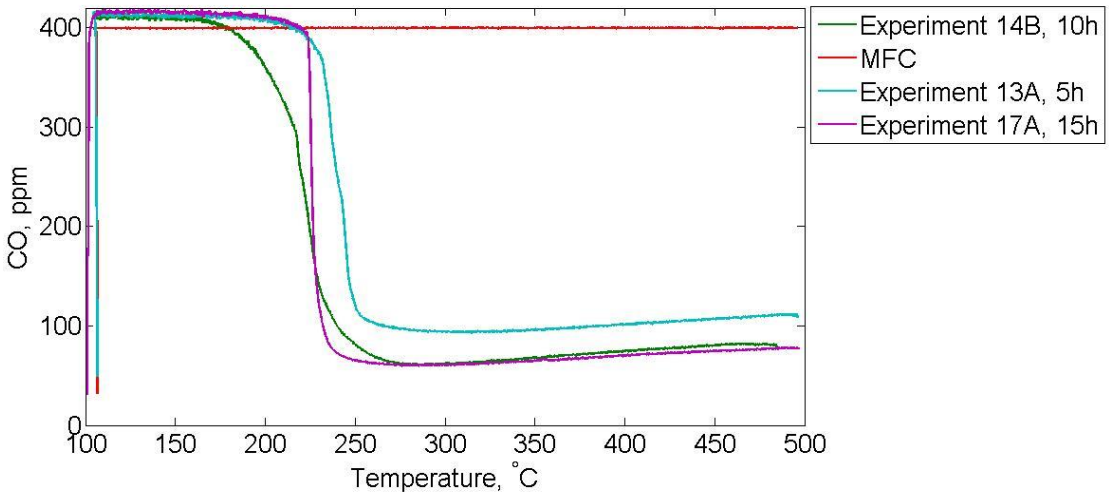

Figure 29 Effect of time duration on CO formation; pre-treatment:C_3H_6+O_2 (refer to Table 8 for further details).

It is clearly observed that evaporation duration of 15h (Experiment 17A) resulted in higher CO oxidation than the 5h case (Experiment 13A), indicating the presence of higher amounts of Pt and confirming the trend observed in NH_3 oxidation. Evaporation duration of 10h (Experiment 14B) also clearly resulted in higher CO oxidation levels when compared to 5h (Experiment 13A). However, the relation between Experiments 14B and 17A regarding consumption is not visually clear.

CO consumption was integrated over time, and the results are presented in Table 22. The visual trend was confirmed, and the CO consumption of Experiments 14B and 17A was close. However, Experiment 17A had a slightly lower consumption, which was unexpected.

Table 22 CO consumption from the integration of CO concentration vs. time (150°C-475°C, Experiments 13A, 14B and 17A).

Experiment	Time duration (h)	CO consumption ($x10^{-4}$ mol)
13A	5	4.0
14B	10	4.9
17A	15	4.6

In Figure 30, the results from Table 21 and Table 22 are presented in a graphical comparison against time to ease visualisation of the discussion carried out. The increase in NH_3 and CO consumption from 5 to 10h (Experiments 13B and 14B) is clearly noticed. However, practically no difference can be seen between Experiments 13A and 17A.

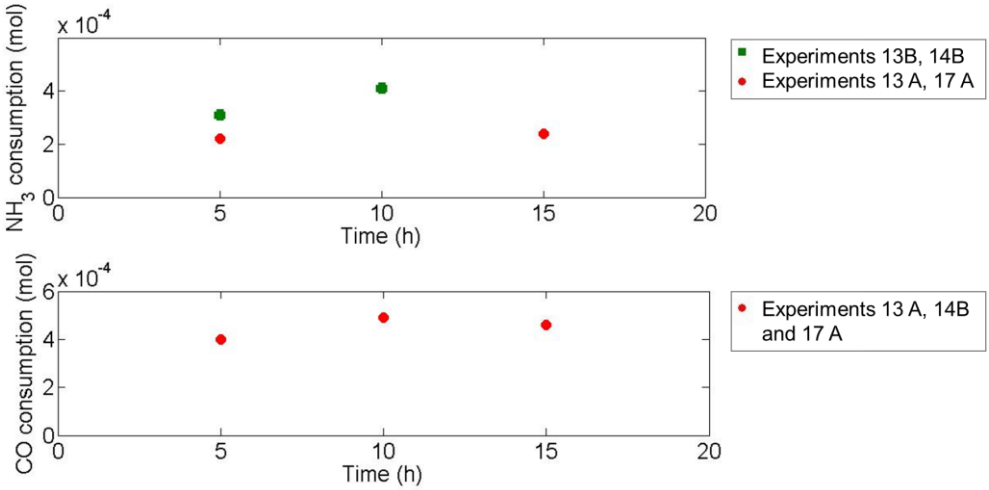

Figure 30 Comparison of NH_3 consumption and CO consumption (mols) and DOC evaporation durations (h); Experiments 13B and 14B: two NH_3 oxidations, Experiments 13A and 17A: one NH_3 oxidation.

4.1.2.2 ICP-MS analysis

The capturing monolith samples used in these experiments (C10, C11, and C13) were sent to ICP analysis to quantify the amount of Pt captured on one-half (longitudinal direction) of the monolith. The results are presented in Table 23.

Table 23. ICP analysis results for monoliths C10, C11, and C13.

	C10 – 5h	C11 - 10h	C13 - 15h
Pt (%wt)	7.3E-05±1.1E-05	7.2E-05±1.1E-05	7.9E-05±1.2E-05

The results from ICP-MS analysis showed very low differences between the amounts captured in the different samples if uncertainty is taken into consideration. We, therefore, propose that during high temperature, both sintering and evaporation occurs simultaneously, and when the Pt particles become larger, the evaporation rate decreases. This results in that the amount of Pt found for all three durations are similar.

4.1.3 Effect of oxygen concentration

4.1.3.1 Flow reactor experiments

In total, the effect of three different oxygen concentrations was investigated: 2%, 5% and 8%. All evaporation experiments aiming the study of this effect on Pt migration had a duration of 15h and were carried out at temperatures of 700°C, in the presence of water vapour. Experiments 11, 15 and 16 were used for this investigation.

Results from experiments 11B, 15B and 16B were obtained after two NH_3 oxidation trials whereas results from experiments 11A, 15A and 16A, after one NH_3 oxidation trial. The results from Experiment 15A showed some small irregularities in the NH_3 oxidation curve for approximately 5 minutes during the temperature ramp, most likely attributed to an instrument issue. Therefore, to obtain more accurate results in the NH_3 consumption calculation, the results from Experiments 11B (8% O_2), 16B (5% O_2) and 15B (2% O_2) are presented and discussed in this section.

In Table 24, the reactor and DOC temperatures, as well as the observed capturing monolith temperatures, are presented for each experiment.

Table 24 Temperature values for the DOC, capturing monolith and reactor (experiments 11, 15 and 16).

	Temperature (°C)		
Experiment	Reactor	Capturing monolith	DOC
11	700	301	683
15	700	279	693
16	700	301	693

In Figure 31, the behaviour of NH_3 oxidation as a function of oxidation temperature for samples submitted to evaporation at an O_2 concentration of 2%, 5% and 8% are presented. MFC represents the amount of NH_3 injected into the system, equivalent to 400 ppm.

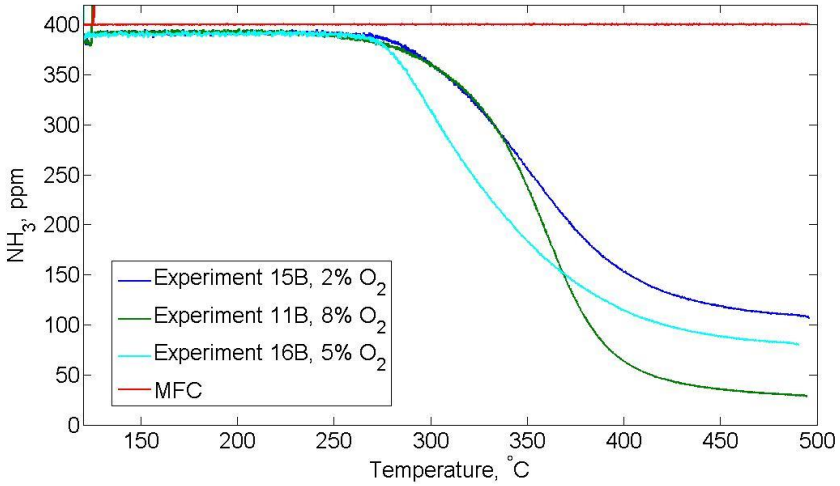

Figure 31 Effect of evaporation temperature on NH_3 oxidation; pre-treatment:C_3H_6+O_2; # of NH_3 oxidations: 2 (refer to Table 8 for further details).

It can be observed that there was an increase in NH_3 oxidation with increasing O_2 concentration, especially when comparing Experiments 11B and 16B with Experiment 15B, suggesting that a higher amount of Pt volatilized in an environment with a higher concentration of O_2. In studies of Pt evaporation from metal surfaces at high temperatures, it was found that the evaporation rate of Pt increased in a non-linear proportion with increasing O_2 partial pressure (Jehn 1981; Fryburg & Petrus 1961).

The integration of NH_3 concentrations over time for Experiments 11B, 15B and 16B are presented in Table 25. The observed trend is confirmed. However, the amount of NH_3 consumption of Experiment 11B is close to the one of Experiment 16B, suggesting that the change in concentration from 5% to 8% did not result in major changes in Pt evaporation.

Table 25 NH_3 consumption from integration of NH_3 concentration vs. time (200°C-480°C, Experiments 11B, 15B and 16B).

Experiment	O_2 concentration (%)	NH_3 consumption ($x10^{-4}$ mol)
11B	8	2.6
16B	5	2.4
15B	2	2.0

The formation of NO, N_2O and NO_2 from NH_3 oxidation were also studied. The amount of NO_2 produced was below 3 ppm for all experiments, and therefore the curves were omitted. Figure 32 and Figure 33 exhibits the behaviour of NO and N_2O formation as a function of oxidation temperature, respectively.

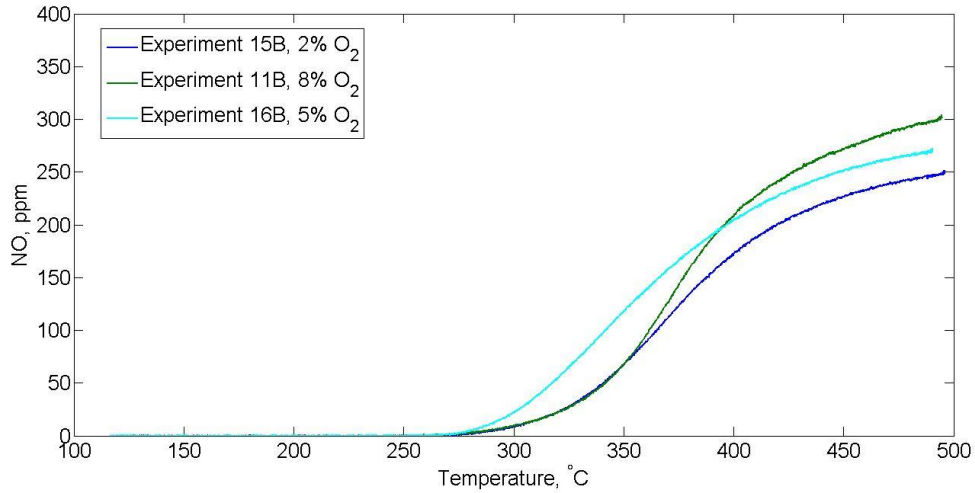

Figure 32 Effect of evaporation temperature on NO formation; pre-treatment:C_3H_6+O_2; # of NH_3 oxidations: 2 (refer to Table 8 for further details).

As expected from previous discussion, the main product obtained from NH_3 oxidation was NO. The behaviour of the curves follow the observations made in Figure 31. The amount of NO formed in Experiment 11B seems to be very similar to the one in Experiment 16B. From Figure 33, the amounts of N_2O produced by these two experiments are also very alike, which may be seen as an indicative that the amount of Pt in these samples are similar. For the lowest oxygen concentration investigated, both NO formation and N_2O formation are much lower, indicating lower amounts of Pt in the capturing monolith.

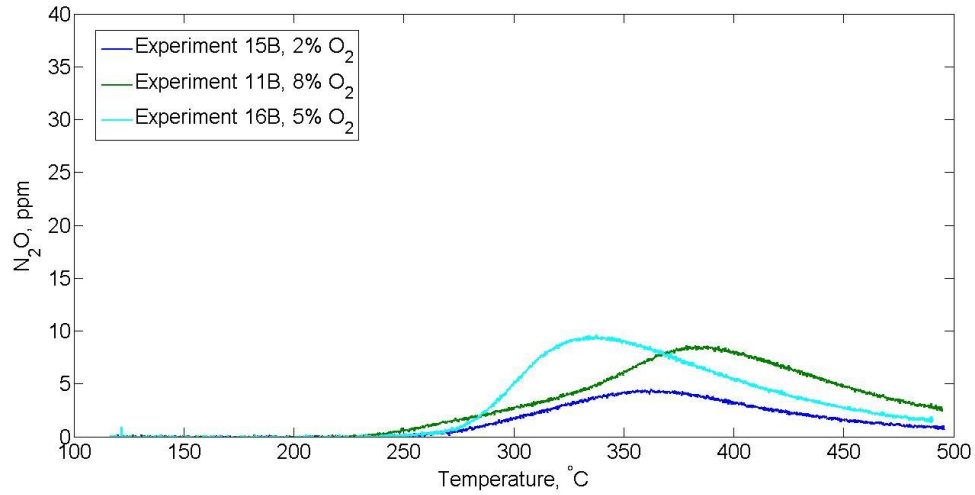

Figure 33 Effect of evaporation temperature on NO_2 formation; pre-treatment:C_3H_6+O_2; # of NH_3 oxidations: 2 (refer to Table 8 for further details).

CO oxidation was also investigated, being the results presented in Figure 34. Confirming the trend observed so far, Experiment 15B resulted in lower CO oxidation, whereas the results from Experiments 11B and 16B were quite similar.

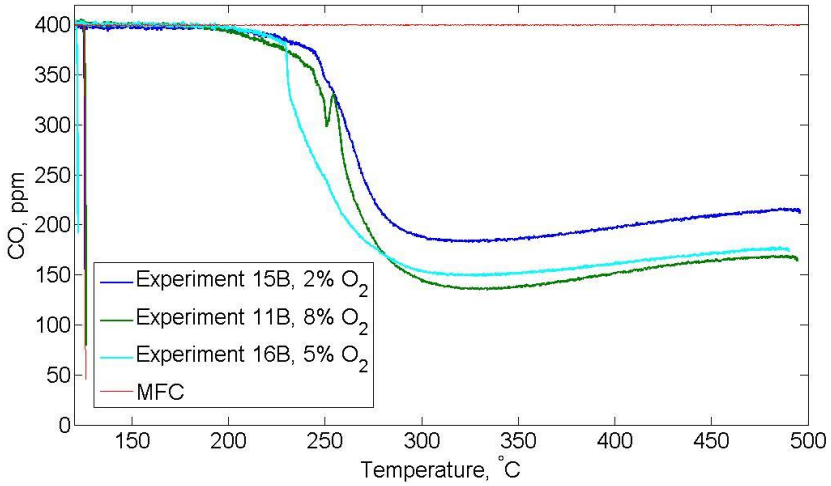

Figure 34 Effect of evaporation temperature on CO oxidation; pre-treatment:C_3H_6+O_2; # of NH_3 oxidations: 2 (refer to Table 8 for further details).

The integration of CO concentration over time during the interval of the oxidation temperature ramp is presented in Table 26. The amount of CO consumption of Experiments 11B and 16B were the same.

Table 26 CO consumption from the integration of CO concentration vs. time (150°C-475°C, Experiments 11B, 15B and 16B).

Experiment	O_2 concentration (%)	CO consumption (x10^{-4} mol)
11B	8	3.0
16B	5	3.0
15B	2	2.4

In Figure 35, a comparison between the amount of NH_3 and CO consumed according to oxygen concentration during the evaporation experiments are presented, respectively.

As observed in Table 25 and Table 26, there is an increasing trend from 2% O_2 to 5% O_2, but the results for 5% O_2 and 8% O_2 are practically the same for NH_3 consumption and actually the same for CO consumption.

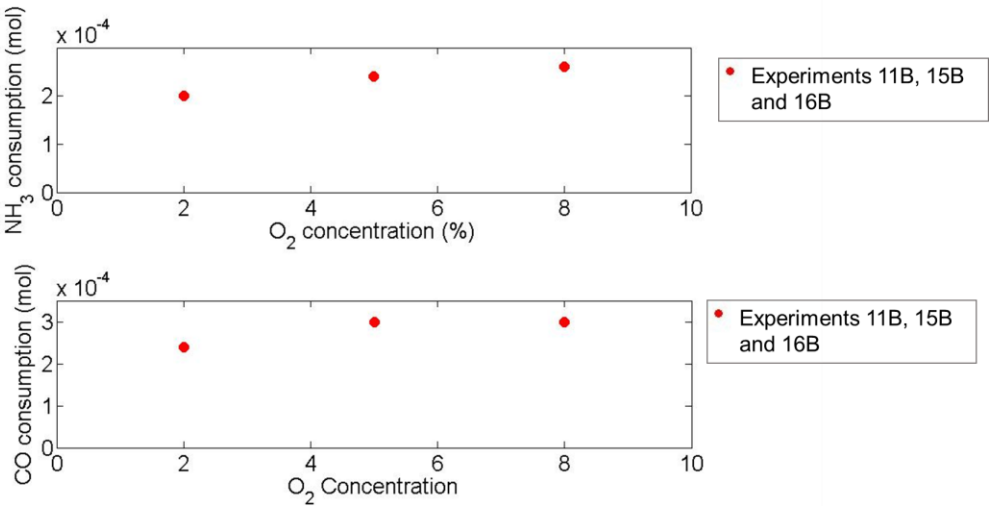

Figure 35 Comparison of NH_3 and CO consumption (mols) and O_2 concentration (%) during evaporation experiments for Experiments 11B, 15B and 16B.

4.1.3.2 ICP-MS Analysis

Despite the similar results obtained for both NH_3 and CO oxidation, ICP-MS analysis of the monoliths showed that the amount of Pt captured increased with increasing oxygen concentration, indicating higher evaporation rates at higher O_2 concentrations, as had been verified by Jehn et al. (1981) and Fryburg & Petrus (1961) in their studies. The results from ICP analysis are presented in Table 27. The samples sent for analysis corresponded to one longitudinal half of the capturing monolith.

Table 27. ICP analysis results for monoliths C16, C17 and C18.

	C16 - 2% O_2	C17 - 5% O_2	C18 - 8% O_2
Pt (%wt)	3.3E-05±0.5E-05	4.0E-05±0.6E-05	6.6E-05±1.0E-05

The results from ICP analysis were plotted in Figure 36. It can be seen that the trend goes in agreement with the observations made regarding the non-linear relation between increasing oxygen concentration and increasing evaporation rate for Pt metal surfaces exposed to high temperatures (Jehn 1981; Fryburg & Petrus 1961).

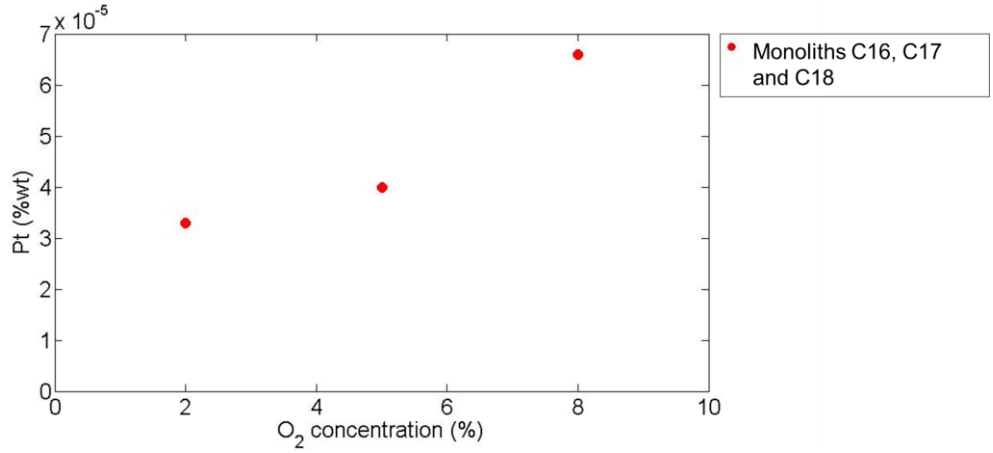

Figure 36 Pt content (%wt) vs. oxygen concentration.

The results obtained in this section indicate once more that NH_3 and CO oxidation experiments should be used as a guidance to trends but that they not precisely reflect the content of Pt in the sample, assuming that Pt deposits in similar manners on the transversal direction.

It has been reported in the literature and observed in this study (Section 4.1.1.2) that differences in the deposited amount of Pt exist on the longitudinal extension of the monolith, being higher quantities found at the side of the monolith facing the DOC. However, no discussion has been found about differences in the transversal extension of the monoliths, and there are no reasons to believe that a high difference would occur. Instead, we propose that it is possible that different Pt particle shapes are possible in the capturing monoliths, which could influence the activity.

4.1.4 Effect of Pd doping

4.1.4.1 Flow reactor experiments

Pd has a different reactivity towards oxygen when compared to Pt. It has been observed to oxidise into PdO at approximately 300-400°C and, unlike Pt, to be stable in air at atmospheric pressure until approximately 800°C (Gélin & Primet 2002). PtO_2 is formed already at room temperature, as detailed in Section 2.3. Chaston (1964) reported that when temperatures between 280°C-450°C are reached, PtO_2 dissociates into Pt and O_2. Grandadam in Beamish (1966) observed that PtO_2, under atmospheric pressure, decomposed into PtO at 380°C-400°C, that then decomposed into Pt at 560°C. Despite the differences when it comes to the dissociation temperature of PtO_2, it can be noticed that Pd is more stable than Pt in the presence of O_2.

Pd also has good activity towards HC oxidation. Cavataio et al. (2009) investigated the effect of different Pt/Pd ratios in the DOC and found that Pd had an effect of stabilising the Pt, reducing volatilization and contamination of the SCR.

Doping the model Pt/Al_2O_3 with Pd was tested to observe the effects on Pt volatilization.

The experiment had a duration of 15h and was carried out at 700°C, with 8%O_2 in the presence of water vapour. The temperature obtained in the capturing monolith during evaporation was 300°C. As with the model Pt/Al_2O_3, one and two NH_3 oxidations were performed. The first NH_3 oxidation is denoted A and the second, denoted B. The results were then compared to Experiments 11A and 11B (see Table 8), performed under the same conditions with model DOC.

In Figure 37, a comparison between NH_3 oxidation levels between capturing monoliths exposed to evaporation with Pd-doped DOC and model DOC, at the same experimental conditions, is presented.

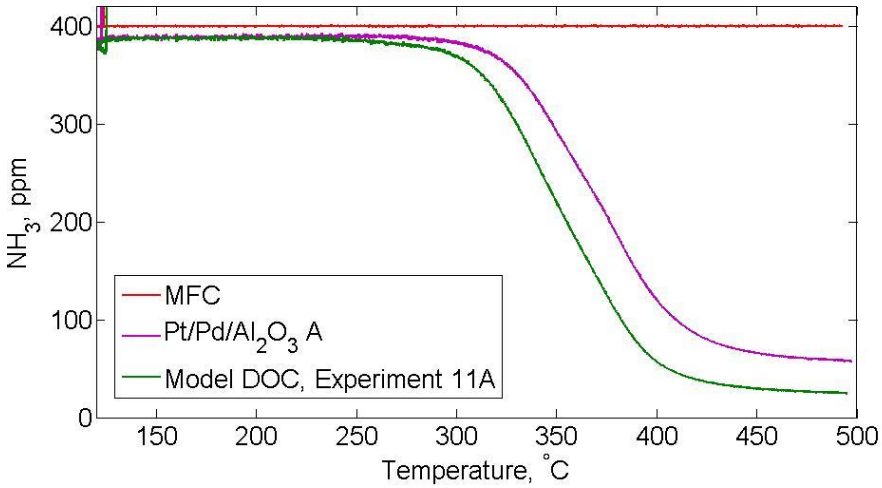

Figure 37 Effect of Pd doping on NH_3 oxidation; pre-treatment:C_3H_6+O_2; # of NH_3 oxidations: 1.

It is seen that the doped DOC has a lower NH_3 oxidation activity, supporting the findings of Cavataio et al. (2009) that Pd stabilises Pt, reducing Pt volatilization. Since the Pt content was kept the same and the experimental conditions of the experiments presented were the same, the difference in oxidation can be attributed to the effect of Pd.

The results obtained for two NH_3 oxidations showed a different behaviour though. As presented in Figure 38, the NH_3 oxidation activity was higher for the capturing monolith exposed to evaporation with the Pd-doped DOC. As seen in Figure 39, there were no major differences between the NH_3 oxidation levels for the capturing monoliths exposed to model DOC in Experiment 11 when "one NH_3 oxidation" and "two NH_3 oxidations" are compared, suggesting that the presence of Pd on the DOC catalysts had an effect on the redistribution of Pt on the capturing monolith surface that resulted in the behaviour observed in Figure 38.

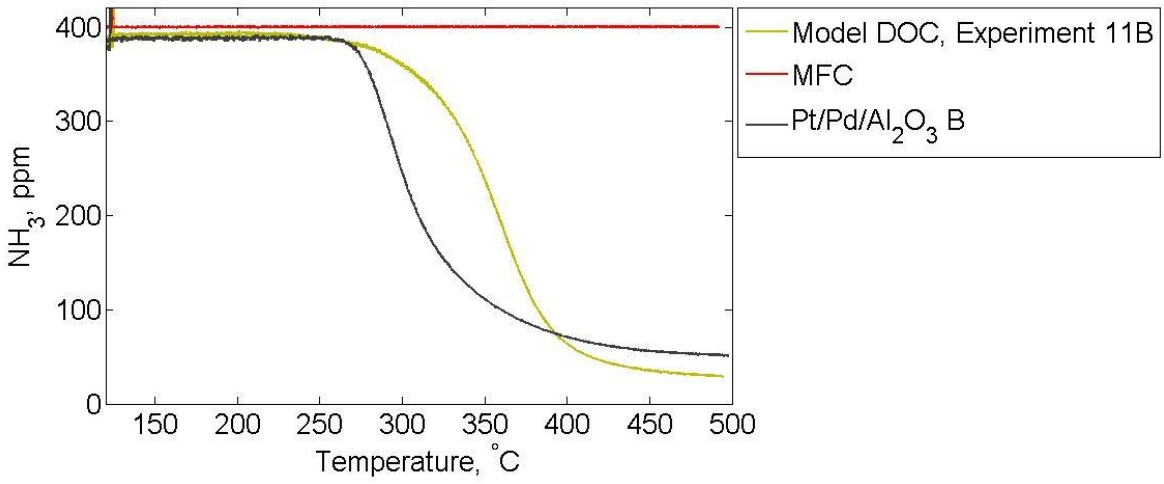

Figure 38 Effect of Pd doping on NH_3 oxidation; pre-treatment:C_3H_6+O_2; # of NH_3 oxidations: 2.

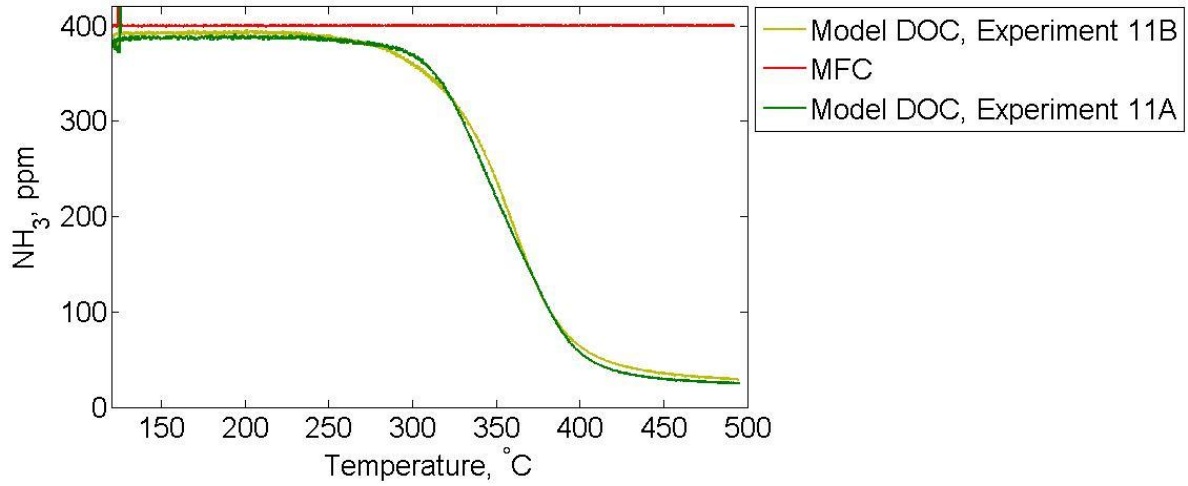

Figure 39 Comparison between NH_3 consumption for samples exposed to "one NH_3 oxidation" and "two NH_3 oxidations" (Experiment 11).

The results from the integration of NH_3 consumption for the presented cases is shown in Table 28.

Table 28 NH_3 consumption from the integration of NH_3 concentration vs. time (200°C – 480°C, Experiments 11 and Pt/Pd/Al_2O_3).

Experiment	Evaporation Temp. (°C)	NH_3 consumption (x10^{-4} mol)
Pt/Pd/Al_2O_3 A	700	2.1
11 (A and B) – Pt/$Al_2O_{3=}$	700	2.6
Pt/Pd/Al_2O_3 B	700	3.1

Figure 40 and Figure 41 show the NO and N_2O formation levels, respectively. Results from both "one" and "two NH_3 oxidations" are presented. It is seen that Pt/Pd/Al_2O_3 B resulted in the formation of higher levels of NO in the temperature range of about 280°C-420°C when compared to Pt/Pd/Al_2O_3 A. Also, a significant difference in N_2O formation was observed. The change in selectivity indicates differences in the active sites on the capturing monolith surface.

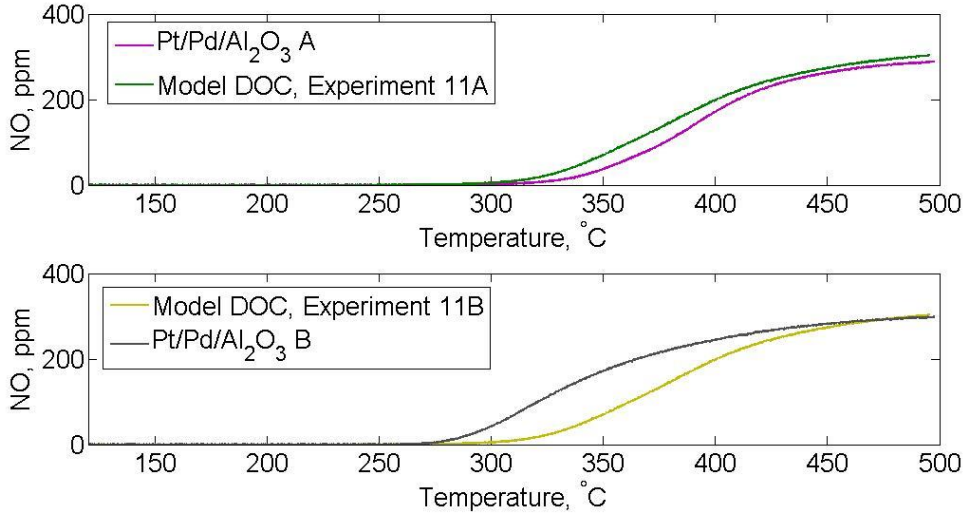

Figure 40 Effect of Pd doping duration on NO formation; pre-treatment:C_3H_6+O_2; # of NH_3 oxidations: Experiments "A" = 1, Experiments "B"=2.

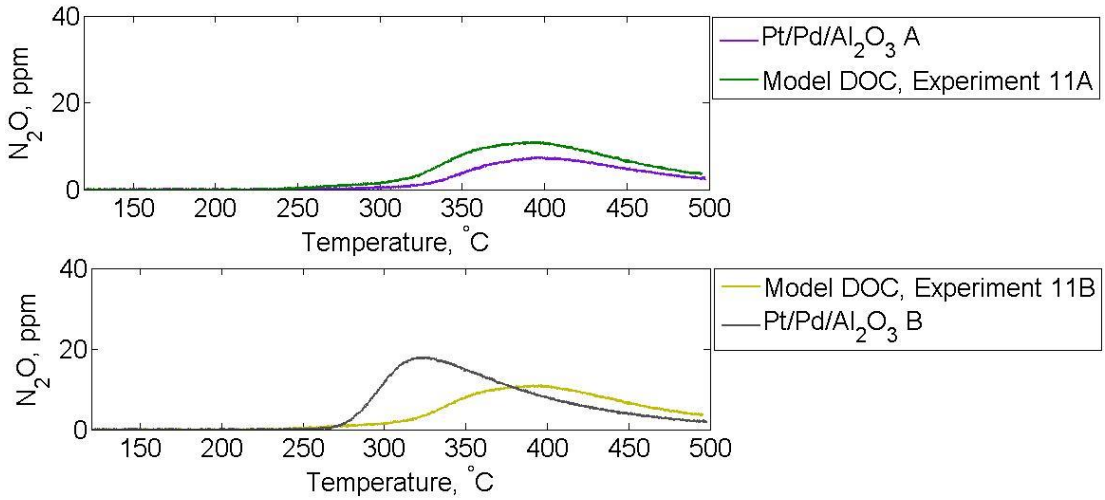

Figure 41 Effect of Pd doping duration on N_2O formation; pre-treatment:C_3H_6+O_2; # of NH_3 oxidations: Experiments "A" = 1, Experiments "B" = 2.

The relation between NO and N_2O formed and Model DOC/Pd-doped DOC supports the observations of Figure 37 and Figure 38. NO_2 levels were below 2 ppm, so the results were omitted.

In Figure 42, the results of CO oxidation are presented. The presence of Pd in the DOC resulted in a higher activity for CO oxidation in the capturing monolith sample when compared to the one observed with the model DOC. Unlike the observed differences between "one NH_3 oxidation" and "two NH_3 oxidations" in NH_3 consumption, the CO consumption was kept practically equal, as seen in Figure 43. The reason for this is likely to be that NH_3 oxidation is the first experiment on the capturing monolith, and during this experiment redistribution occurs while for CO oxidation, the capturing monolith is already stable due to the earlier NH_3 oxidation.

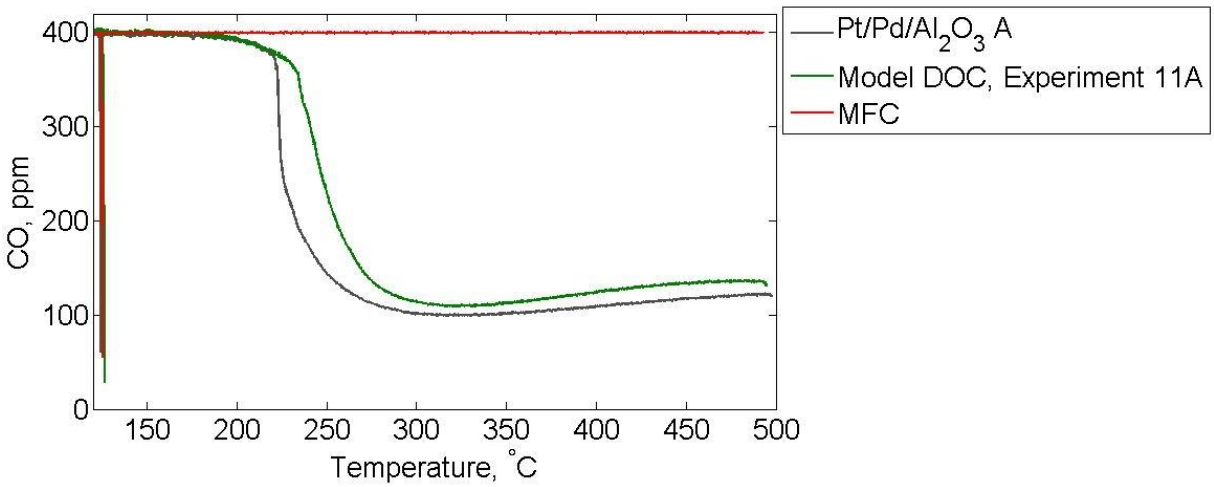

Figure 42 Effect of Pd doping on CO oxidation; pre-treatment:C_3H_6+O_2; # of NH_3 oxidations: 1.

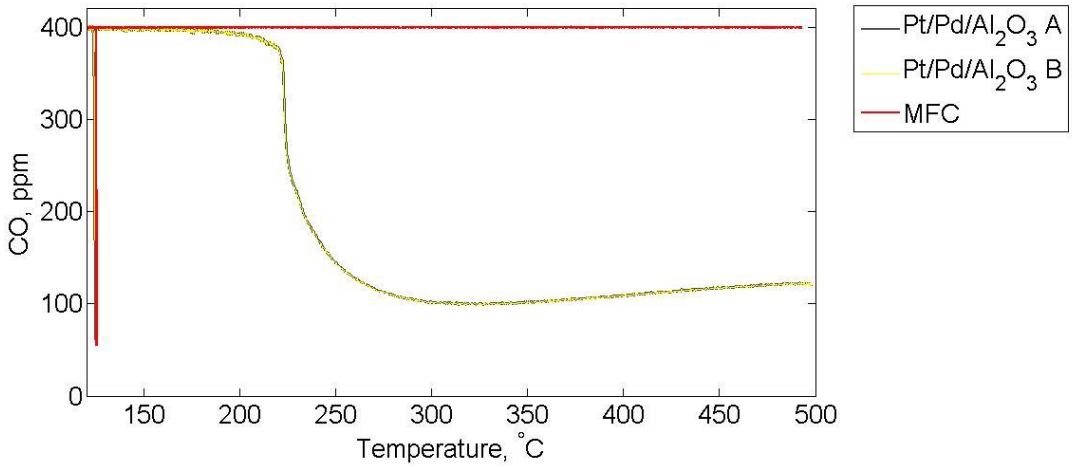

Figure 43 Comparison between CO consumption for samples exposed to "one NH_3 oxidation" and "two NH_3 oxidations" (Pd-doped DOC).

The results of integration of CO consumption over are presented in Table 29, confirming the observed behaviour from Figure 42.

Table 29 CO consumption from the integration of CO concentration vs. time (150°C-475°C, Experiments $Pt/Pd/Al_2O_3$ and 11A).

Experiment	Evaporation Temp. (°C)	CO consumption ($x10^{-4}$ mol)
$Pt/Pd/Al_2O_3$	700	3.9
11A	700	3.5

4.1.4.2 ICP-MS Analysis

The capturing monolith sample used in this experiment (C19) was sent to ICP analysis to quantify the amount of Pt captured on one-half (longitudinal direction) of the monolith. The amount of Pd was also quantified, but no significant levels were detected. The results obtained for Pt content are presented in Table 30, together with the results obtained for C18 (Experiment 11), for comparison.

Table 30. ICP analysis results for monoliths C18 and C19.

	C19 - $Pt/Pd/Al_2O_3$	C18 - Model DOC
Pt (%wt)	1.4E-04±0.2E-04	6.6E-05±1.0E-05

From Table 30, the amount of Pt evaporated from the Pd-doped DOC was found to be higher than the one evaporated from model DOC without Pd. This supports the observed behaviour for "two NH_3 oxidations" (Figure 38) and of CO consumption. Since Pd probably is stabilising Pt against sintering, it is possible that the Pt-Pd particles are smaller compared to Pt particles. This will likely result in less evaporation from the Pt-Pd particles.

4.1.5 Commercial DOC

4.1.5.1 Flow reactor experiments

A commercial DOC provided by Cummins Inc. was tested in an evaporation trial with a duration of 15h, a temperature of 700°C and an O_2 concentration of 8%. As with the model Pt/Al_2O_3, one and two NH_3 oxidations were performed, being DOC A done with one NH_3 oxidation and DOC B with two. The results were then compared to Experiments 11A and 11B (see Table 8), performed under the same conditions with model DOC.

The exact composition of the catalyst was not provided by the company, but it was known that it contained PGM, among which Pt, and that the support contained Al_2O_3.

A comparison between the results obtained for the model and commercial DOC when it comes to NH_3 oxidation is presented in Figure 44 for samples that were subjected to "one NH_3 oxidation". The results were found to be very similar.

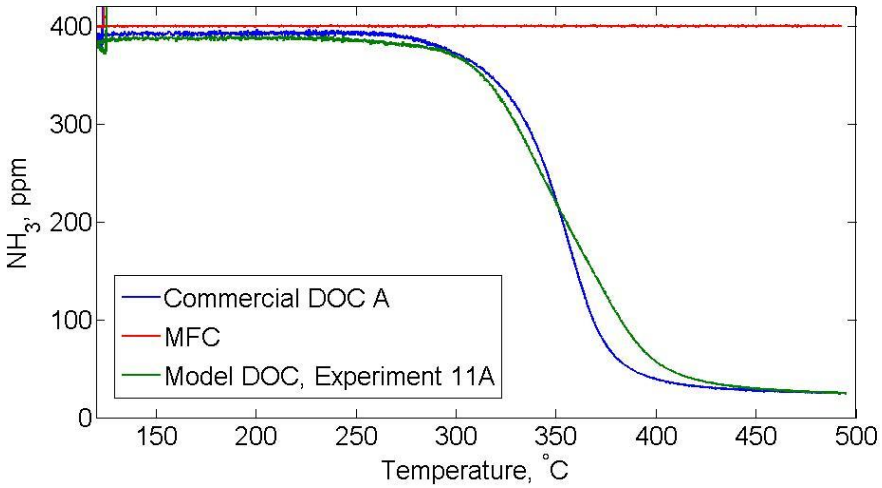

Figure 44 Investigation of Commercial DOC - NH_3 oxidation; pre-treatment:C_3H_6+O_2; # of NH_3 oxidations: 2.

However, as observed for investigation of Pd doping (refer to Section 4.1.4), a big difference was observed between the results for "one NH_3 oxidation" and "two NH_3 oxidations", which was not observed for the model DOC (Experiments 11A and 11B – see Figure 39). The comparison of the results obtained for the experiments performed with the commercial DOC is shown in Figure 45.

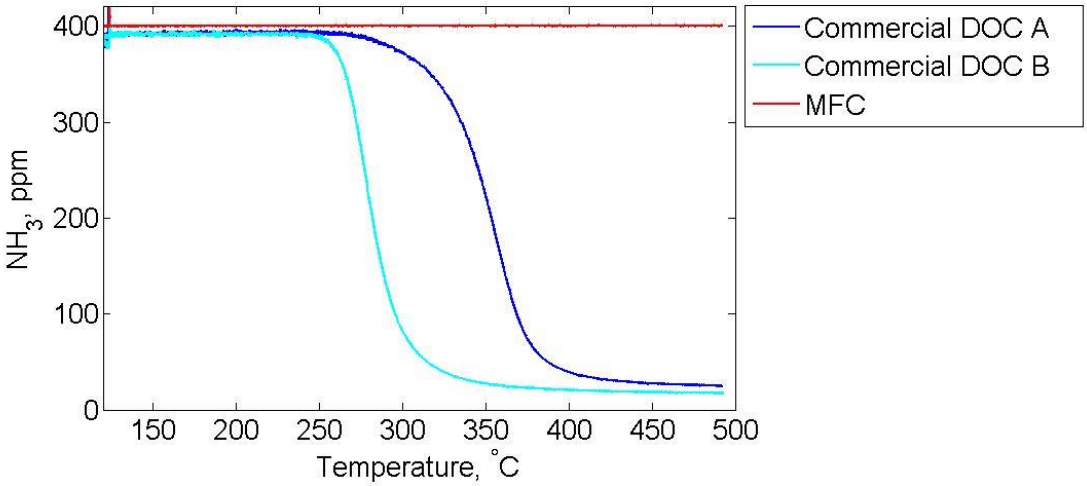

Figure 45 Comparison between NH_3 consumption for samples exposed to "one NH_3 oxidation" and "two NH_3 oxidations" (Commercial DOC).

The results from the integration of NH_3 consumption for the presented cases is presented in Table 31.

Table 31 NH_3 consumption from integration of NH_3 concentration vs. time (200°C – 480°C, (Experiments 11 and Commercial DOC).

Experiment	Evaporation Temp. (°C)	NH_3 consumption ($x10^{-4}$ mol)
Commercial DOC A	700	3.5
11 (A and B)	700	2.6
Commercial DOC B	700	7.9

Figure 46 and Figure 47 show the NO and N_2O formation levels, respectively. Results from both "one" and "two NH_3 oxidations" are presented. The behaviour is similar to the one obtained for Pd-doped DOC, which might be due to the presence of this element in the commercial DOC. There was a change in selectivity in the results obtained for Commercial DOC A and Commercial DOC B, indicating differences in the active sites on the capturing monolith surface.

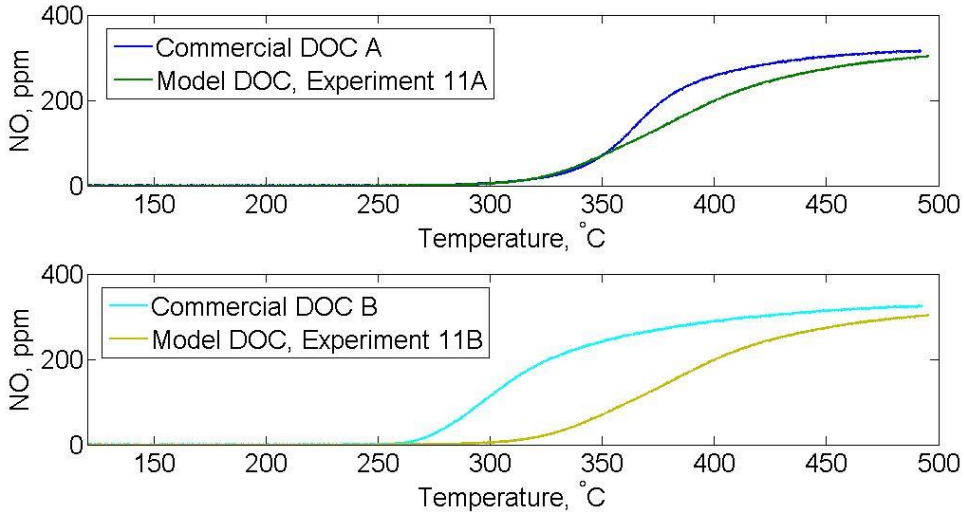

Figure 46 Investigation of Commercial DOC - NO formation; pre-treatment:C_3H_6+O_2; # of NH_3 oxidations: Experiments "A" = 1, Experiments "B"=2.

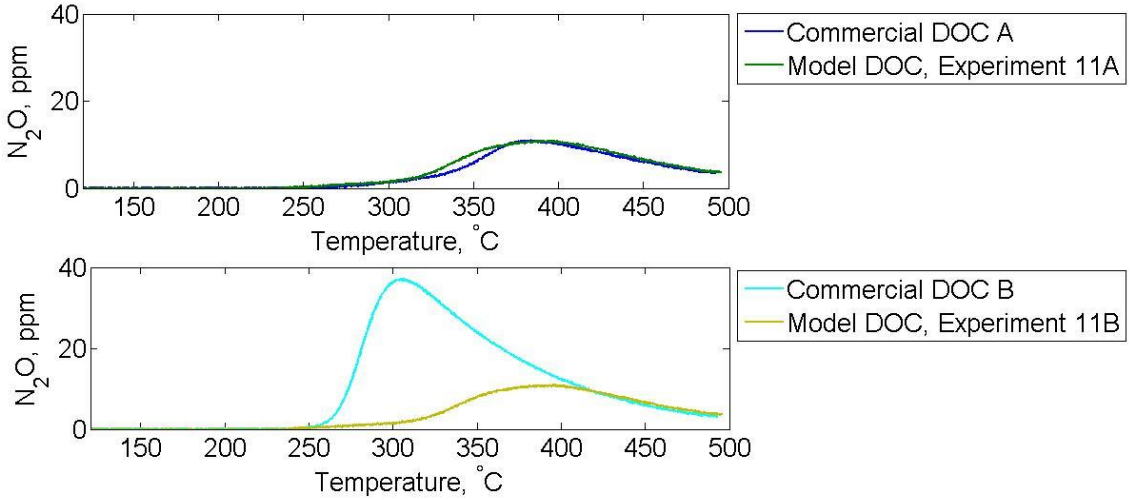

Figure 47 Investigation of Commercial DOC – N_2O formation; pre-treatment:C_3H_6+O_2; # of NH_3 oxidations: Experiments "A" = 1, Experiments "B" = 2.

In Figure 48, the results of CO oxidation are presented. The results from commercial DOC exhibited a higher activity for CO oxidation if compared with the model DOC. As observed in the investigation of the effects of Pd doping, no differences were observed between CO consumption between the trials with "one NH_3 oxidation" and "two NH_3 oxidations", unlike the observed for NH_3 oxidation. This can be seen in Figure 49.

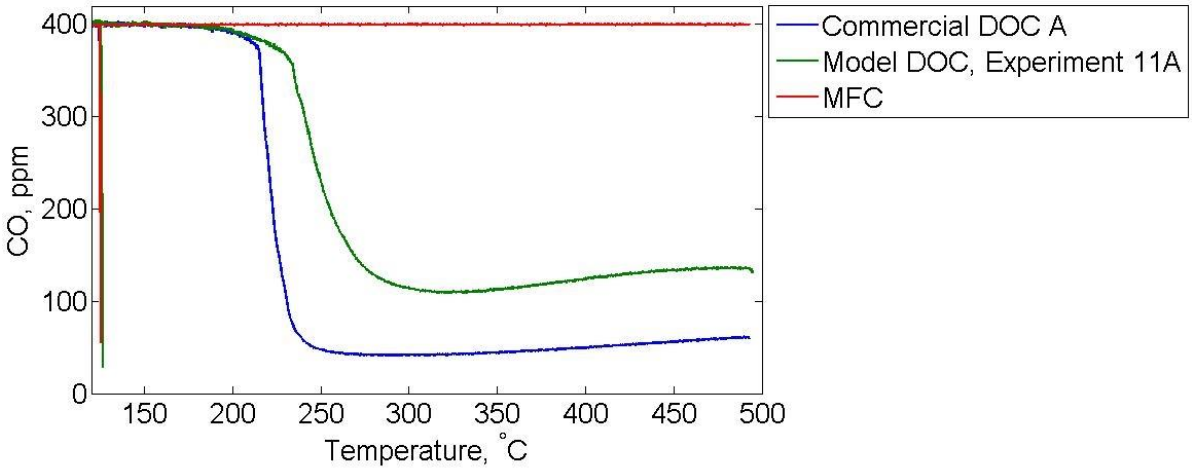

Figure 48 Investigation of Commercial DOC - CO oxidation; pre-treatment:C_3H_6+O_2; # of NH_3 oxidations: 1.

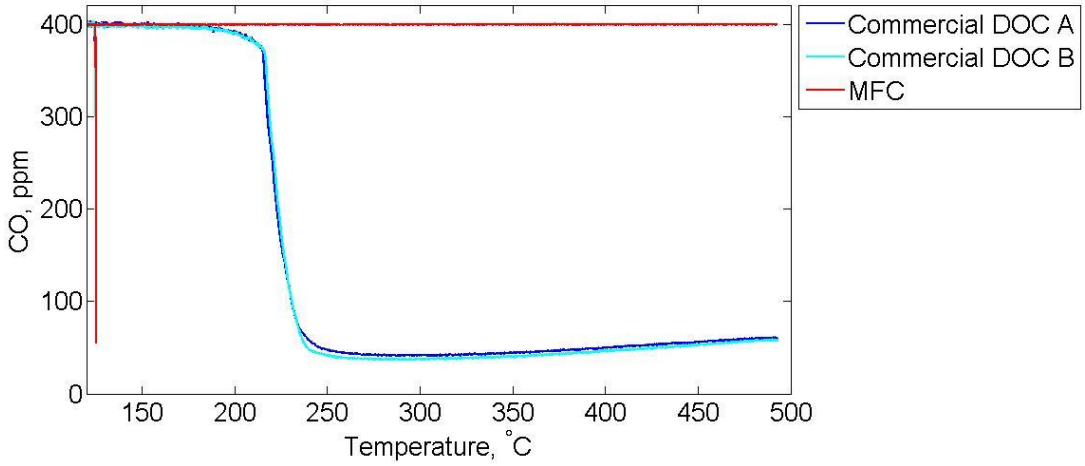

Figure 49 Comparison between CO consumption for samples exposed to "one NH_3 oxidation" and "two NH_3 oxidations" (Commercial DOC).

The results of integration of CO consumption over time are presented in Table 32, confirming the observed behaviour from Figure 48.

Table 32 CO consumption from the integration of CO concentration vs. time during the duration of the temperature ramp (150°C-475°C, Experiments Commercial DOC and 11A).

Experiment	Evaporation Temp. (°C)	CO consumption (x10^{-4} mol)
Commercial DOC	700	5.0
11A	700	3.5

4.1.5.2 ICP-MS analysis

The capturing monolith sample used in this experiment (C12) was sent to ICP analysis to quantify the amount of Pt captured in one-half (longitudinal direction) of the monolith. The amount of Pd was also quantified, but no significant levels were detected. The results obtained

for Pt content are presented in Table 33, together with the results obtained for C18 (Experiment 11), for comparison.

Table 33. ICP analysis results for monoliths C12 and C18.

	C12 - Commercial DOC	C18 - Model DOC
Pt (%wt)	4.7E-05±0.7E-05	6.6E-05±1.0E-05

Despite CO consumption for the commercial DOC being higher and also the NH_3 consumption for the "two NH_3 oxidations" experiment, the amount of evaporated Pt was lower for the commercial DOC when compared to the Model DOC, suggesting that some component in its composition has a stabilizing effect over Pt. The results from oxidation combined with ICP results can be an indicative that there is migration of other species besides Pt that can oxidize NH_3 and CO.

4.1.6 Reproducibility

Figure 50 exhibits the comparison between Experiments 11A and 17A when it comes to NH_3 oxidation. Both samples were submitted to one NH_3 oxidation. The differences observed are quite small.

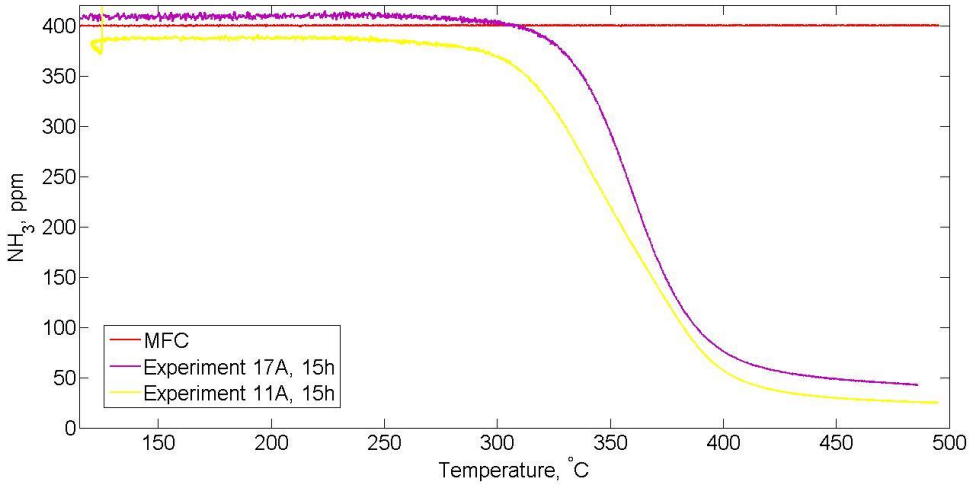

Figure 50 Reproducibility – Comparison of experiments 11A and 17A (NH_3 consumption).

In Figure 51, the Experiments are compared when it comes to CO oxidation, larger deviations are observed.

The monoliths used in Experiments 11 and 17 were sent to ICP-MS analysis, and the results confirmed the results of the comparison between the oxidation experiments. Monolith C18 (Experiment 11) resulted in a Pt content of 6.6E-05±1.0E-05 %wt, whereas Monolith C13 (Experiment 17) in a content of 7.9E-05±1.2E-05 %wt. Taking into account the uncertainty of the analysis though, it can be seen that despite the variability, the results are still comparable and relatively close, suggesting that the difference observed could mainly be attributed to experimental uncertainties.

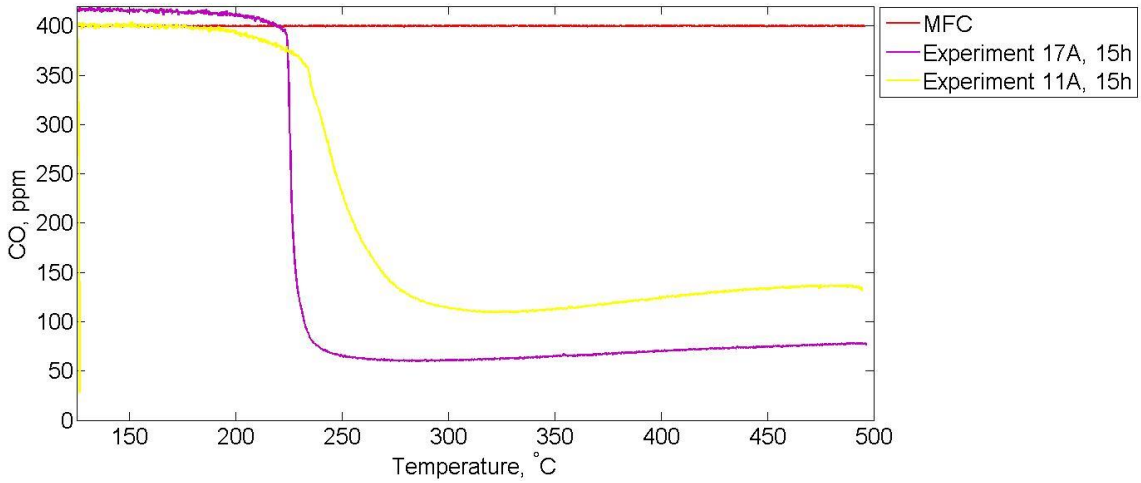

Figure 51 Reproducibility – Comparison of experiments 11A and 17A (CO consumption).

4.1.7 SEM/EDX

SEM/EDX was one of the physical characterization techniques tested, being performed prior to any ICP-MS analysis. The sample used was the capturing monolith C3, exposed to evaporation at 775°C. The SEM image obtained is exhibited in Figure 52, and one of the spectra from the EDX is depicted in Figure 53.

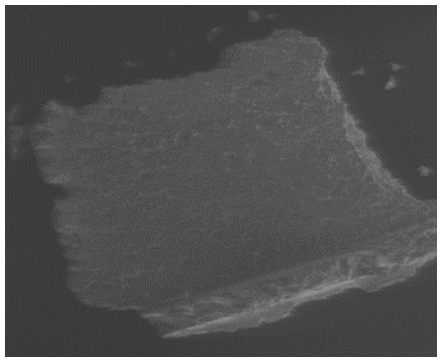

Figure 52 SEM image from a "contaminated" capturing monolith (C3).

Several elements that are expected to be found in cordierite were present, according to Figure 52. A peak of Al is observed which can also be attributed to the Al_2O_3 washcoating that was performed. However, no Pt was detected. As mentioned in the Section 2.6.3, the detection limits from EDX is approximately 0.1 %wt (Kuisma-Kursula 2000), which is too high for the amount of Pt that was found, as shown by the ICP-MS analysis results.

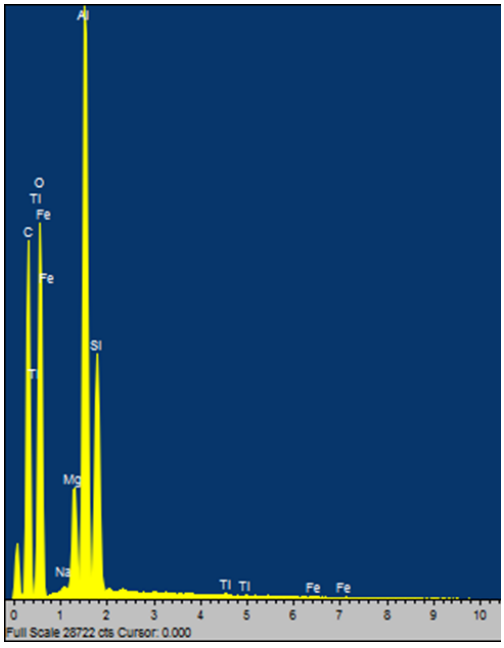

Figure 53 EDX spectrum from a "contaminated" capturing monolith (C3).

4.2 Kinetic model

To develop the kinetic model, the experimental results and the simulation results needed to be comparable. As detailed in Section 3.2, from the results of ICP-MS analysis, the amount of PtO_2 evaporated was estimated. The results are presented in Section 4.2.1.

In Section 4.2.2, the model parameters found are presented, and discussion regarding those is carried out.

4.2.1 Estimation of PtO_2 formed from experiments

ICP-MS analysis of monoliths C10, C11, C13, C14, C15, C16, C17 and C18 were used for developing the kinetic model of Pt evaporation. The ICP-MS results for this samples, already presented in the discussion in Section 4.1, are summarised in Table 34 for easier reference.

Table 34 Summary of ICP-MS data used for the kinetic modelling

Monolith sample	Pt content (%wt)	Evaporation conditions
C10	7.3E-05±1.1E-05	700°C, 5h, 8% O_2
C11	7.2E-05±1.1E-05	700°C, 10h, 8% O_2
C13	7.9E-05±1.2E-05	700°C, 15h, 8% O_2
C14	1.2E-05±0.2E-05	550°C, 15h, 8% O_2
C15	2.1E-04±0.3E-04	850°C, 15h, 8% O_2
C16	3.3E-05±0.5E-05	700°C, 15h, 2% O_2
C17	4.0E-05±0.6E-05	700°C, 15h, 5% O_2
C18	6.6E-05±1.0E-05	700°C, 15h, 8%O_2

The ICP-MS results for varying durations (monoliths C10, C11 and C13) are very similar. The rate of Pt evaporation increased with time (Fryburg & Petrus 1961; Jehn 1981) but this was observed for metals only, not supported particles.

Based on the Pt content determined by ICP-MS, the amount of PtO_2(g) necessary to result in that content, assuming the reaction Pt(s) + $O_2 \leftrightarrow PtO_2$ (g), was determined. The routine for that, as well as assumptions made in the process, were presented in Section 3.2. The results can be found in Table 35.

Table 35 Estimated amounts of PtO_2 formed, in mg.

Monolith sample	Estimated PtO_2 formed (kg)	Evaporation conditions
C10	8.8E-10±1.3E-10	700°C, 5h, 8% O_2
C13	9.3E-10±1.4E-10	700°C, 15h, 8% O_2
C14	1.5E-10±0.2E-10	550°C, 15h, 8% O_2
C15	2.4E-09±0.4E-09	850°C, 15h, 8% O_2
C16	3.8E-10±0.6E-10	700°C, 15h, 2% O_2
C17	4.8E-10±0.7E-10	700°C, 15h, 5% O_2
C18	7.9E-10±1.2E-10	700°C, 15h, 8%O_2

In Figure 54, the results from Table 35 are presented graphically. The uncertainty was not added.

The plots in Figure 54 were scaled based on the results for varying temperature, to be comparable. At this scale level, the PtO_2 formed during the evaporation experiments carried out at 700°C, 15h, 8%O_2 is practically the same (monoliths C13 and C18).

To proceed with the modelling, it was chosen that the results of the evaporation experiment carried out with monolith C13 would be used as the basis for the "700°C, 15h, 8% O_2" case because this monolith was subjected to evaporation in the same reactor booking as C10. As previously mentioned, ideally, the evaporation experiments with 5h and 10h duration should have been repeated and longer evaporation durations could have been investigated to assess the presence of a decrease, but there were time constraints that did not allow that.

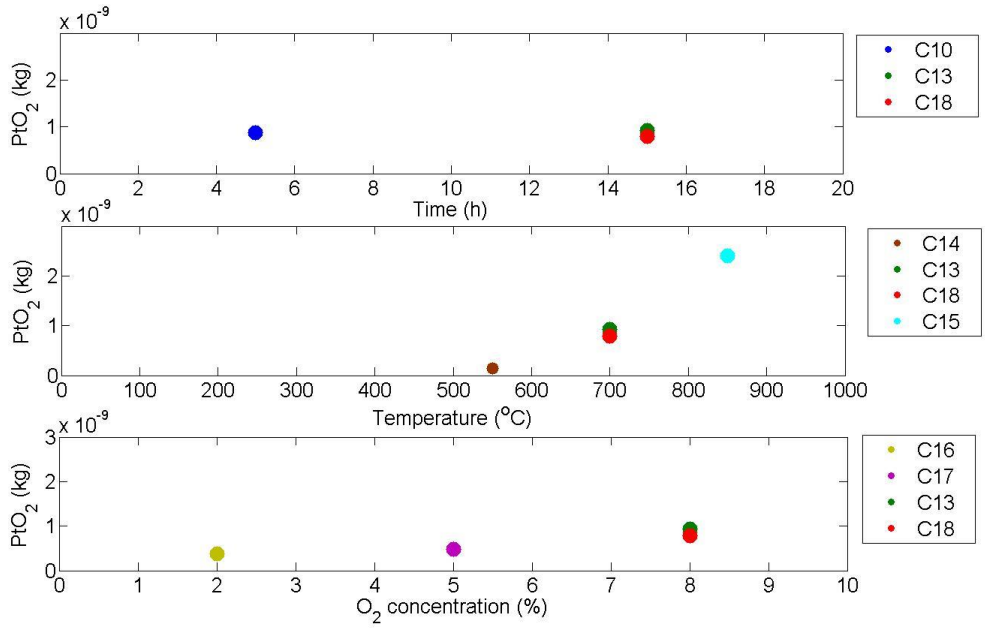

Figure 54 PtO_2 formed (kg) as a function of duration, temperature and O_2 concentration.

4.2.2 Model parameters

As detailed in Section 3.2, the rate expression given by Equation 38 was implemented on BOOST and simulations were performed to find values for E1, E2, K1, K2 and α that adjusted to the experimental results (presented in Section 4.2.2), resulting in a model of the simplified kinetics of Pt evaporation from model DOC.

Values for these parameters, when found in the literature, were used as a guideline to start the simulations. Fryburg & Petrus (1961), in their study of electrically heated Pt ribbons, found the activation energy of the Pt oxidation reaction to be 42.5 kcal/mol (177.9 kJ/mol), based on the collision efficiency of O_2 molecules to the Pt surface.

Fryburg & Petrus (1961) also determined the equilibrium constant for the reaction Pt(s) + O2 ↔ PtO2(g) and compared it to values from other studies, as presented in Section 2.4. The equilibrium constants there presented showed an order of magnitude of 10^{-5} and 10^{-6} for temperatures of 1500°C and 1200°C, respectively (see Table 4). Bartlett (1967) also determined values for the equilibrium constant of the same reaction: an order of magnitude of 10^{-5}, 10^{-6} and 10^{-7} was found for temperatures of 1400°C, 1200°C and 1060°C. As the temperature range of the experiments carried out in this work was much lower, a lower order of magnitude for the equilibrium constants was expected to be found. The order of magnitude of the equilibrium constants obtained with the different combination of parameters was monitored based on that.

Three sets of parameters were found to adjust to the experimental data as presented in Figure 55, Figure 56 and Figure 57.

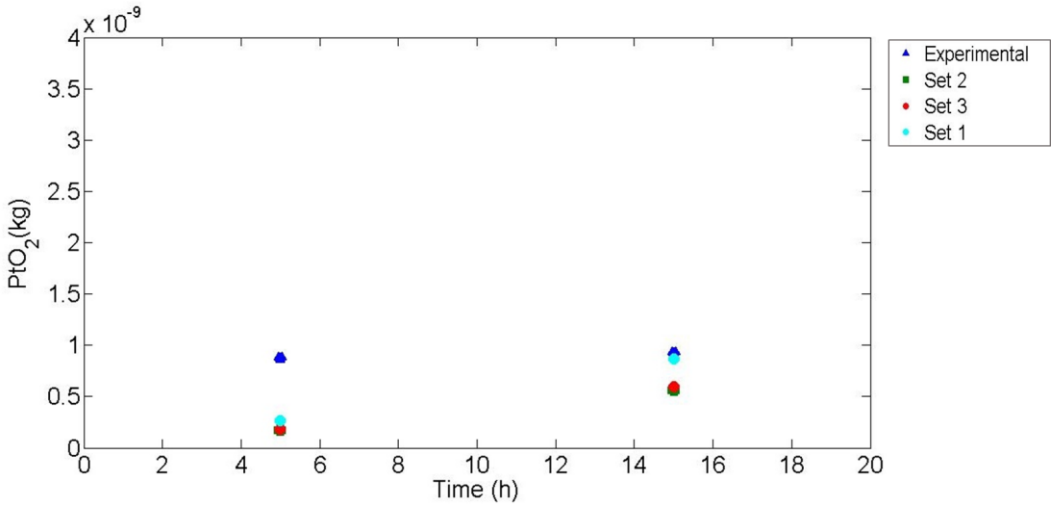

Figure 55 Simulation vs. experimental results for varying durations

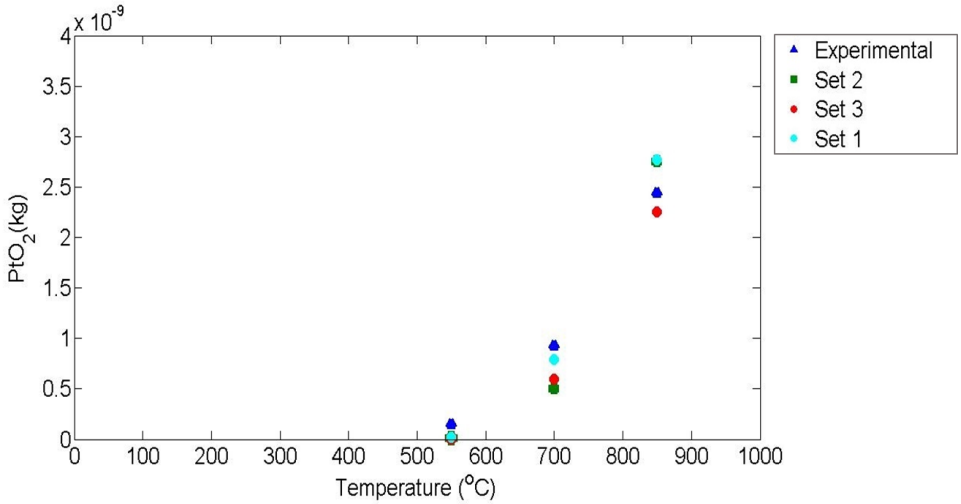

Figure 56 Simulation vs. experimental results for varying temperature.

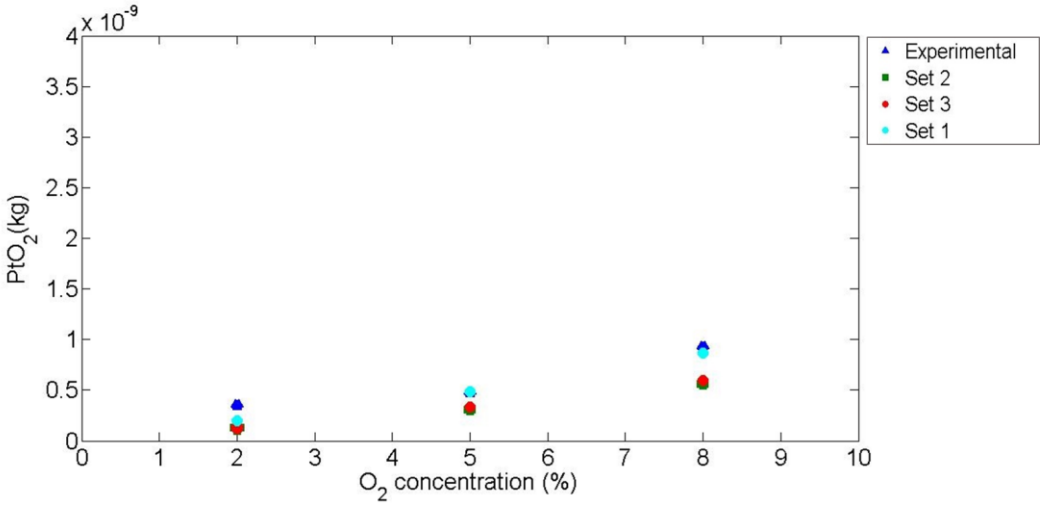

Figure 57 Simulation vs. experimental results for varying oxygen concentration.

The corresponding parameters that resulted in these plots are given in Table 36. The activation energy values found for the forward reaction are comparable to the one observed by Fryburg & Petrus (1961) of 177.9 kJ/mol.

Table 36 Model parameters

Set #	α	K1 (kmol/m²s)	E1 (kJ/mol)	K2 (kmol/m²s)	E2 (kJ/mol)
1	1	4.50E-05	175	1.00E+03	165
2	1	9.00E-05	185	1.00E+03	170
3	1	1.00E-04	185	3.70E+03	178

The corresponding equilibrium constants, for each temperature, are presented in Table 37. The orders of magnitude are lower than the reference values presented for higher temperatures at the beginning of this section, which follows the expected.

Table 37 Equilibrium constants from found model parameters.

Set #	Equilibrium constants (Keq)		
	850 °C	700 °C	550 °C
1	1.5E-08	1.3E-08	1.0E-08
2	1.8E-08	1.4E-08	1.0E-08
3	1.3E-08	1.1E-08	9.7E-09

The absolute values for PtO_2 formed in kg, for each simulated case using the sets of parameters found is presented in Table 38, together with the calculated values obtained based on the experiments.

The error for each case in relation to the experimental value was calculated and presented in Table 39. An important factor to be considered is that the uncertainty of the experimental values was of about 15% in average.

For some of the cases, especially “550°C”, the deviation between the simulated values and the experimental ones was quite big. However, as seen in Figure 56, it still allowed for a fair fit to the results because of the low absolute value of this point, which is likely to lie within the experimental uncertainty. There was no time for repeating that experiment. However, it is kept as a suggestion.

As previously discussed in this section, the experimental values found for cases “5h”, and “15h” were very close. However, the model did not incorporate the sintering effect and could, therefore, not describe this feature.

Due to time constraints, further adjustment of the model parameters could not be performed. By considering the uncertainty of the experimental values, the errors and the curves for all cases, the parameters defined in Set 1 gave the better adjustment to the experiments at this point. However, an important factor to be considered in further adjustments is that according to the experimental results, Pt migration is still significant at lower temperatures, implying that the reaction $PtO_2(g) \rightarrow Pt\ (s) + O_2$ occurs. Thus, the activation energy for that reaction is

expected to be lower so that the reaction can indeed overcome the energy barrier and occur at lower temperatures, reflecting the behaviour observed experimentally.

Table 38 Simulation vs. experimental results – Formed PtO_2 (kg)

	Formed PtO_2 (kg)			
	Experimental	Set 1	Set 2	Set 3
Time (h)				
5	8.8E-10	2.7E-10	1.7E-10	1.80E-10
15	9.3E-10	8.7E-10	5.6E-10	6.0E-10
Temperature (°C)				
550	1.5E-10	2.5E-11	1.4E-11	1.5E-11
700	9.3E-10	7.9E-10	5.0E-10	6.0E-10
850	2.4E-09	2.8E-09	2.8E-09	2.3E-09
O_2 Concentration (%)				
8	9.3E-10	8.7E-10	5.6E-10	6.0E-10
5	4.8E-10	4.9E-10	3.1E-10	3.3E-10
2	3.8E-10	2.0E-10	1.3E-10	1.4E-10

Table 39 Error of simulated values in relation to experimental.

	Experimental	Set 1	Set 2	Set 3
Time (h)				
5	0	-70%	-81%	-79%
15	0	-6%	-39%	-36%
Temperature (°C)				
550	0	-83%	-91%	-90%
700	0	-15%	-46%	-36%
850	0	13%	13%	-8%
O_2 concentration (%)				
8	0	-6%	-39%	-36%
5	0	3%	-34%	-30%
2	0	-49%	-67%	-65%

5 Conclusions and final remarks

In this study, the effect of different parameters on Pt volatilization from model DOC was investigated, allowing for a deeper understanding of this phenomenon that has been problematic in diesel exhaust aftertreatment systems due to the deactivation caused in the downstream located SCR catalyst, that, in turn, results in poor NOx conversion.

The effects of temperature, duration and oxygen concentration were studied and based on the results obtained, it was possible to develop a model of the simplified kinetics of Pt evaporation from model DOC.

Exposing the DOC to increasing temperatures, resulted in increasing Pt volatilization, as expected. Temperatures in the range of 550-850°C were tested, and for all cases, volatilization was observed to occur at levels that could be detected both by NH_3 and CO oxidation experiments and by ICP-MS analysis. Also, the Pt evaporation rate was observed to increase at a non-linear rate with increasing temperature. From ICP-MS analysis, for the lower temperature tested, the amount of Pt that migrated was found to be of 0.00001%wt whereas for the higher temperature tested, of 0.0002 %wt.

Subjecting the DOC to a high temperature (700°C) during different durations allowed for observing that there is a variation in Pt migration according to duration. It was expected that the Pt evaporation rate would increase linearly with time and an increase was indeed observed. However, the Pt levels of evaporation obtained for all experiments were quite close, especially considering the uncertainty of the ICP-MS analysis. A possible reason for this could be that sintering occurs simultaneously with evaporation and that when the large particles are formed, the rate for evaporation decreases.

The study of the effect of varying oxygen concentrations on Pt evaporation revealed that an increasing oxygen concentration resulted in a higher Pt evaporation rate. Furthermore, based on the ICP-MS analysis, this rate was found to increase in a non-linear way with increasing concentration, as expected from the literature. The oxygen concentration was varied from 2% to 8%. For the lowest tested oxygen concentration, from ICP-MS analysis, the amount of Pt that migrated was found to be of 0.00003 %wt and for the highest, of 0.00007 %wt.

The kinetic model was based on the literature finding that the main form of evaporation of Pt is as PtO_2 and on the global reaction $Pt(s)+O_2 \leftrightarrow PtO_2(g)$. The ICP-MS results obtained from the study of the effects of temperature, duration and oxygen concentration were used to extrapolate the amount of $PtO_2(g)$ that corresponded to the captured Pt(s) amounts, based on the global reaction. This was found to lie in the range of 1.5E-10 to 2.4E-09 kg. Through simulations based on the proposed oxidation reaction rate, using the software AVL BOOST™, parameters for the activation energies and rate constants were found. The activation energy for the forward reaction was found to be 175 kJ/mol for the best set of parameters determined in this study, which was reasonable based on the experiments behaviour and results from the literature. However, further adjustments need to be made since the activation energy found for the backward reaction was quite high (165-178 kJ/mol), considering that this reaction is active at low temperatures, as observed experimentally.

Pd is known to have a different oxidation behaviour when compared to Pt, being stable in its oxide form at temperatures up to 800°C whereas PtO_2 is extremely volatile. Pd has been reported to act as a stabiliser to Pt, hindering its migration. However, the experiment carried out in this study that investigated the effect of Pd doping revealed a significantly higher Pt

evaporation for the Pd-doped catalyst, based on the ICP-MS analysis results. The NH_3 oxidation results showed different scenarios; when the sample was submitted to one NH_3 oxidation, the Pd-doped catalyst resulted in a lower activity towards oxidation than the Pt/Al_2O_3 DOC. However, when NH_3 oxidation was repeated, the opposite was observed, and the activity towards oxidation was significantly higher for the Pd-doped catalyst. A change in selectivity was also observed, indicating a restructuring of the active surface sites. When it comes to CO oxidation, the Pd-doped catalyst had a higher oxidation activity in all tests. To better understand the effect of Pd-doping on Pt stability, further experiments investigating this parameter are suggested for future studies.

The Commercial DOC provided by Cummins, Inc. resulted in a similar behaviour as the observed for the Pd-doped DOC when it comes to the NH_3 and CO oxidation experiments. However, ICP-MS analysis showed a lower Pt migration from the commercial DOC when compared to the model one. No information about the exact composition of the commercial DOC was provided, but the behaviour observed can be an indicative of migration of other species that are active in NH_3 and CO oxidation.

Investigation of how Pt distributes along the monolith positioned downstream of the DOC resulted in the confirmation of the observations in the literature; high amounts of Pt were deposited on the monolith inlet (side facing the DOC), and no significant amounts of Pt were found at the outlet of the monolith, also indicating that there was no Pt flowing out of the reactor system. ´

The results obtained from NH_3 and CO oxidation could be used as a good overall guidance to trends regarding Pt migration. However, during the first NH_3 oxidation experiment, redistribution of the noble metal particles likely occurred and it is therefore better to use the second NH_3 oxidation experiment and CO oxidation experiments for the comparisons. The results should preferentially be combined with other characterization methods, and repeated trials should be performed to gain a better understanding of the variability and the possible relation with the restructuring of deposited Pt species.

As previously observed by other studies, characterization techniques that are employable in the investigation of Pt migration from DOC are restricted due to the ultra-low amounts of Pt that migrate. This challenging aspect was confirmed, and SEM/EDX, for example, was not suitable for detecting the Pt deposited in the downstream positioned monolith.

Reproducibility among the experiments was another challenging factor. Many parameters were subjected to small variations from experiment to experiment even though it was aimed to keep them the same, i.e. positioning of the monoliths, thermocouples, and heating coil. Despite the variation under the same experimental conditions, the results obtained were relatively close.

To gain an even broader understanding of the Pt migration behaviour from DOC, investigation of the form in which Pt is deposited on the downstream monolith would be interesting, being the ultra-low amounts a challenging factor to be overcome. Refinement and further development of the kinetic model, with the inclusion of more steps such as adsorption, desorption and surface reactions are kept as suggestions for future studies.

Also, performing a similar study with the use of SCR-catalysts instead of capturing monoliths would be interesting to deepen the understanding of how Pt migration affects the NOx aftertreatment system.

References

Alcock, C.B., 1961. The Gaseous Oxides of the Platinum Metals. *Platinum Metals Review*, 5(4), pp.134–139. Available at: http://www.platinummetalsreview.com/dynamic/article/view/pmr-v5-i4-134-139 [Accessed May 17, 2017].

Anderson, J.A., 1992. CO oxidation over alumina supported platinum catalyst. *Catalysis Letters*, 13(4), pp.363–369. Available at: http://link.springer.com/10.1007/BF00765039 [Accessed May 25, 2017].

AVL, 2017. AVL BOOST. Available at: https://www.avl.com/boost [Accessed June 5, 2017].

AVL, 2013. AVL BOOST FIRE Aftertreatment Users Guide. Available at: https://www.avl.com/-/avl-boost-aftertreatment.

Bartholomew, C.H. & Farrauto, R.J., 2010. Environmental Catalysis: Stationary Sources. In *Fundamentals of Industrial Catalytic Processes*. Hoboken, NJ, USA: John Wiley & Sons, Inc., pp. 753–819. Available at: http://doi.wiley.com/10.1002/9780471730071.ch11 [Accessed May 25, 2017].

Bartlett, R.W., 1967. Platinum Oxidation Kinetics with Convective Diffusion and Surface Reaction. *Journal of the Electrochemical Society*, 114(6), pp.547–550.

Beamish, F.E., 1966. Chapter 1 – the Action of Acids, Bases, Oxygen and Chlorine on the Noble Metals. In *The Analytical Chemistry of the Noble Metals*. pp. 1–38.

Bobaru, S.C., 2006. *High-Pressure STM Studies of Oxidation Catalysis*. Faculty of Mathematics and Natural Sciences, Leiden University.

Brandenberger, S. et al., 2008. *The State of the Art in Selective Catalytic Reduction of NOx by Ammonia Using Metal-Exchanged Zeolite Catalysts*,

Cavataio, G. et al., 2009. Impact and prevention of ultra-low contamination of platinum group metals on SCR catalysts due to DOC design. *SAE Technical Paper*, 2(1), pp.2009-01–0627.

Chaston, J.C., 1964. Reaction of Oxygen with the Platinum Metals. I-The Oxidation of Platinum. *Platinum Metal Review*, 8, pp.50–54.

Chen, X. et al., 2013. Mitigation of Platinum Poisoning of Cu-Zeolite SCR Catalysts. , 2013, pp.4–9.

Citir, M. et al., 2008. Direct Determination of the Ionization Energies of PtC, PtO, and PtO2 with VUV Radiation. *Phys. Chem.*, A(112), pp.9584–9590.

Cornils, B., 2004. Handbook of Commercial Catalysts. Heterogeneous Catalysts. By Howard F. Rase. *Angewandte Chemie International Edition*, 43(18), pp.2324–2325. Available at: http://doi.wiley.com/10.1002/anie.200385146 [Accessed May 20, 2017].

Cybulski, A. & Moulijn, J.A., 1994. Monoliths in Heterogeneous Catalysis. *Catalysis Reviews: Science and Engineering*, 36(2), pp.179–270.

Domesle, R. et al., 1992. Catalyst for purification of exhaust gases of diesel engines and method of use. Available at: https://www.google.ch/patents/US5157007.

Dunn-Rankin, D., Miyasato, M.M. & Pham, T.J., 2008. Introduction and perspectives. *Lean combustion : technology and control*.

Egerton, R.F., 2016. *Physical Principles of Electron Microscopy*, Cham: Springer International Publishing. Available at: http://link.springer.com/10.1007/978-3-319-39877-8.

Fryburg, G.C. & Petrus, H.M., 1961. Kinetics of the Oxidation of Platinum. *Journal of Electrochemical Society*, 108, pp.496–503.

Gélin, P. & Primet, M., 2002. Complete oxidation of methane at low temperature over noble metal based catalysts: A review. *Applied Catalysis B: Environmental*, 39(1), pp.1–37.

Hannevold, L. et al., 2005. Chemical vapor transport of platinum and rhodium with oxygen as transport agent. *Journal of Crystal Growth*, 279(1), pp.206–212. Available at: http://www.sciencedirect.com/science/article/pii/S0022024805002034 [Accessed May 20, 2017].

Hauff, K. et al., 2013. Platinum oxide formation and reduction during NO oxidation on a diesel oxidation catalyst-Macrokinetic simulation. *Applied Catalysis B: Environmental*, 129, pp.273–281. Available at: http://dx.doi.org/10.1016/j.apcatb.2012.09.022.

Heck, R.M. & Farrauto, R.J., 2001. Automobile exhaust catalysts. *Applied Catalysis A: General*, 221(1–2), pp.443–457.

Heck, R.M., Farrauto, R.J. & Gulati, S.T., 2009. Diesel Engines. In *Catalytic Air Pollution Control: Commercial Technology*. New Jersey: John Wiley & Sons, Inc., pp. 238–280.

Heck, R.M., Gulati, S. & Farrauto, R.J., 2001. The application of monoliths for gas phase catalytic reactions. *Chemical Engineering Journal*, 82(1–3), pp.149–156.

Horiuchi, M., Ikeda, Y. & Saito, K., 1991. Exhaust gas purification catalyst. Available at: http://www.google.si/patents/US5000929.

Imelik, B. & Vedrine, J.C., 1994. *Catalyst Characterization: Physical Techniques for Solid Materials*, Available at: http://books.google.cz/books?id=eChU6eD5M48C.

Jehn, H., 1984. High temperature behaviour of platinum group metals in oxidizing atmospheres. *Journal of the Less Common Metals*, 100, pp.321–339. Available at: http://linkinghub.elsevier.com/retrieve/pii/0022508884900729 [Accessed May 17, 2017].

Jehn, H., 1981. Platinum losses during high temperature oxidation. *Journal of the Less Common Metals*, 78(2), pp.33–41. Available at: http://linkinghub.elsevier.com/retrieve/pii/0022508881901417 [Accessed May 28, 2017].

Jen, H. et al., 2008. Detection , Origin and Effect of Ultra-Low Platinum Contamination on Diesel-SCR Catalysts. *SAE International 2008*, 1(2488), pp.1553–1559.

Kamasamudram, K. et al., 2011. New Insights into Reaction Mechanism of Selective Catalytic Ammonia Oxidation Technology for Diesel Aftertreatment Applications. *SAE International Journal of Engines*, 4(1), pp.1810–1821.

Khair, M.K., 2003. A Review of Diesel Particulate Filter Technologies. In *SAE Technical Paper*. SAE International. Available at: http://dx.doi.org/10.4271/2003-01-2303.

Koebel, M., Elsener, M. & Kleemann, M., 2000. Urea-SCR: a promising technique to reduce NOx emissions from automotive diesel engines. *Catalysis Today*, 59(3), pp.335–345.

Kong, Y. et al., 2005. Active DPF Regeneration for 2007 Diesel Engines. In *SAE Technical Paper*.

SAE International. Available at: http://dx.doi.org/10.4271/2005-01-3509.

Kuisma-Kursula, P., 2000. Accuracy, precision and detection limits of SEM–WDS, SEM–EDS and PIXE in the multi-elemental analysis of medieval glass. *X-Ray Spectrometry*, 29(1), pp.111–118. Available at: http://dx.doi.org/10.1002/(SICI)1097-4539(200001/02)29:1%3C111::AID-XRS408%3E3.0.CO;2-W.

Llopis, J., 1969. Corrosion of Platinum Metals and Chemisorption. *Catalysis Reviews*, 2(1), pp.161–220. Available at: http://dx.doi.org/10.1080/01614946908066543.

Manasilp, A. & Gulari, E., 2002. Selective CO oxidation over Pt/alumina catalysts for fuel cell applications. *Applied Catalysis B: Environmental*, 37, pp.17–25. Available at: http://cheresearch.engin.umich.edu/gulari/32.pdf [Accessed May 25, 2017].

McCabe, R.W., Wong, C. & Woo, H.S., 1988. The passivating oxidation of platinum. *Journal of Catalysis*, 114(2), pp.354–367.

Rankovic, N., Nicolle, A. & Da Costa, P., 2010. Detailed Kinetic Modeling Study of NOx Oxidation and Storage and Their Interactions over Pt/Ba/Al 2 O 3 Monolith Catalysts. *The Journal of Physical Chemistry C*, 114(15), pp.7102–7111. Available at: http://pubs.acs.org/doi/pdf/10.1021/jp100192u [Accessed June 1, 2017].

Ritchie, I.M. & Hunt, G.L., 1969. The kinetics and pressure dependence of surface controlled metal oxidation reactions. *Surface Science*, 15(3), pp.524–534.

Ross, J.R.H., 2012. Catalytic Reactors and the Measurement of Catalytic Kinetics. *Heterogeneous Catalysis*, pp.97–121. Available at: http://linkinghub.elsevier.com/retrieve/pii/B9780444533630100052.

Schäfer, F. & van Basshuysen, R., 1995. Exhaust aftertreatment methods. In *Reduced Emissions and Fuel Consumption in Automobile Engines*. pp. 86–116.

Thomas, R., 2013. *Practical Guide to ICP-MS: A Tutorial for Beginners* 3rd editio., CRC Press.

Toops, T.J. et al., 2010. Deactivation of accelerated engine-aged and field-aged Fe-zeolite SCR catalysts. *Catalysis Today*, 151(3–4), pp.257–265.

Torborg, C. & Beller, M., 2009. Recent Applications of Palladium-Catalyzed Coupling Reactions in the Pharmaceutical, Agrochemical, and Fine Chemical Industries. *Advanced Synthesis & Catalysis*, 351(18), pp.3027–3043. Available at: http://doi.wiley.com/10.1002/adsc.200900587 [Accessed May 20, 2017].

Twigg, M. V., 2007. Progress and future challenges in controlling automotive exhaust gas emissions. *Applied Catalysis B: Environmental*, 70(1–4), pp.2–15.

Wang, C.-B. & Yeh, C.-T., 1998. Effects of Particle Size on the Progressive Oxidation of Nanometer Platinum by Dioxygen. *Journal of Catalysis*, 178(2), pp.450–456. Available at: http://linkinghub.elsevier.com/retrieve/pii/S0021951798921212 [Accessed May 17, 2017].

Wyatt, M. et al., 1993. The Design of Flow-Through Diesel Oxidation Catalysts. , (412). Available at: http://papers.sae.org/930130/ [Accessed June 5, 2017].

Yu, T. et al., 2017. Insight of platinum poisoning Cu/SAPO-34 during NH3-SCR and its promotion on catalysts regeneration after hydrothermal treatment. *Applied Catalysis B: Environmental*, 204, pp.525–536. Available at:

http://www.sciencedirect.com/science/article/pii/S0926337316309389 [Accessed May 16, 2017].

Appendix

A.1 – Details about the produced model DOC and capturing monoliths

Table 40 Washcoat amount per model DOC produced.

Sample #	Washcoat mass (mg)	Sample #	Washcoat mass (mg)
P1	259	P10	254
P2	257	P11	257
P3	262	P12	262
P4	262	P13	248
P5	259	P14	268
P6	258	P15	254
P7	250	P16	248
P8	258	P17	240
P9	252	$Pt/Pd/Al_2O_3$	272

Table 41 Washcoat amount per capturing monolith produced.

Sample #	Washcoat mass (mg)	Sample #	Washcoat mass (mg)
C1	19	C11	88
C2	31	C12	82
C3	21	C13	84
C4	21	C14	72
C5	22	C15	66
C6	16	C16	67
C7	17	C17	70
C8	20	C18	68
C9	18	C19	76
C10	81		

Table 42 Deviation (%) from aimed washcoat amount.

Sample #	Deviation from aimed value (%)	Sample #	Deviation from aimed value (%)
P1	3.4	P10	1.8
P2	2.9	P11	2.8
P3	4.8	P12	4.6
P4	4.9	P13	-0.8
P5	2.6	P14	7.2
P6	3.3	P15	1.6
P7	3.4	P16	-0.8
P8	3.1	P17	-4.0
P9	0.6		

Sample #	Deviation from aimed value (%)	Sample #	Deviation from aimed value (%)
C1	-5.0	C10	1.3
C2	55.0	C11	10.0
C3	10.0	C12	2.5
C4	5.0	C13	5.0
C5	5.0	C14	-10.0
C6	-20.0	C15	-17.5
C7	-15.0	C16	-16.3
C8	0.0	C17	-12.5
C9	-10.0	C18	-15.0
		C19	-5.0

A.2 – Flow reactor experiments results

A.2.1 – Effect of repeating NH_3 oxidation on the same capturing monolith sample

It was found that repeating NH_3 oxidation after an NH_3 – CO oxidation sequence resulted, in some cases, in a different NH_3 oxidation behaviour when compared to the "first" NH_3 oxidation. This is probably due to a restructuring of the Pt species on the capturing monolith.

To illustrate this, two cases are presented. Experiments 12A and 12B and Experiments 13A and 13B are presented.

For Experiment 12, executed at 850°C with 8% O_2 and a duration of 15h, the NH_3 consumption when only one NH_3 oxidation had been performed was higher than when the total number of NH_3 oxidations was two, as seen in Figure 58. For Experiment 13, executed at 700°C with 8% O_2 and a duration of 5h, the opposite was observed, as shown in Figure 59.

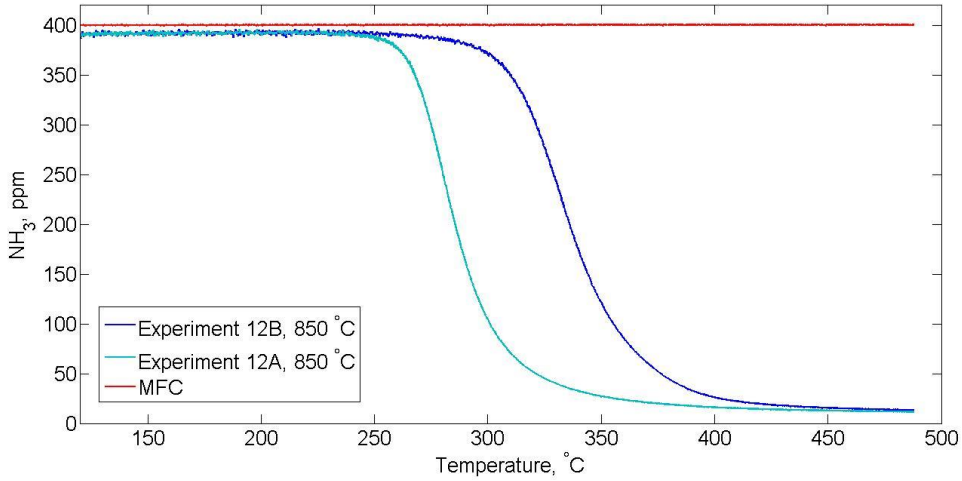

Figure 58 Comparison of the effect of number of NH_3 oxidations performed on the sample (NH_3 consumption, Experiments 12A and 12B).

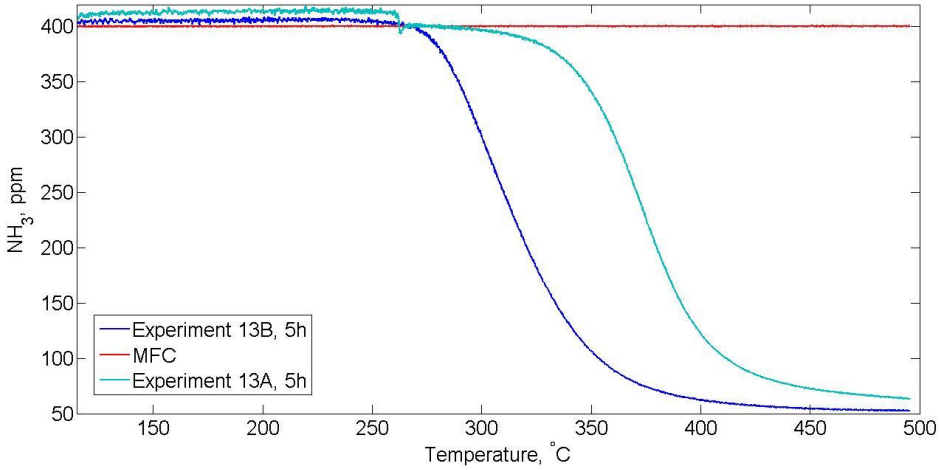

Figure 59 Comparison of the effect of number of NH_3 oxidations performed on the sample (NH_3 consumption, Experiments 13A and 13B).

In Section 4.1.4.1, a comparison between Experiments 11A and 11B is made when it comes to NH_3 consumption. There, the differences between the total number of NH_3 oxidations

performed on the sample was negligible. Thus, the same pattern was not found and the cases needed to be analysed each by each.

Differences in CO oxidation were also observed. In general, they were smaller than the differences observed in NH_3 oxidation, as seen in Figure 60 and Figure 61. The reason for this is likely that during the first experiment, which always is NH_3 oxidation, the Pd is redistributing and for the following CO oxidations, the capturing monolith is stable.

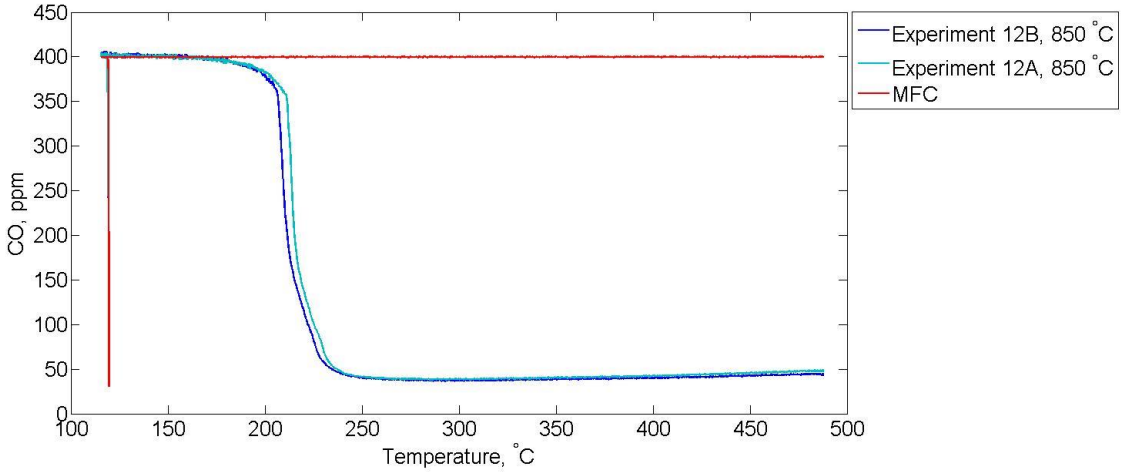

Figure 60 Comparison of the effect of number of NH_3 oxidations performed on the sample (CO consumption, Experiments 12A and 12B).

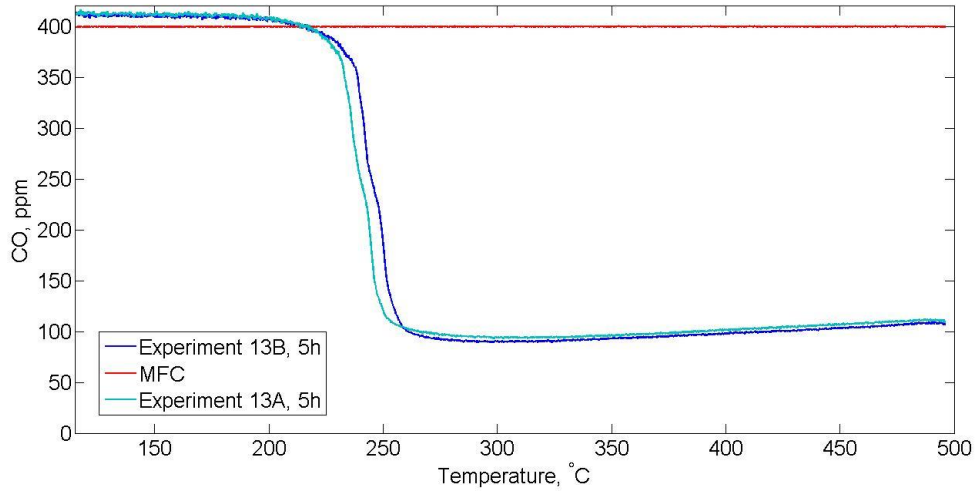

Figure 61 Comparison of the effect of number of NH_3 oxidations performed on the sample (CO consumption, Experiments 13A and 13B).

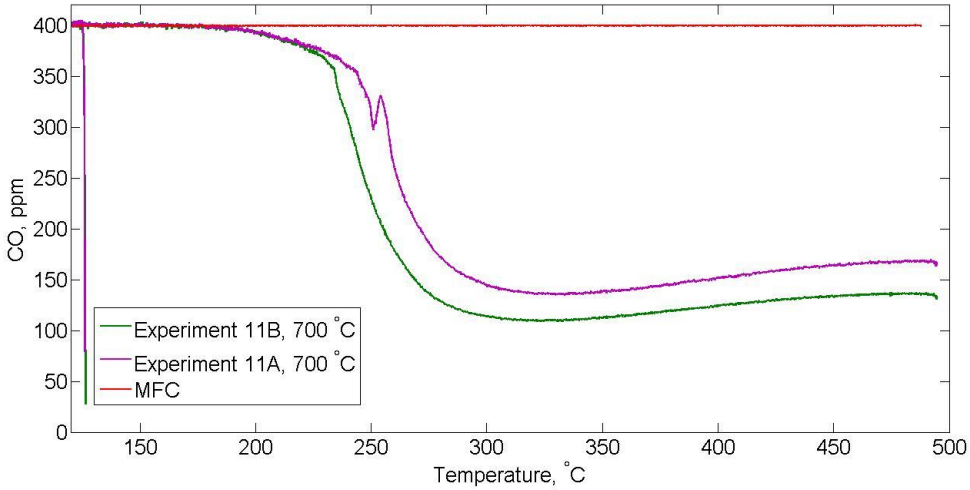

Figure 62 Comparison of the effect of number of NH_3 oxidations performed on the sample (CO consumption, Experiments 11A and 11B).

A.2.2 - NH_3 oxidation test with "non-contaminated" capturing monolith

To ensure that the capturing monolith washcoated with Al_2O_3 was not being responsible for part of the oxidation observed in the trials, giving misleading results regarding Pt migration, an NH_3 oxidation test with a "non-contaminated" capturing monolith was performed. That is, a capturing monolith that had not been exposed to evaporation. The result is presented in Figure 63. No NH_3 oxidation was observed.

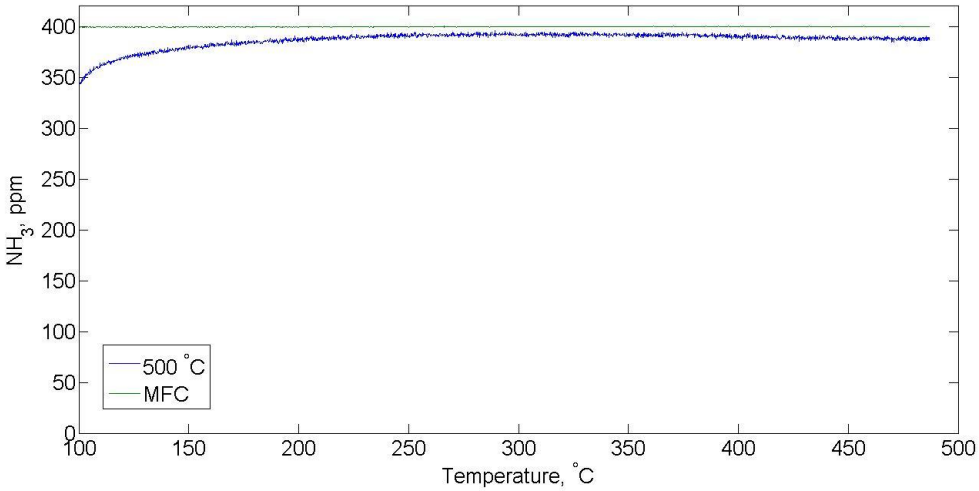

Figure 63 NH_3 oxidation test with "non-contaminated" capturing monolith.

A.2.3 – Effect of surface cleaning

During execution of Experiments 1-4, surface cleaning was mistakenly not performed prior to the first sequence of NH_3 – CO oxidations. A comparison between the NH_3 oxidation results obtained for Experiment 2, with and without surface cleaning is presented to illustrate the differences resulting from that. The NH_3 oxidation results show that the sample that was not subjected to surface cleaning showed a higher activity towards oxidation, which is logical if it is thought that species might be weakly adsorbed on the capturing monolith surface and that they oxidise NH_3. However, based on the discussion of the effect of the number of NH_3

oxidations, it is not clear what is a result of surface cleaning and what is a result of different number of NH_3 oxidations.

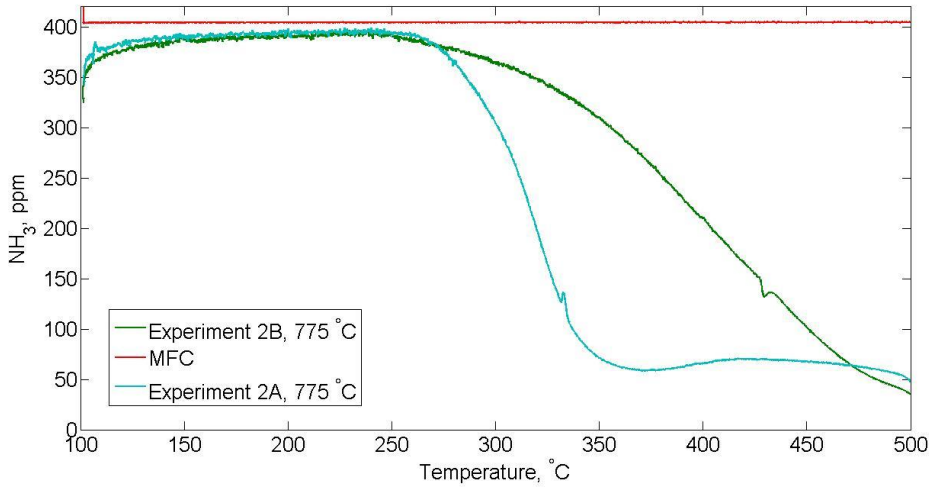

Figure 64 Comparison of Experiments 2A (with surface cleaning) and 2B (without surface cleaning).

In Figure 65, all Experiments 1A, 2A and 3A are exhibited for illustration purposes since the significance of the results cannot be evaluated due to the lack of surface cleaning. It is noticed that, if compared to the results presented in Section 4.1.1.1, curves 2A and 3A are "sharper" than curves 2B and 3B. Differences regarding this characteristic were not observed when the number of oxidations was compared, suggesting that this is likely to be connected to surface cleaning.

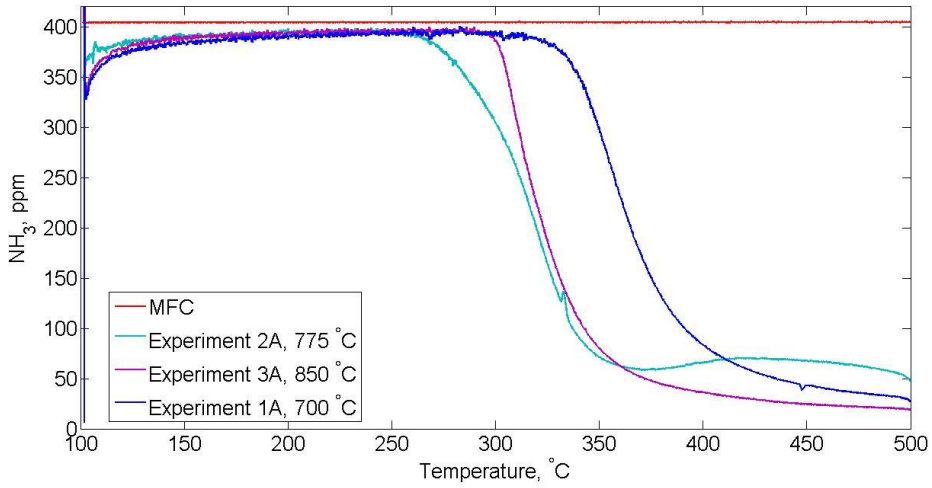

Figure 65 NH_3 oxidation results from Experiments 1A-3A (without surface cleaning).

A.2.4 – Effect of temperature: 10B-12B results

The results of Experiments 10B-12B, omitted from Section 4.1.1.1 for conciseness are here presented. Despite differences inherent to a different number of NH_3 oxidations being observed for some of the samples, the overall behaviour and trend were the same for all investigated parameters.

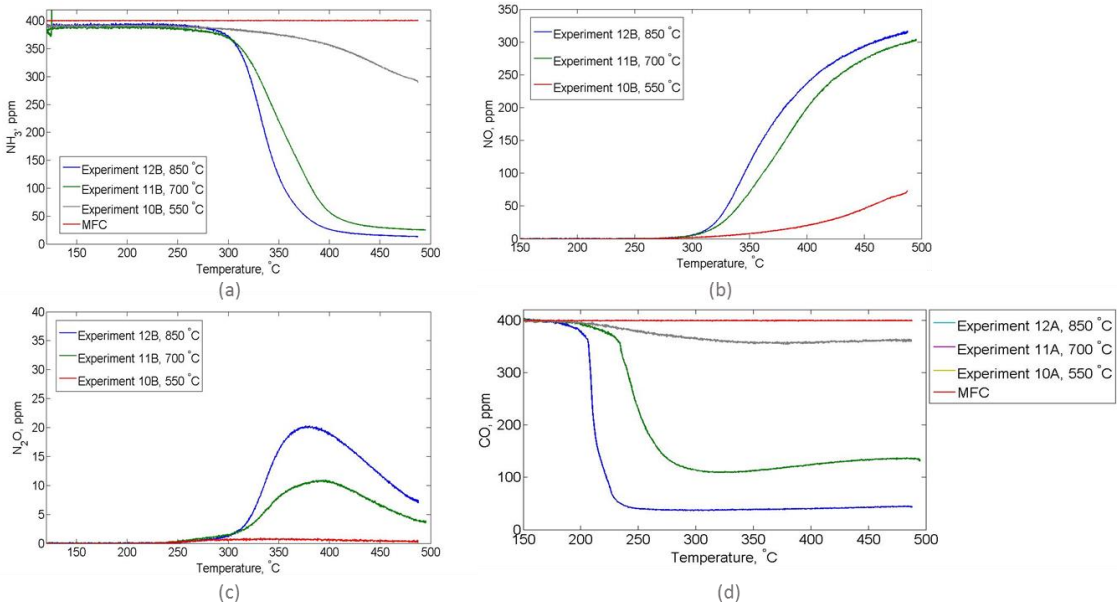

Figure 66 Effect of temperature - Results from experiments 10B-12B: (a) NH_3 oxidation; (b) NO formation; (c) N_2O formation; (d) CO oxidation.

A.3 – BOOST

A.3.1 – Catalyst specifications

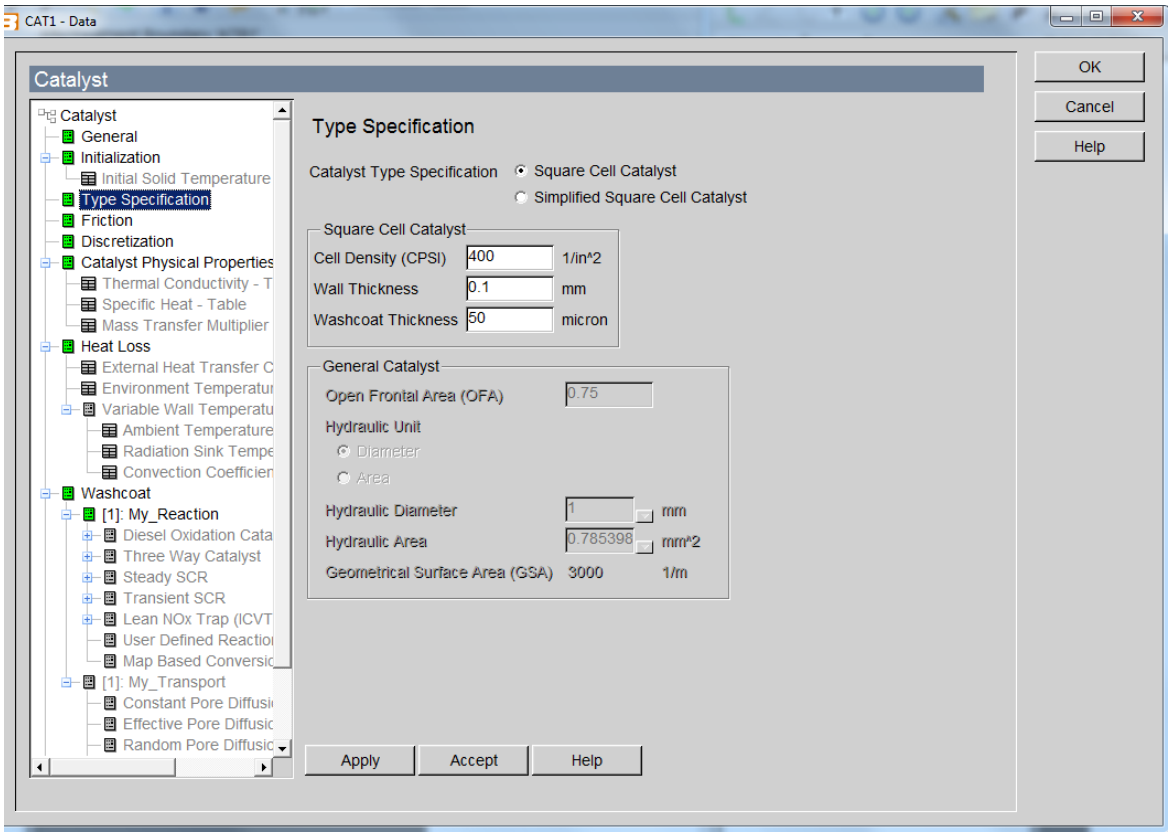

Figure 67 BOOST: Catalyst specifications – Type.

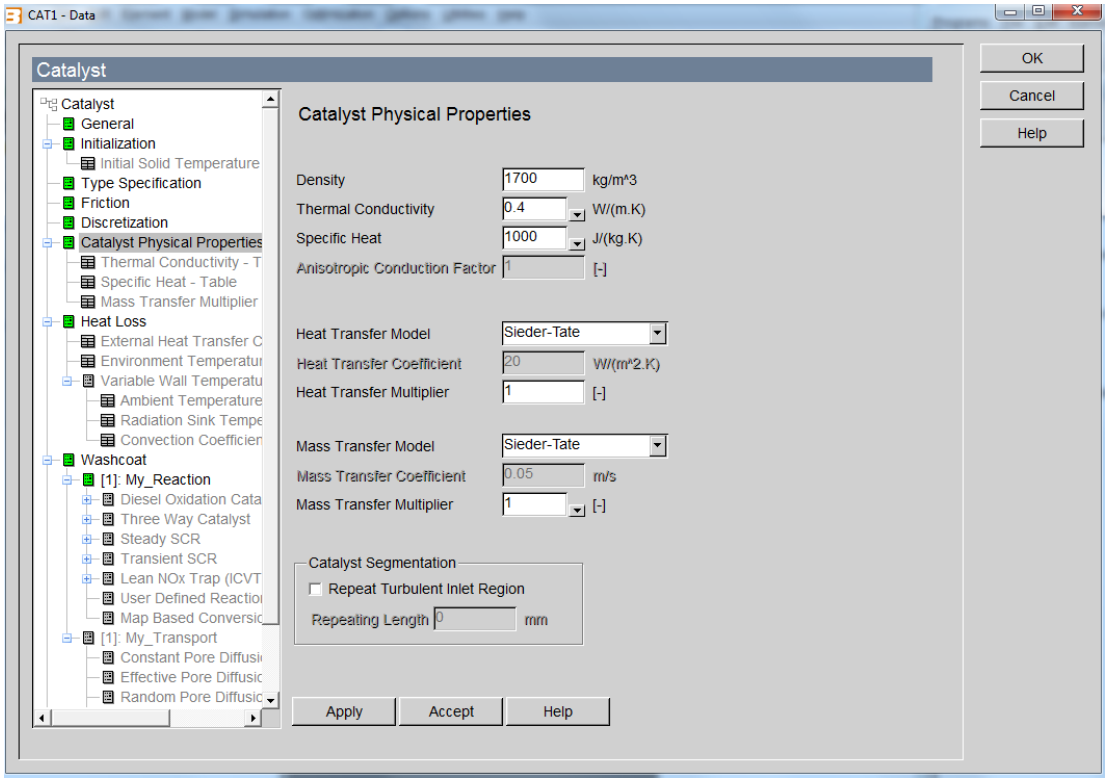

Figure 68 BOOST: Catalyst specifications – Physical properties.

A.3.2 – User defined reaction details

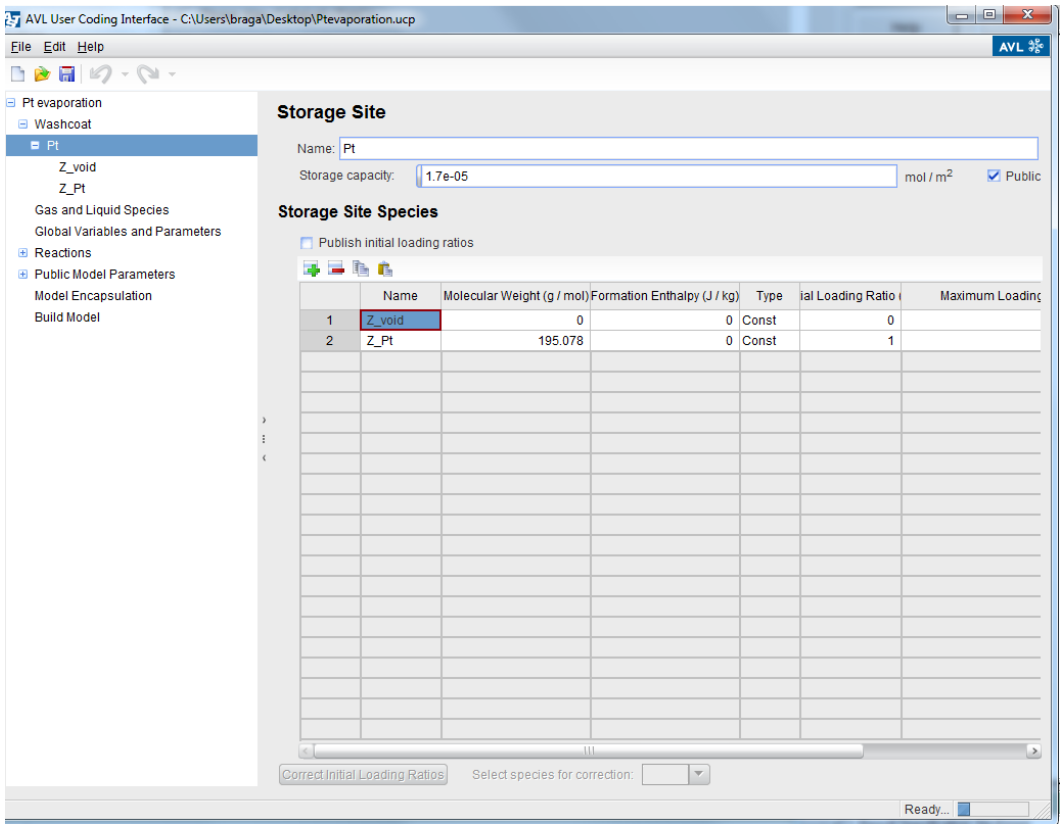

Figure 69 BOOST: User defined reactions – Surface sites.

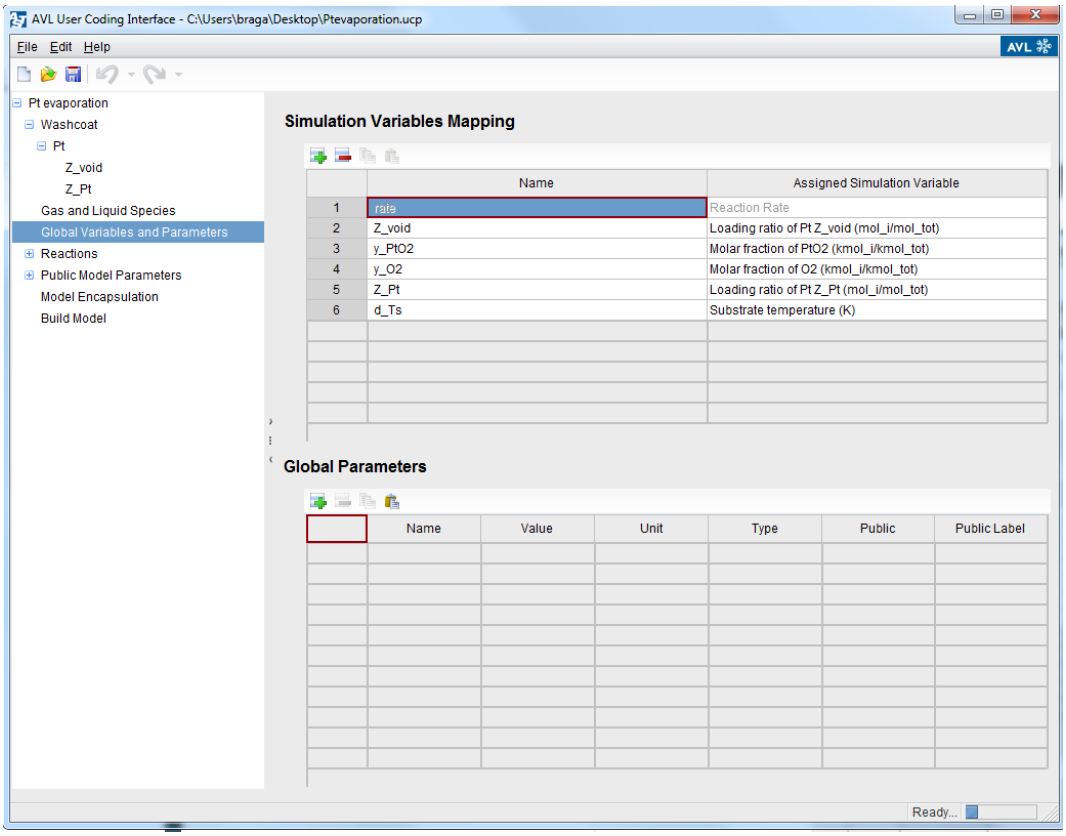

Figure 70 BOOST: User defined reactions – Global Variables and Parameters.

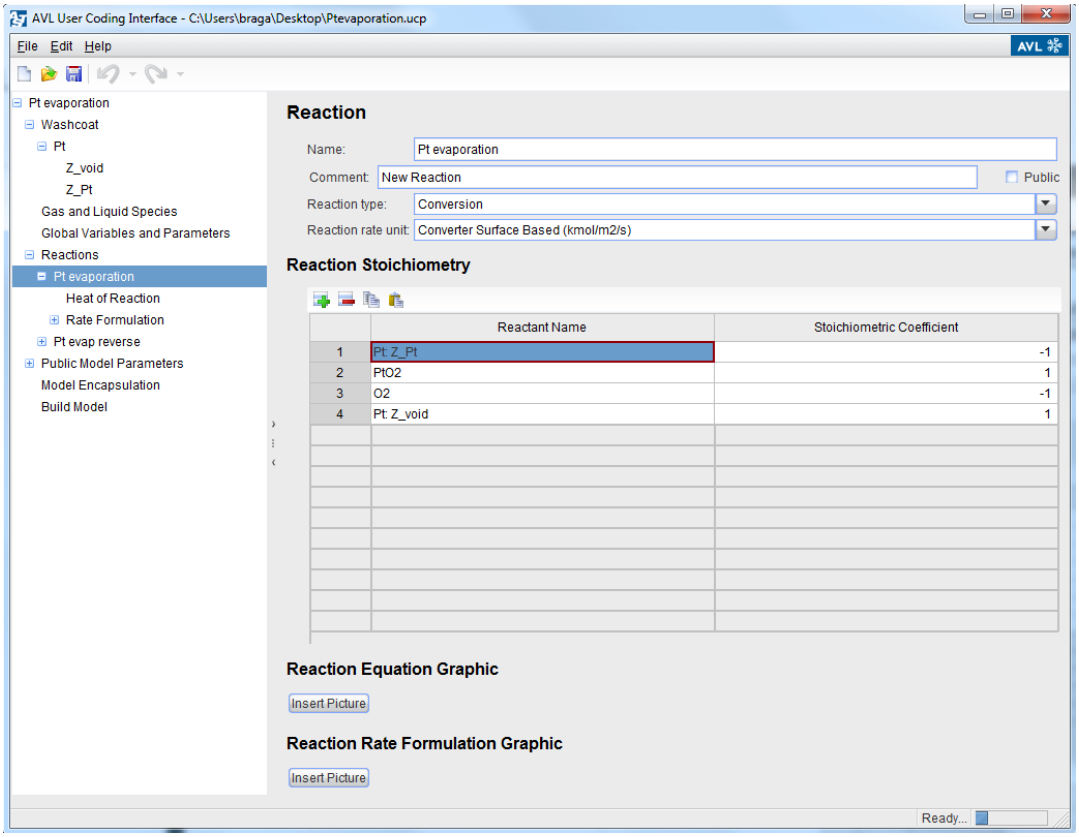

Figure 71 BOOST: User defined reactions – Forward reaction stoichiometric coefficients.

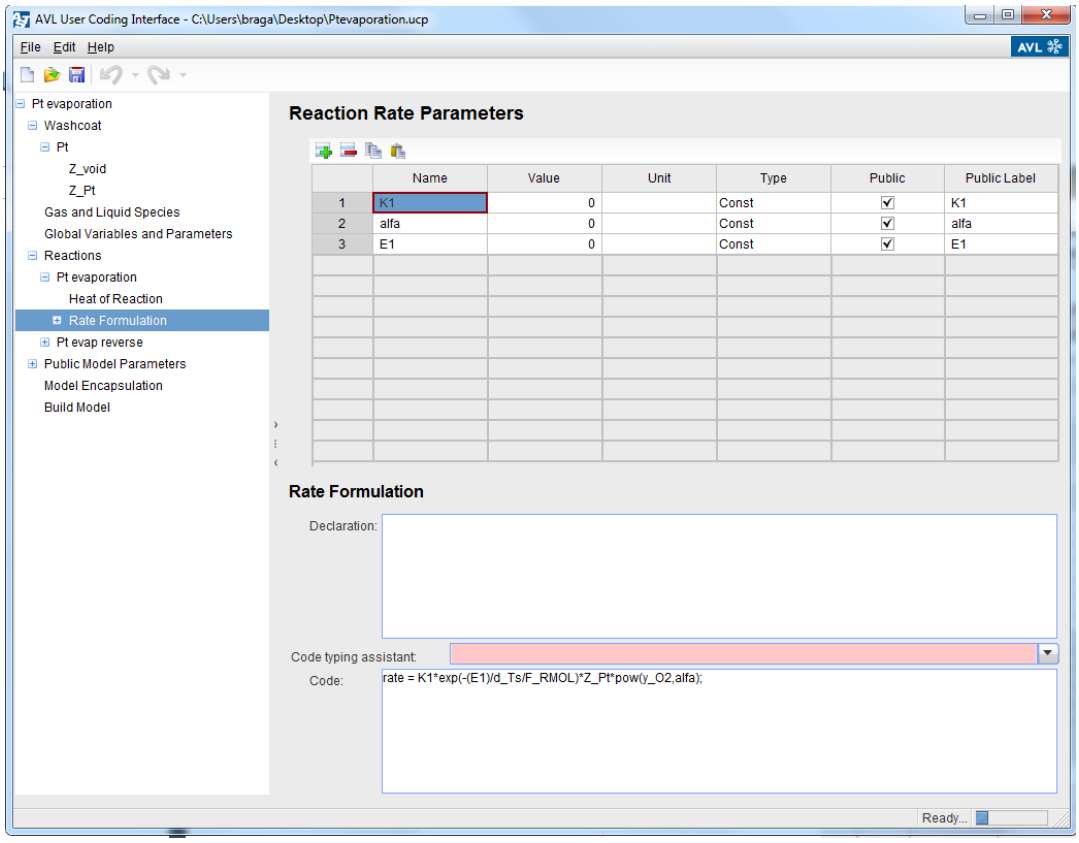

Figure 72 BOOST: User defined reactions – Forward reaction rate formulation.

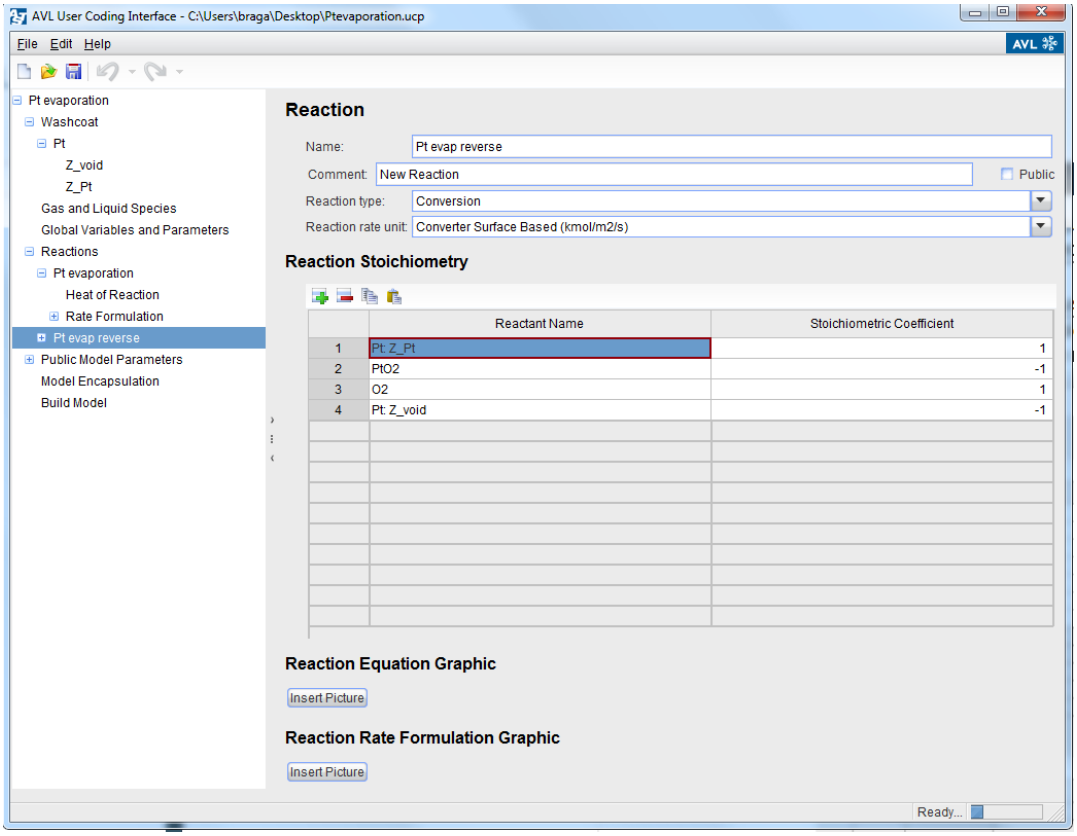

Figure 73 BOOST: User defined reactions – Backward reaction stoichiometric coefficients.

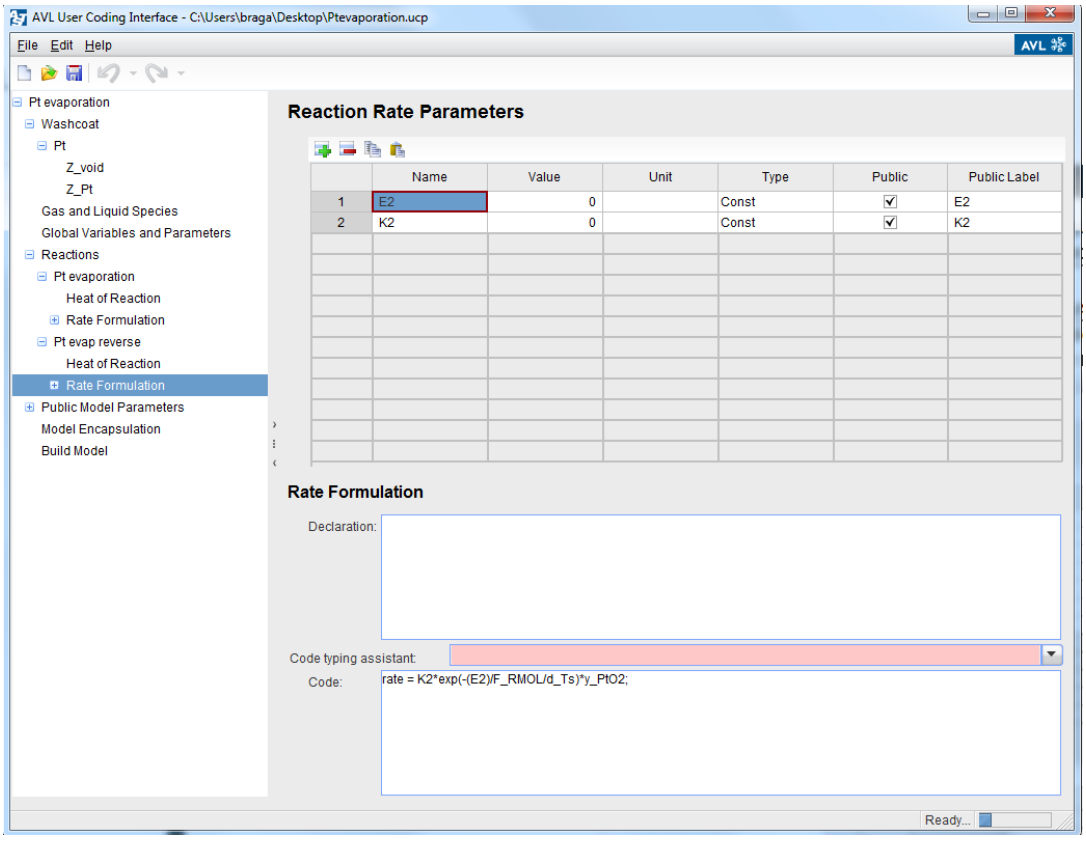

Figure 74 BOOST: User defined reactions – Backward reaction rate formulation.